THE PROPERTIES AND REGULATION OF THE HEPATIC CYTOPLASMIC LIPID DROPLET

by

AMANDA ELIZABETH CRUNK

B.S., California State Polytechnic University, Pomona 2004

A thesis submitted to the

Faculty of the Graduate School of the

University of Colorado in partial fulfillment

of the requirements for the degree of

Doctor of Philosophy

Molecular Biology Program

2013

This thesis for the Doctor of Philosophy degree by

Amanda Elizabeth Crunk

has been approved for the

Molecular Biology Program

by

Rytis Prekeris, Chair

James L. McManaman, Advisor

Andrew P. Bradford

Jerome Schaack

David J. Orlicky

Date 10/25/13

Crunk, Amanda, Elizabeth (Ph.D., Molecular Biology)

The Properties and Regulation of the Hepatic Cytoplasmic Lipid Droplet

Thesis directed by Professor James L. McManaman.

ABSTRACT

Liver steatosis, a serious complication of obesity, results from the excess accumulation of TG stored in the core of cytoplasmic lipid droplets (CLD). CLD are organelle like structures that contain a neutral lipid core surrounded by a phospholipid monolayer and covered in various coat proteins. Perilipin-2, the most abundant coat protein of hepatic CLD, functions as an important regulator of cellular lipid metabolism and trafficking. Electron microscopy experiments showing direct interaction between CLD and organelles raise the possibility that CLD contribute to how cells integrate cellular lipid synthesis, storage and metabolic demands. I hypothesize that Plin2 serves as a scaffolding protein for CLD interactions with organelles and metabolic enzymes, and that loss of Plin2 function will disrupt hepatic metabolism and metabolic homeostasis. To test this hypothesis I characterized lipid accumulation and CLD physical and biochemical proteins in livers from WT and Plin2-null mice that were fasted and refed low fat (LF) or high fat (HF) diets. Loss of Plin2 resulted in decreased accumulation of hepatic lipids and smaller CLD. In the absence of Plin2, perilipin family members Plin3 and Plin5 were identified on the isolated CLD from animals on both LFD and HFD. Proteomics analysis of CLD isolated from livers of fasted and re-fed WT and Plin2-null animals revealed that the loss of Plin2 alters the distribution of enzymes related to carbohydrate and lipid metabolism, and that dietary fat content influenced the effects of Plin2 loss on CLD

protein properties. Furthermore, CLD deficient of Plin2 have fewer organelle associated proteins compared to CLD from WT animals. KEGG pathway of CLD proteins indicated that the loss of Plin2 influences the CLD association of enzymes in multiple metabolic pathways including, carbohydrate, amino acid and lipid metabolism. Collectively, my data show that the protein compositions of hepatic CLD of both WT and Plin2 KO mice are dynamically influenced by diet, and that loss of Plin2 induces specific reorganization of CLD protein composition when animals were re-fed a HF diet. These results provide the first evidence that CLD are dynamically regulated by diet and Plin2, and that they may function as platforms to coordinate lipid metabolism in hepatocytes.

The form and content of this abstract are approved. I recommend its publication.

Approved: James L. McManaman

DEDICATION

I dedicate this work to my parents Chris and John who have always encouraged me to pursue my dreams, no matter how difficult or insurmountable they may seem, and to Dr. Alan Wilkinson whose encouragement and gift of a new life will never be forgotten.

ACKNOWLEDGMENTS

The body of work that encompasses the thesis dissertation cannot be accomplished by a single individual. Without the help and guidance of many people over the last several years, I would not be where I am today. I have so many people that I would like to acknowledge for their role in this process, and I am certain I will forget many. I would like to thank my thesis committee members, Andrew Bradford and Jerry Schaack for their guidance and mentoring. In particular, I would like to thank my thesis committee member David Orlicky who truly enjoys teaching and was instrumental in helping me with all of the histology throughout this project. I especially want to thank my committee chair Rytis Prekeris, who has been irreplaceable as a sounding board, mentor, teacher, and most importantly an anchor who brings me back to earth when get too far off my path.

I also want to thank the Molecular Biology Program Administrator, Jean Sibley, who has become a friend over the last several years. I will miss dropping into her office to let off steam or just have a quick chat about the week's recent activities. I want to thank the faculty of the Molecular Biology Program, who were able to look past my flaws and recognized my tenacity and determination were not merely words I used to describe myself in an admissions essay, but are integrated elements of my personality. The words thank you cannot express how much it means to have the strong unwavering support of my program director James DeGregori; never the less thank you.

I want to thank the Maclean lab for their help with all things dealing with metabolism. In particular, I want to thank Matthew Jackman for taking the time to teach me how to use the metabolic monitoring system. I want to thank Melanie Scully for her

western blot expertise, and working together with me to learn all about on our new baby the Li-cor.

Finally, I want to thank the women in my lab who have taught me so much. Shannon Cain has run more than her share of lipolysis, TLC and triglyceride assays for which I am extremely grateful for all of her help. Elise Bales maintains our huge mouse colony, and she always made sure I had animals available when I needed them, and helped me with the countless slides that were stained for this project. I want to thank Jenifer Monks who is an enormous resource when it comes to microscopy. Without her help and hours in front of the microscope I would never have been able to finish as quickly as I have, if ever. She is a great teacher, mentor and friend.

I want to thank my thesis mentor James McManaman who took a leap of faith when he brought me into his lab so late in my graduate student career. I will miss our long roundabout conversations, the initial subject of which neither can remember. You have allowed me the freedom to explore and contemplate ideas which on the surface may have seen crazy or insane, but eventually lead to many fruitful projects in the end. Working in your lab truly encompasses my favorite quotation seen many times in my emails but never as appropriate as now.

“The most exciting phrase to hear in science, the one that heralds new discoveries, is not Eureka! (I found it!) but, That's funny...."

Isaac Asimov

TABLE OF CONTENTS

CHAPTER

LIST OF TABLES

TABLE

LIST OF FIGURES

FIGURE

LIST OF ABBREVIATIONS

ABC: Ammonium Bicarbonate

ACN: Acetonitrile

ADRP: Adipophilin

ADRP: Adipocyte Differentiation Related Protein

ALT: Alanine Aminotransferase

AFLD: Alcoholic Fatty Liver Disease

ASO: Anti Sense Oligonucleotides

AST: Aspartate Transaminase

BAT: Brown Adipose Tissue

BMHT: Betaine Homocysteine Methyltransferase

CARS: Coherent Anti-Stokes Raman Scattering

CLD: Cytoplasmic Lipid Droplet

CV: Central vein

D5KO: Perilipin 2, Delta 5 Knock Out

DAG: Diacylglycerol

DGAT: Diacylglycerol Transferase

FA: Fatty Acid

FFA: Free Fatty Acid

GO: Gene Ontology

H&E: Hematoxylin and Eosin

HCV: Hepatitis C

HFD: High Fat Diet

HPLC: High Performance Liquid Chromatography

HSL: Hormone Sensitive Lipase

KEGG: Kyoto Encyclopedia of Genes and Genomes

LCFA: Long Chain Fatty Acid

LFD: Low Fat Diet

MCFA: Medium Chain Fatty Acid

mRNA: Messenger RNA

MEF: Mouse Embryonic Fibroblasts

MS: Mass spectrometry

NAFLD: Non-Alcoholic Fatty Liver Disease

PDI: Protein Disulfide Isomerase

Plin: Perilipin

Plin1: Perilipin 1, Perilipin

Plin2: Perilipin 2, Adipophilin, ADRP, ADPH

Plin3: Perilipin 3, TIP47

Plin4: Perilipin 4, S3-12

Plin5: Perilipin 5, Oxpat

PEX3: Peroxisomal biogenesis factor 3

PNS: Post Nuclear Supernatant

PPAR: Peroxisome Proliferator Activated Receptor

PPAR-α: Peroxisome Proliferator Activated Receptor – alpha

PPAR-β/δ: Peroxisome Proliferator Activated Receptor - beta/delta

PPAR-γ: Peroxisome Proliferator Activated Receptor – gamma

PPRE: Peroxisome Proliferator Response Element

PT: Portal Triad

QRT-PCR: Quantitative Real Time - Polymerase Chain Reaction

RER: Respiratory Exchange Ratio

RXR: Retinoid X Receptor

TFA: Triflouric Acid

TG: Triacylglycerol, Triglyceride

VDAC: Voltage-dependent anion channel

WAT: White Adipose Tissue

WT: Wild Type

VLDL: Very Low Density Lipoprotein

CHAPTER I

INTRODUCTION AND BACKGROUND

Introduction

Obesity is the number one preventable cause of death worldwide, and can lead to cardiovascular disease, cancer, type II diabetes, and nonalcoholic fatty liver disease with an annual cost in the US of almost $215 billion a year [1, 2]. A common pathological feature of obesity is the excess accumulation of triglycerides (TG) in the form of cytoplasmic lipid droplets (CLD) in non-adipose tissues, which can lead to hepatic steatosis [3]. CLD are organelle-like structures that are increasingly recognized to play critical roles in cellular lipid metabolism by regulating lipid storage, utilization and trafficking [4]. Knowledge of the molecular mechanisms by which CLD regulate these processes are important for understanding the pathophysiological roles CLD play in obesity and other metabolic diseases, and for developing new treatments and therapies to combat these disorders. The proteins that coat CLD have been emerging as an important regulator of CLD functions. Specifically, five members of the perilipin family of proteins found in mammals, Plin1 (perilipin), Plin2 (adipophilin, ADPH), Plin3 (TIP 47), Plin4 (S3-12), and Plin5 (Oxpat), are increasingly recognized to be important as regulators of lipid metabolism and storage in most tissues. In the normal mouse liver, CLD are coated by Plin2, and it has been shown that Plin2 is required for hepatic TG accumulation associated with chronically feeding mice a high fat (HF) diet

In this chapter, I will briefly discuss how various metabolic alterations can lead to hepatic steatosis, and finally I will review the current literature regarding cytoplasmic lipid droplets.

Non-Alcoholic Fatty Liver Disease

Impaired hepatic lipid metabolism can have dramatic pathophysiological consequences. These alterations can lead to insulin resistance, diabetes, and hepatic steatosis which can progress to non-alcoholic fatty liver disease (NAFLD), hepatic stenosis, and in rare cases hepatic carcinoma [5]. The rise in NAFLD has made it the most prevalent form of liver disease in western society [6], and has directly increased the number of patients now awaiting liver transplants by nearly 15 fold in the last two decades. In the U.S., approximately 75% of all obese individuals have some form of hepatic steatosis compared to 15% of the non-obese individuals [7]. In children the occurrences of NALFD have almost doubled in the last decade from 2.6% to 5% in normal weight children, increased 38% in obese children, and 48% of children with type 2 diabetes [8-10].

NAFLD is a spectrum of disorders ranging from simple steatosis, which is relatively benign, to nonalcoholic steatohepatitis, and finally progression into fibrosis/cirrhosis. The clinical definition of NAFLD is the accumulation of lipid in hepatocytes that constitutes more than 5%-10% of the liver weight [11]. NAFLD has been recently included in part of the larger metabolic syndrome. A group of symptoms that include insulin resistance, diabetes, obesity, and high serum blood lipid profiles. NAFLD is rarely found without at least one of these accompanying pathologies, most commonly insulin resistance [12]. Clinical manifestation usually presents with increased serum biomarkers of liver injury, alanine aminotransferase (ALT) and aspartate aminotransferase (AST), although in early stages of simple steatosis elevation of liver enzymes are not always present. Like many organ specific diseases, few non-invasive diagnostic techniques are definitive. Liver biopsy is used to determine the severity, and

classification of the disease to determine if an individual has progressed beyond simple steatosis to steatohepatitis that includes signs of inflammation, or the presence of fibrosis [5]. Imaging techniques can determine the relative amount of hepatic lipid accumulation, but these techniques are not sensitive enough to determine the stage of the disease [13].

In the past two decades, research into the mechanisms causing hepatic steatosis has greatly increased due to the focus on diabetes and obesity. Several mouse models of hepatic steatosis have been developed to identify these mechanisms. Although there appear to be multiple genes and metabolic alterations leading to increased prevalence of steatosis, the primary cause is the dysregulation of lipids. Increasing hepatic lipid synthesis, uptake of fatty acids (FA), decrease in TG exports via very low density lipoproteins (VLDL), or increase in adipocyte lipolysis can lead to TG accumulation in the liver in the form of CLD.

Cytoplasmic Lipid Droplets

CLD were first identified in the 1890's by Richard Altmann and E.B. Wilson [14, 15], these structures were initially ignored for nearly a century until 1991, when Greenberg identified perilipin, a phosphorylated protein that coated the CLD in adipocytes [16]. In the past two decades, with the increasing health problems associated with obesity, CLD have been identified as important structures involved in the accumulation of excess neutral lipids. CLD are organelle like structures that contain a neutral lipid core surrounded by a phospholipid monolayer, and coated in a variety of proteins (Figure I.1) [17]. CLD function as critical regulators of cellular metabolism by sequestering these neutral lipids within the phospholipid monolayer, and providing a regulatory network of coat proteins that can respond to specific cellular demands. The

five members of the perilipin family, Plin1 (perilipin), Plin2 (adipophilin), Plin3 (tail interacting protein 47), Plin4 (S3-12), and Plin5 (OXPAT), are the most abundant structural proteins on the CLD, and are the most well characterized CLD coat proteins.

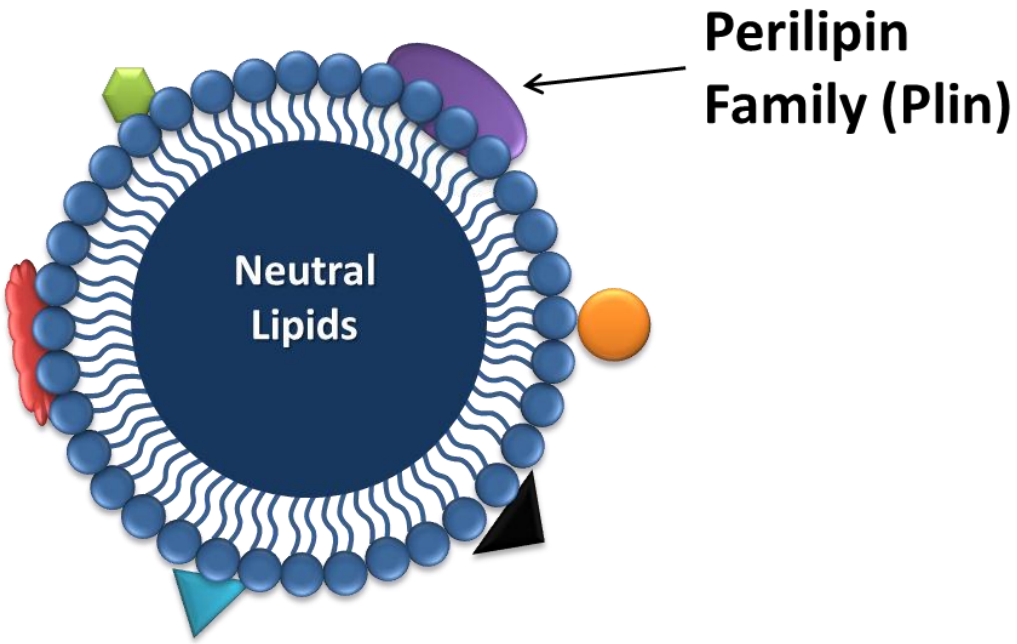

Figure I.1 Diagram of Cytoplasmic Lipid Droplet
Diagram of CLD. Neural lipid core surrounded by phospholipid monolayer and coated in various proteins. Perilipin family members are the most abundant coat proteins on CLD.

Biogenesis

There are several competing hypotheses regarding the mechanism by which CLD are formed. A common feature of each hypothesis is that CLD formation begins through the deposition of lipids in the ER. The initial accumulation of lipids in the ER begins from the increased concentration of intracellular FA, derived either from lipolysis of lipoproteins, from free fatty acids (FFA) carried by albumin, or from activation of cellular de novo lipogenesis. Intracellular FA's are activated by conjugation with acyl-CoA through an ATP dependent enzymatic reaction, catalyzed by various acyl-CoA

ligases, to produce pools of activated fatty acyl-CoA's. Glycerolipid-synthesis enzymes in the ER use fatty acyl-CoA's and glycerol to form diacylglycerol (DAG). DAG's are then converted to TG, or enter phospholipid synthesis pathways through enzymatic reaction with various diacylglycerol transferases (DGATs) [18]. The mechanisms by which DAG's enter either pathway are still unclear.

The canonical model of CLD biogenesis (ER-budding model hypothesis) suggests, that de novo synthesized TG accumulates between the leaflets of the ER membrane bilayer forming a lens. The lens subsequently buds from the membrane, generating a nascent CLD composed of TG core, surrounded by a phospholipid monolayer with associated proteins [19] (Figure I.2A). The bicelle model proposes that neutral lipids accumulate between the leaflets of the ER membrane, and rather than budding, CLD with associated lipid and protein portions of the ER membrane, are somehow excised from the membrane leaving behind a transient pore in the ER membrane [20] (Figure I.2B). There have been no definitive direct observations of any of these proposed mechanisms. Dissenting from the consensus that lipid is deposited within the leaflet of the ER, Robenek et al suggests the site of CLD synthesis occurs within the cytoplasm along specialized cups of the ER [21]. Freeze fracture experiments indicate the site of CLD formation along these ER cups are coated with Plin2, and it was proposed that the Plin2 enriched sites are what trigger the accumulation of CLD (Figure I.2C).

Perilipin Family of Proteins

The Perilipin family is highly conserved throughout evolution. Mammalian homologs have been identified in species that include frogs, flies, yeast, fungi, plants and slime molds [22]. The fact that lipids are important components of all living organisms,

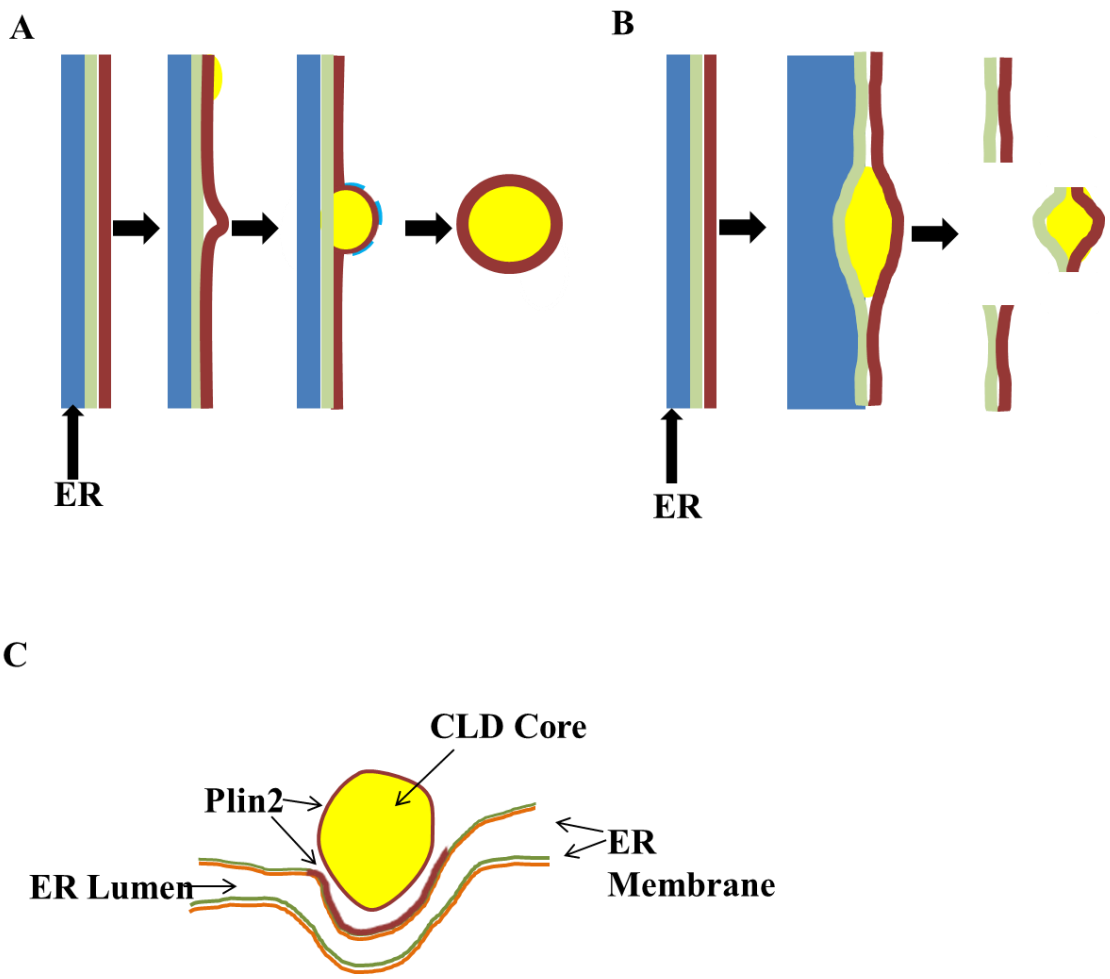

Figure I.2 Models of CLD Biogenesis
Lipid droplet biogenesis by ER budding. Neutral lipids (yellow) are synthesized and bulge from the outer leaflet of the ER membrane (red). The nascent droplet may be coated by proteins (light blue) that facilitate the budding process. (B) Bilayer excision. Newly synthesized neutral lipids accumulate between the inner (green) and outer (red) leaflets of the ER membrane and cause bulging. This entire lipid lens is then excised from the ER, leaving a transient hole in the membrane. ER contents (yellow) might leak through this hole into the cytosol. (C) Lipid is deposited along the Plin2 coated (red) cups at the ER outer membrane.

points to the general importance of this family as possible regulators of cellular lipid homeostasis. Despite their overall genetic conservation, members of the Perilipin family exhibit various degrees of sequence and structural differences [22]. Of the five mammalian perilipin proteins, Plin2 and Plin3 exhibit the greatest degree of sequence and structural homology, including an N-terminal PAT domain, 11-mer helical repeats in their N-terminal regions, a four helix bundle, and hydrophobic cleft in their C-terminal regions [22] (Figure I.2). At present, only the structure of the C-terminal region of Plin3 has been solved [31], but modeling studies suggest that, overall, the structures of Plin2 and Plin3 are very similar [23]. Nevertheless, the question of how closely the functions of Plin2 and Plin3 are related has not been established. Moreover, there is increasing recognition that despite significant sequence homology and structural similarities, the two proteins differ in their functions

Perilipin 2

Plin2 was first identified as an RNA transcript significantly induced during differentiation of cultured adipocytes and was termed adipocyte differentiation related protein (ADRP) [24]. Sequence analysis revealed Plin2 had similarity to other perilipin proteins (Plin1 and Plin3) alluding to a potential function of the protein. Indeed, upon lipid loading, Plin2 was found to coat CLD in a variety of cells and tissues including 3T3L1 cells, fibroblasts, liver and mammary gland [25-31]. In differentiating adipocytes, Plin2 coats the CLD early during differentiation and its mRNA levels remain elevated throughout differentiation. Adipocyte Plin2 protein levels, which rise during differentiation, gradually decrease suggesting that these levels are subject to translational or posttranslational regulation. Masuda et al demonstrated that Plin2 is subject to

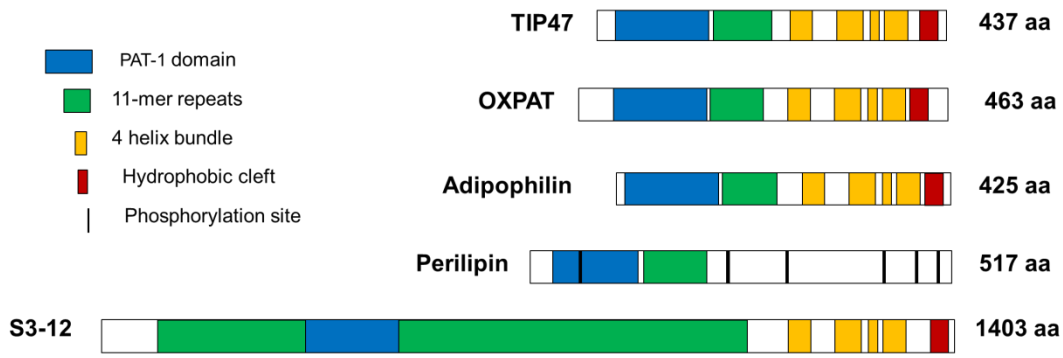

Figure I.3 Schematic Diagram of the Structural Features of the Mouse Perilipin Proteins.

The PAT-1 domain is a 100 amino acid sequence that is similar in all 5 proteins (blue). The 11-mer helical repeat region is required for CLD binding, S3-12 is unique in that it contains 87 tandem repeats (green). The four-helix bundle (gold) and the 14 aa is identified in all but perilipin (gold).

posttranslational regulation via ubiquitination and subsequent degradation by the proteasome [32]. In 3T3L1 cells the observation of decreased protein levels of Plin2 also coincide with increased levels of Plin1 on the CLD. These observations lead to the hypothesis that Plin2 might compete for CLD localization during differentiation of 3T3L1 cells [33, 34]. In the liver, Plin2 was found to be upregulated in both human and murine NAFLD and alcoholic fatty liver disease (AFLD) [35]. In NAFLD and AFLD, Plin2 promotes the incorporation of TG into CLD resulting in enlarged CLD and prevention of β-oxidation [36]. Plin2 anti-sense oligonucleotide (ASO) treatment was shown to decrease the severity of hepatic steatosis in the leptin deficient obese mouse model and the diet induced obesity mouse model. ASO's against Plin2 suppressed expression of lipogenic genes and reduced liver triglyceride content without affecting cholesterol levels. Reduced Plin2 expression also attenuated triglyceride secretion, and decreased serum triglyceride and ALT levels [37]. Chan et al generated a Plin2 KO animal through the deletion of exons 2 and 3 (Δ2,3KO) [38]. Livers of Δ2,3KO animals

had significant reduction in hepatic lipid accumulation and lower serum TG levels. However, β-oxidation, VLDL secretion, and lipogenesis were unchanged compared to WT controls. Measurements of Plin3 mRNA and protein expression in the liver were also unchanged compared to controls. Russell et al determined a flaw in the gene deletion strategy used to generate the Δ 2,3KO mouse [39]. Although there were no detectable transcripts in white adipose tissue (WAT), brown adipose tissue (BAT) or liver, further analysis showed a truncated transcript in the mammary gland of the Δ 2,3KO mouse, upon further analysis this transcript was found to produce a truncated protein that retained at least some Plin2 function. A second Plin2 KO mouse was generated by the deletion of exon 5 (D5KO). The D5KO animal was resistant to HF diet-induced hepatic steatosis, obesity, and adipose inflammation. The liver phenotype in D5KO mice appears to be specifically related to Plin2 loss, since D5KO's had both Plin3 and Plin5 expression as determined by western blot and immunofluorescent microscopy [40]. These studies have demonstrated the importance of Plin2 in hepatic metabolism and hepatic steatosis.

Perilipin 3

Plin3 was initially identified as a protein that bound to the cytoplasmic tail of the mannose 6-phosphate receptor during its transport from the endosomal compartment to the trans-Golgi network. Subsequently, Plin3, was shown to have a role in viral infections, where it has been identified as a necessary cofactor in HIV viral assembly [41]. In hepatoma cell lines infected with hepatitis C virus (HCV) core protein, Plin3 was found to redistribute from the cytosol to CLD upon lipid loading, the authors speculated this phenomenon may be due to the lack of Plin2 in the hepatoma cell lines [42]. Indeed Plin3 protein expression increases in the absence of Plin2 in the liver, mammary gland,

and in mouse embryonic fibroblasts (MEF) [39, 43]. Treatment with ASO's against Plin3 was found to decrease the severity of CLD accumulation in the liver without affecting Plin2 expression [44].

Perilipin 5

Plin5 was identified as a perilipin protein that is primarily expressed in oxidative tissues that utilize large amounts of lipid during β-oxidation [45]. Plin5 is most notably localized to skeletal muscle, heart, and brown fat. Both in vivo and in vitro studies have shown that expression of Plin5 correlates with both increased TG storage, and FA oxidation[46] . Electron micrographs have been used to demonstrate the interaction between mitochondria and Plin5 coated CLD. It has been suggested that these interaction between Plin5 coated CLD and mitochondria may actively control the fate of FA either by directing them towards FA oxidation or storage. Recently, it has been shown that Plin5 has the potential to modulate the interaction of adipose triglyceride lipase (ATGL) with CLD as well as with its co-factor CGI-58 [47] in order to modulate CLD lipolysis [48] . Similar to Plin2, Plin5 appears to be in part regulated by the nuclear receptor peroxisome proliferator activated receptor PPAR [49]. Studies have shown that the induction with ligand FFA increases the expression of both Plin5 mRNA and protein.

Regulation of Lipid Droplets

With the exception of Plin1, the precise functions of the perilipin proteins are not well known. One suggestion is that they act as regulators of lipolysis by controlling access of specific lipases to the CLD core. Lipases are the major enzymes that control lipolysis, the conversion of TG to monoglyceride and fatty acids [50]. Hormone sensitive lipase (HSL) was thought to be the major contributor of TG lipolysis, studies with HSL-

KO mice are resistant to obesity, and rather than having increased concentrations of TG, they have significant high levels of DG [51]. In 2004 ATGL was identified as the enzyme that catalyzed the first, and rate, limiting step in TG hydrolysis having a much higher affinity for TG than HSL, and ATGL deficient animals were shown to develop sever hepatic steatosis [52, 53]. ATGL is activated by the interaction with CGI-58, a member of the esterase/lipase family. Specific domains within both ATGL and CGI-58 have been identified that target the proteins to the CLD [54, 55]. Deletion of the tryptophan rich stretch in the N-terminal region of CGI-58 caused complete inactivation of ATGL without interference with binding between the two proteins [55]. Lu et al speculated that CGI-58 at the surface of CLD may remodel the phospholipid monolayer and thereby allow the access to the TG core by ATGL [54]. The perilipin proteins Plin2 and Plin5 may influence the ability of ATGL or CGI58 to gain access to the CLD core. While Plin2 is thought to prevent ATGL from interacting with the CLD, Plin5 interacts with both ATGL and CGI-58 [56, 57]. The significance of these mechanisms has yet to be defined. What has become clear is how protein interaction with the CLD can modulate the TG core. The loss or changes to the expression of perilipin proteins may influence the modulation of CLD lipolysis.

Summary of Background and Relation to Thesis work

This thesis set out to test the hypothesis that CLD protein composition could be influenced by diet and the loss of the primary coat protein Plin2. Accumulation of CLD is the hallmark of liver steatosis, therefore understanding how CLD are influenced by the metabolic status of the liver and in turn how altering CLD properties influences hepatic metabolic properties are important steps towards understudying how to target therapies to

combat steatosis. Numerous studies have demonstrated interactions between organelles, such as mitochondria, peroxisomes, ER, and even intracellular pathogens and CLD [58]. It has been hypothesized that these interactions occur because of effector proteins on both the CLD and organelles. In order to test these hypotheses I utilized a fasting and re-feeding model, whereby animals are fasted for 24 hours and re-fed for 18 hours either low fat diet (LFD) or high fat diet (HFD). Chapter 2 outlines the various methods and model system used to perform experiments. Chapter 3 profiles how fasting and re-feeding WT animals with diets of different compositions of fat impacts the proteomic profile of the CLD. Chapter 4 examines how the loss of Plin2 changes the CLD protein profile in response to different diets. Chapter 5 examines the physiological effect of fasting on the D5KO mouse compared to the WT mice. Finally, chapter 6 summarizes the culmination of my thesis work, and suggests further investigations that will provide more insight into the role of Plin2 and diet on the proteomic composition of the CLD, and how alterations in proteomic make up can influence hepatic metabolism.

CHAPTER II

METHODS

Materials

Chemicals used were purchased from Sigma Chemical Company (St. Louis, MO). Antibodies to N- and C-terminal regions of Plin2 and to Plin3 were raised in rabbits as described [39]. Guinea pig antibodies specific to the N-terminal 25 amino acids of mouse Plin2 were purchased from Fitzgerald (North Acton, MA). Rabbit antibodies to GRP78 and PDI were purchased from Novus Biologicals (Littleton, Colorado), and Fitzgerald Inc. (North Acton, MA) respectively. Rabbit anti-BHMT was purchased from Santa Cruz Biotechnology (Santa Cruz, CA). Horseradish-peroxidase-conjugated and Alexfluor-conjugated secondary antibodies were purchased from Life Technologies (Grand Island, NY). IR dye-conjugated secondary antibodies were purchased from Li-COR Biosciences (Lincoln, Nebraska). High fat (60 kcal%; D12492) and low fat (10 kcal%, D12045B) diets were purchased from Research Diets Inc. (New Brunswick, NJ).

Animals

Male C57BL/6J mice were purchased from Jackson Labs (Bar Harbor, Maine) at 9 weeks of age, and acclimated for 3 weeks prior to studies. Mice were individually housed and allowed to acclimate for one day prior to fasting and re-feeding.

Generation of Plin2(Δ5) Mice

Mice lacking exon 5 of the Plin2 locus were generated by Genoway (Lyon, France). Briefly, a replacement targeting vector containing a distal *lox*P site and a FRT-neomycin-FRT-*lox*P cassette were inserted into introns 4 and 5 of the Plin2 locus replacing exon 5 (Figure II.1). 129/SvPas ES cells were then transfected with the

linearized targeting vector and positive clones were selected by culturing in G418 containing media. Homologous recombinations were identified by PCR and Southern blotting. Targeted ES clones were injected into C57BL/6 blastocysts. Chimeras were backcrossed with C57BL/6 females and the neomycin cassette was removed by breeding heterozygous animals with Flippase expressing mice. Neomycin excised mice were then bred to CMV-Cre expressing mice to delete exon 5, generating Plin2(Δ5) mice. Mixed background Plin2(Δ5) mice were backcrossed to C57BL/6 mice for 15 generations to generate congenic C57Bl/6-Plin2(Δ5) mice. WT and Plin2(Δ5) were genotyped by PCR using the following mixture of primer sequences that target exon 5 and adjacent intronic regions of the mouse Plin2 locus: 5'- AGC AAC CTG ATG GAG ACA CTC AG -3'(Forward); 5'- CAC TGT TCA TGA ACT GCA CCA TC -3'(Reverse 1); 5'- CCG GA GCA GAG CTT GGT AGA -3'(Reverse 2).

Animal Procedures

All procedures involving animals were approved by the Institutional Animal Care and Use Committee of the University of Colorado, Anschutz Medical Campus and were performed in accordance with published National Institutes of Health Guidelines. Twelve-week-old mice were fasted for 8, or 24 hours, with access to water ad libitum, and refed with LF (10.0% fat-derived calories, 24.0% protein-derived calories and 60% carbohydrate-derived calories) or HF (60.3% fat-derived calories, 18.4% protein-derived calories and 21.3% carbohydrate-derived calories) diets for 18 hours. Livers were removed from refed animals euthanized by carbon dioxide, and weighed. A portion of each liver was removed and used for CLD isolation; portions of the remainder were fixed

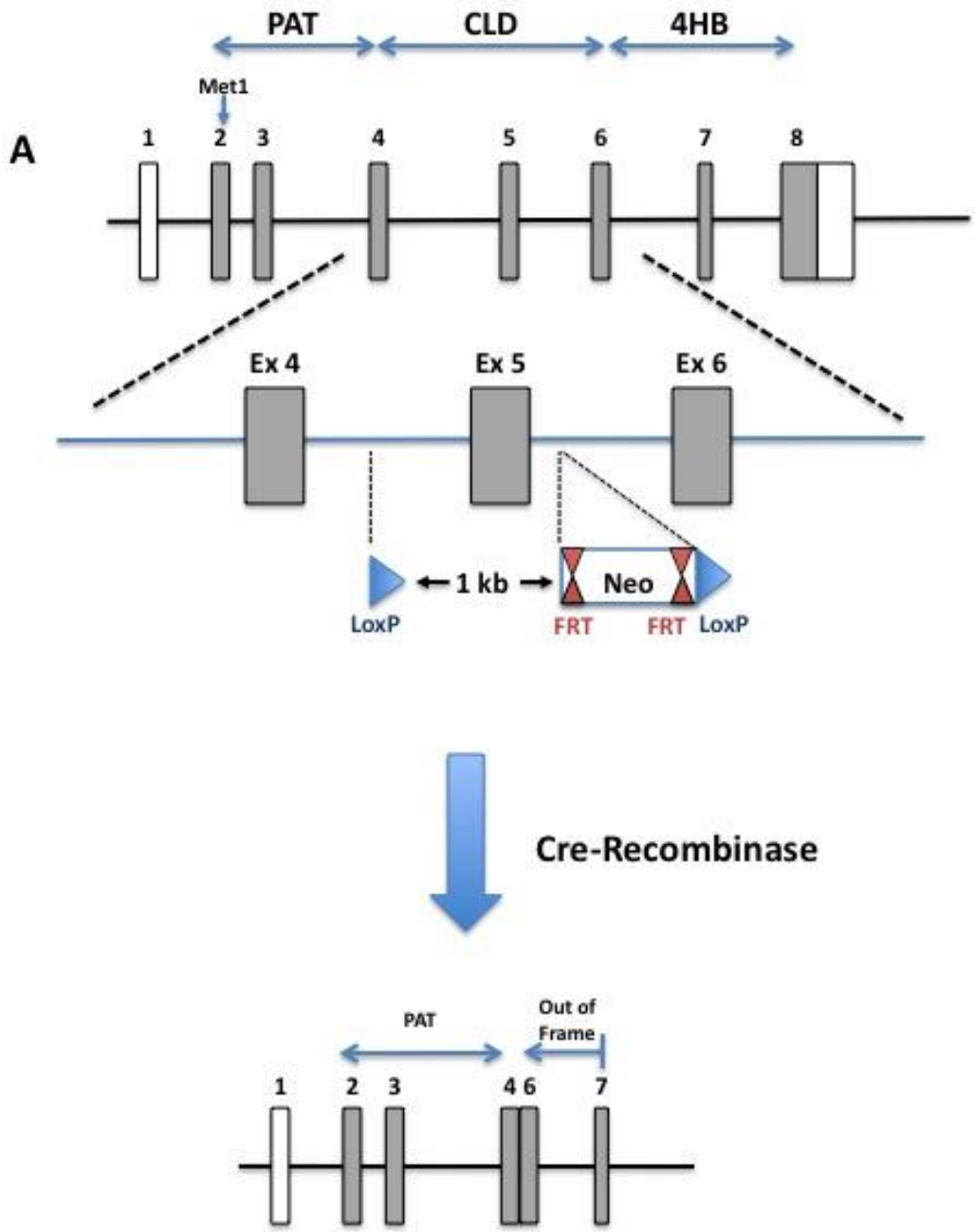

Figure II.1 Schematic Diagram Representing the Process Used to Make the D5KO Mouse

in 4% paraformaldehyde and processed for paraffin imbedding [59] or flash frozen in liquid nitrogen for RNA and protein analyses.

Metabolic Monitoring

Three separate cohorts of mice were placed in a metabolic monitoring system that provided measurements of energy balance (intake and expenditure), the respiratory exchange ratio (RER), and activity levels (Columbus 8M Oxymax) [60]. Mice were individually housed in metabolic chambers and allowed to acclimate for one week prior to fasting and re-feeding.

CLD and Organelle Isolation

CLD were isolated as described previously [61] with minor modifications. Briefly, freshly dissected livers were homogenized on ice with an equal volume of ice cold homogenization medium (37.5 mM TRIS-malate, pH 6.4; 0.5 M sucrose; and 5mM $MgCl_2$ pH 6.4) plus protease inhibitors (Aprotinin, Leupeptin, Peptstatin, AEBSF, PIC1, PIC2) per gram of tissue, using 10 strokes in a dounce homogenizer. Samples were divided into 4 equally loaded 1.5 ml centrifuge tubes and overlaid with PBS (1/2 volume of PBS/weight of liver) and centrifuged for 15 minutes at 5000 X g at 4^oC. The postnuclear supernatant (PNS) layer and debris was removed with a glass pasture pipette. Floating fractions containing CLD was combined and washed 3 times at 4^oC by successively resuspending them 300 ul of cold PBS and centrifuging for 10 minutes at 8500 X g. For proteomics analysis, the CLD sample was diluted in 100 ul of 10 mM Tris pH 7.4. For western blot analysi,s the samples were diluted in 100 ul of 5% SDS in 10mM Tris pH 7.4 plus protease inhibitors and stored at -80^oc. Organelles were isolated by sucrose density gradient centrifugation according to Croze and Morre [62].

RNA Extraction and Transcript Quantitation

Total RNA was extracted from frozen tissue using Trizol (Life Technologies) according to the manufacturer's instructions. The purity, concentration, and integrity of total RNA from each sample were verified using a NanoDrop spectrophotometer (NanoDrop Technologies, Wilmington, DE). Transcript copy numbers were determined by quantitative real-time (QRT)-PCR analysis using a multiplexing strategy to provide an internal standard for normalization (18s ribosomal). QRT-PCR assays were performed in the Quantitative Genomics Core Laboratory at the University of Texas Health Sciences Center, using previously validated primers and probes (Table II.1). All QRT-PCR assays used were validated at the Quantitative Genomics Core Laboratory to ensure that they passed the minimum requirements for efficiency, sensitivity, and selectivity. At least three tissue replicates were analyzed at least twice with similar results.

Protein Extraction and Quantitation

Protein concentrations in extracts and isolated fractions were measured using Bio-Rad Protein Assay (Hercules, CA). CLD-associated proteins were extracted in 5% SDS and stored at -80^{o}C prior to analysis by SDS-PAGE and immunoblotting. Proteins were separated on 10% polyacrylamide gels and stained with Coomassie blue or transferred to nitrocellulose membranes for immunoblot analysis, using the following primary antibodies and dilutions. Guinea pig anti-Plin2 (1:1,000); rabbit anti-PDI (1:500); rabbit anti-GRP78 (1:1000); rabbit anti-BHMT (1:500). Infrared dye-conjugated secondary antibodies (Li-COR, Lincoln, Nebraska) were used according to the manufacturer's specifications. Antibody staining intensity was quantified using an Odyssey CLX system (Li-COR, Lincoln, Nebraska).

Table II.1 QPCR Primers

mPerilipin1

Assay crosses the Exon 5/6 boundary

582(+)	CGAGAAGGTGGTAGAGTTCC
660(-)	AGCCTTCTGGGTCCTCTG
604(+)	CTGCCACCAGACAAGGAGTCAGCC

mPerilipin2

Assay crosses the Exon 4/5 boundary

436(+)	CAGCCAACGTCCGAGATTG
495(-)	CACATCCTTCGCCCCAGTT
456(+)	CACATCCTTCGCCCCAGTT

mPerilipin2#2

Assay crosses the Exon 1/2 boundary

77(+)	GACCGTGCGGACTTGCTC
146(-)	GCCATTTTTTCCTCCTGGAGA
96(+)	TCCCTCAGCTCTCCTGTTAGGCGTCTC

mPerilipin2#3

Assay is within exon 8

1553(+)	AGCTCAGTTATGGTCTTG
1639(-)	TCCTCACAAGACTAACAC
1611(-)	CCAGCCAGGTAAGAGAACTCC

mPerilipin3

Assay is within exon 5

423(+)	GGTTTTGGCGGATACTAA
490(-)	AGCTAGATACCATTTCTTGAG
467(-)	CCAGACACTGTAGATGACACCA

mPerilipin4

Assay crosses the exon 4/5 boundary

304(+)	CCCCTCATCTAAAGTGTC
382(-)	AGCTGTCTGTTCAGAAG
323(+)	ACCAACTCACAGATGGCAGG

mPerilipin5

Assay is within exon 7

742(+)	GCAACAGGGCTACTTTG
806(-)	GTTCATAGGCGAGATGG
770(+)	TCCCTATCGGCACGCCTC

m18s rRNA

1335(+)	CGGCTTAATTTGACTCAACAC
1401(-)	ATCAATCTGTCAATCCTGTCC
1359(+)	AAACCTCACCCGGCCCG

In Solution Digest and LC-MS/MS

Proteins from the isolated CLD was precipitated using methanol:chloroform (1:2). After the protein pellet was dissolved in 2 ul of 1% Protease Max Surfactant in 50mM ammonia bicarbonate (ABC) (Promega, Madison, WI), 83.5 ul of ABC was added to the sample followed by DTT to a final concentration of 5mM. The sample was incubated for 20 minutes at 56^{o}C and then cooled to RT. Iodoacetamide was added to a final concentration of 15 mM and incubated at RT in the dark for 15 minutes to block the sulfhydryl groups. A second addition of 1ul of 1% Protease Max Surfactant was added to the sample followed by 1ug of Trypsin (Promega, Madison, WI). The sample was digested overnight at 37^{o}C. The condensate was collected by centrifugation at 12,000 x g for 10 seconds. The reaction was quenched by the addition of trifluroacetic acid (TFA) to a final concentration of 0.5% and incubated for 5 minutes at RT. The peptide fragments were purified and concentrated using a 10 ul μ-c18 ZipTip (Millipore, CA) according to the manufactures directions. The peptides were eluted in 60%acetonitrile(ACN)/0.1% formic acid (FA).

LTQ XL

HPLC-MS/MS was performed by the University of Colorado, Anschutz Medical Campus Mass Spectrometry/Proteomics Core Facility. Samples were analyzed by microcapillary HPLC tandem mass spectrometry (μLC-MS/MS) using an LTQ XL mass spectrometer (Thermo, San Jose, CA). Samples (2.5 μL) were injected onto a reverse-phase column via a cooled (12°C) autosampler (Eksigent, Dublin, CA) connected to an HPLC system (Agilent 1100, Agilent Technologies, Santa Clara CA) that was set at 70 μL/min before the split and ~350 nL/min after the split. HPLC buffers used were Buffer

A: 94.9% water, 5% acetonitrile, and 0.1% formic acid and Buffer B: 94.9% acetonitrile, 5% water, and 0.1% formic acid. A 90-minute HPLC gradient was used to separate peptides. The gradient changed from 5% to 28% acetonitrile over 60 minutes followed by organic and aqueous washes on a 15 cm microcapillary HPLC column with a pulled 5 μm nanospray tip for nano-electrospray ionization. The column was packed in-house with reverse-phase stationary phase Synergi 4u, 100 Å C_{18} (Phenomenex, Torrance, CA). The column was heated to 60 °C using a column heater constructed in-house.

LTQ Orbitrap

Samples were measured on an LTQ Orbitrap Velos mass spectrometer (Thermo Fisher Scientific) coupled to an Eksigent nanoLC-2D system through a nanoelectrospray LC−MS interface. Peptide desalting and separation was achieved using 8 μl of sample was injected into a 10 μL loop using the autosampler. To desalt the sample, material was flushed out of the loop and loaded onto a trapping column (ZORBAX 300SB-C18, dimensions 5x0.3 mm 5 μm) and washed with 5% ACN, 0.1% formic acid at a flow rate of 1 μL/min for 10 minutes. At this time the trapping column was put online with the nano-pump at a flow rate of 350 nL/min. The mobile phase included water with 0.1% formic acid (solvent A) and 99.9 % acetonitrile with 0.1% formic acid (solvent B). A 90 minute gradient from 6% ACN to 40% ACN was used to separate the peptides. Peptides were separated on a house-made 100 μm i.d. × 150 mm fused silica capillary packed with Jupiter C_{18} resin (Phenomex; Torrance, CA). Data acquisition was performed using the instrument supplied Xcalibur (version 2.0.6) software. The mass spectrometer was operated in the positive ion mode; the peptide ion masses were measured in the Orbitrap mass analyzer, whereas the peptide fragmentation was performed by collision-induced

dissociation (CID) in the linear ion trap analyzer using default settings. Twenty most intense ions were selected for fragmentation in each scan cycle; fragmented masses were excluded from further sequencing for 90s.

Data Acquisition

Mass spectrometry data acquisition was performed in data-dependent mode on the Xcalibur instrument software (v. 2.0.6, Thermo, San Jose, CA) with a single MS1 scan (30 ms) followed by up to three data dependent collision induced dissociation scans (MS/MS, 30 ms each). Data were converted from the Thermo *.raw data file format to the *.mgf format using an in-house script. After conversion, data were searched against the mouse Swissprot database (downloaded 12/14/2011) using Mascot® (v. 2.2.07, Matrix Science Ltd., Boston, MA). For searches, mass tolerances were set at ±0.60 Da for both MS peaks and MS/MS fragment ions. Trypsin enzyme specificity was applied allowing one missed cleavage in the database searches. Modifications searched included fixed carbamidomethyl modification of cysteine and the variable oxidation modifications of methionine, protein N-terminal acetylation, peptide N-terminal pyro-glutamic acid formation. Results from the Mascot searches were analyzed and sorted using Scaffold® (v. 3.00, Proteome Software, Portland, OR).

Immunohistochemistry and Fluorescence Imaging

Paraffin sections were processed for immunohistochemistry as described previously [63]. Immunoreactivity was visualized using secondary antibodies conjugated with Alexafluor 488 or Alexafluor 594 at dilutions of 1:500 and 1:250 respectively. Nuclei were stained with DAPI (Sigma Chemical Company, St Louis, MO). Immunofluorescence images were captured on a Nikon Diaphot fluorescence

microscope. For CARS microscopy and BODIPY staining, livers from refed animals were perfused with paraformaldehyde, sectioned at 10 um, collected onto Cell-Tak coated coverslips, and vapor-fixed with paraformaldehyde for 20 min before being gently rehydrated with PBS. Auto-fluorescence was quenched with 2 mg/ml glycine for 10 min. Sections were rinsed with PBS and stained with BODIPY 493/503 at a final concentration of 30 ug/ml, and DAPI at 5 ug/ml. Coverslips were mounted in PBS and imaged within 3 days. Confocal imaging of BODIPY 493/503 and DAPI was performed on a 3i Marianas Inverted Spinning Disk Confocal system. All image analyses and rendering were performed using SlideBook Software (Intelligent Imaging Innovations, Inc., Denver, CO). Coherent anti-Stokes Raman scattering (CARS) images of lipid droplets in tissue sections were acquired with a custom-built multiphoton microscopy platform optimized for CARS as previously described [64]. All images were processed by Photoshop (Adobe Systems Inc., Mountain View, CA).

Immunoelectron Microscopy

Cells were processed for immunoelectron microscopy using a modified Tokuyasu method [65] as described previously [66]. Briefly, pelleted cells were fixed overnight at 4°C in PBS buffered 4% paraformaldehyde containing 5% sucrose and 100 mM HEPES, and infiltrated with PBS containing 2.1 M sucrose over ~10 hours, with repeated solution changes. Fixed cells were transferred to an aluminum cryosectioning stub (Ted Pella, Inc., Redding, CA) and immediately frozen in liquid nitrogen. Semi-thin (90 nm) cryosections were cut at -110°C with an UltraCut UCT/FCS cryomicrotome (Leica), using a diamond knife (Diatome US) and transferred to a Formvar-coated, carbon-coated, glow-discharged 100-mesh copper-rhodium EM grid. Following blocking of non-

specific antibody binding sites with 10% calf serum in PBS, the sections were labeled by sequential incubation with rabbit antibodies to the N-terminal domain of Plin2 [39] and colloidal gold conjugated secondary antibodies (Ted Pella Inc., Redding, CA) and then negatively stained and embedded with 1% uranyl acetate, 1% methylcellulose in distilled water. Samples were viewed in a Tecnai TF20 electron microscope (FEI) operating at 200 KeV and images collected digitally.

Statistical Analysis

Calculations were performed by using Prism 5.0 (GraphPad Software) and Microsoft Excel (Windows 2010, Microsoft). For each variable, 2 to 6 independent experiments were carried out. Differences between diet groups were tested for significance using an unpaired Student *t* test. Differences were considered significant at $P \leq 0.05$.

Bioinformatic Analysis

STRING 9.0 (http://string.embl.de/), Gene ontology database (http://geneontology.org/), and KEGG (http://www.genome.jp/kegg) were used for protein interaction, biological function, and pathway analysis respectively.

CHAPTER III

DYNAMIC REGULATION OF HEPATIC LIPID PROTEOME BY DIET[1]

Introduction

Abnormal intrahepatic fat accumulation (steatosis) in the form of cytoplasmic lipid droplets (CLD) is an early pathophysiological feature of altered liver metabolism that is linked to insulin resistance and potential progression to severe liver disease [67, 68]. Consequently, understanding how CLD affect hepatic metabolism, and how nutritional status influences their functions, are important elements in defining the mechanistic links between hepatic steatosis and metabolic diseases. Gene disruption studies in mice have documented that Plin2 is required for hepatic lipid accumulation in response to high fat diet (HFD) feeding [37, 38]. However, other PLIN family members have been detected on hepatic CLD in humans and mice with fatty liver disease [59, 69], which suggests the possibility that diet and/or altered metabolic properties can dynamically influence hepatic CLD protein composition.

Protein compositions of CLD has been characterized to varying degrees from multiple sources including; yeast (Saccharomyces cerevisiae)[70, 71], Drosophila [72, 73], mouse mammary epithelial cells [61], Chinese hamster ovary K2 cell lines [74, 75], 3T3-L1 adipocytes [76, 77], cultured human A431 epithelial cells [78], HuH7 human hepatoma cell line [79], cultured human hepatocyte HepG2 cell lines [42], liver tissue from Sprague-Dawley rats [80], human lymphoblast U937 cells from lung tissue [81], and mouse skeletal muscle [82]. However, information about the protein composition of

---

[1] Chapter III was taken in its entirety from: Crunk, A.E., et al., *Dynamic Regulaiton of Hepatic Lipid Droplet Properties by Diet.* PLoS One, 2013. **8**(7): p. e67631

hepatic CLD remains relatively limited, and the effects of diet and/or metabolic alterations on CLD protein properties are not known in detail for any tissue.

The highly dynamic and adaptive nature of the liver metabolism is sensitive to nutrient status [83]. In rodents, fasting and re-feeding is associated with alterations in hepatic glucose and lipid metabolism that are reflected in increased expression of lipid metabolizing genes and the accumulation of intrahepatic lipids [84, 85]. The nature of these responses is influenced by the amount of and types of dietary fat [86]. In the work presented here, I use a fasting and re-feeding model to test the hypothesis that the hepatic CLD proteome is influenced by dietary fat composition. My data show that low fat (LF) and high fat (HF) diets differentially affect the types and quantities of CLD associated protein compositions, and these differences are associated with differences in hepatic metabolism and CLD properties. Taken together, these findings indicate the hepatic CLD proteome is dynamically regulated by the nutrient and metabolic status of the liver and provide evidence that CLD may function as a platform for regulating hepatic metabolic activity.

Results

Diet Effects on Metabolism and Hepatic Lipid Storage

Fasting and diet composition are known to influence food intake and liver metabolism, which in turn can affect hepatic lipid storage [87, 88]. Therefore, to define the effects of LF and HF diets on hepatic CLD properties, it was necessary first to establish the effects of these diets on energy intake and metabolism of fasted animals. Figure III.1A shows that energy consumption of fasted animals that were refed the HF diet was significantly greater than that of animals refed the LF diet. I also found

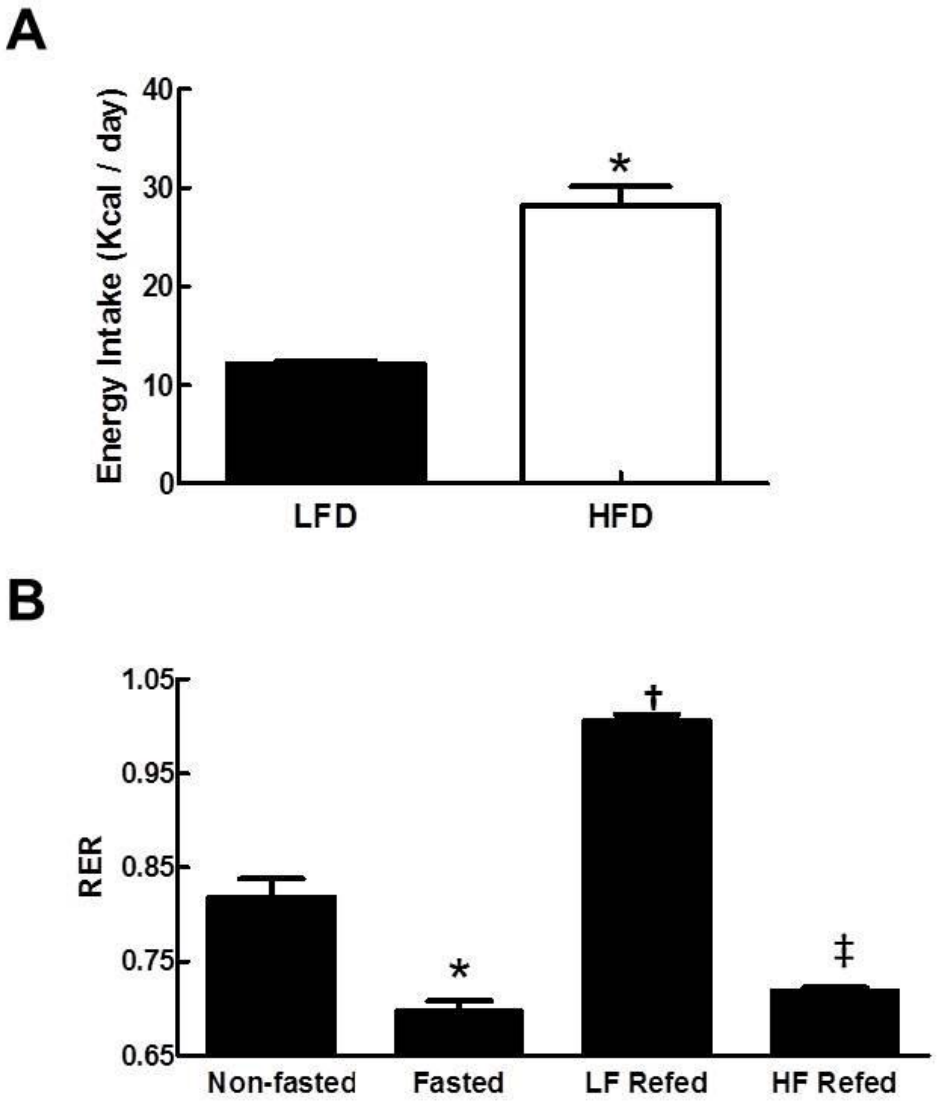

Figure III.1 Diet Effects on Metabolism

(A) Effects of LF- and HF-re-feeding on energy intake in fasted male mice. Values are means (± SD) for 4 animals in each group. Asterisk indicates HFD values differ from LFD values ($p<0.01$). (B) Energy usage in non-fasted, fasted and LF- and HF-refed male mice as determined by RER. Non-fasted and fasted values correspond to averages (± SD) of 8 animals obtained prior to re-feeding. LF- and HF-re-feeding values correspond to averages (± SD) for 4 animals in each group. Asterisk indicates values differ from non-fasted controls ($p<0.001$); dagger indicates values differ from non-fasted and fasted values ($p<0.001$); double dagger indicates values differ from LF refed and non-fasted values ($p<0.001$).

differences in the fuel utilization properties of LF- and HF-refed animals. Figure III.1B shows the respiratory exchange ratio (RER) values of mice prior to fasting, following a 24-hour period of fast, and after re-feeding with LF- or HF-diets. Prior to fasting, RER values were approximately 0.8, as fuel use reflected the broad mixture of carbohydrate, fat, and protein in the diet. During fasting, RER values dropped to approximately 0.7, indicating a switch to fat as the primary source of energy. Re-feeding on a LF diet resulted in RER values that were close to 1, which reflects the preferential use of carbohydrate for energy production and the likelihood that *de novo* lipogenesis was induced [60]. In contrast, mice refed the HF diet had RER values that remained closer to 0.7, which indicated they were oxidizing fat for energy, like fasted animals.

The distribution and properties of CLD in liver sections of LF- and HF-refed mice were visualized by coherent anti-Stokes Raman scattering (CARS) microscopy [89], and by confocal laser microscopy after staining neutral lipids with BODIPY (493/503) (Figure III.2A). CLD were detected throughout the liver in both LF- and HF-refed animals, although both CARS and BODIPY intensities appeared to be greater in the central vein region (zone 3). Consistent with the elevated fat content of HF diets, I found that CARS and BODIPY intensities of livers of HF-refed animals were greater than those of LF-refed mice. CLD properties were further defined by 3D laser confocal microscopy of BODIPY stained liver sections. Representative 3D projection images of CLD from central vein regions of hepatocytes of LF- and HF-refed mice (Figure III.2B), indicate that CLD are larger, and appear to be more numerous, in animals refed the HF diet relative to those refed the LF diet. Diet Effects on Hepatic CLD Protein Composition to determine if LF- and HF-CLD differed in their protein compositions, CLD were isolated

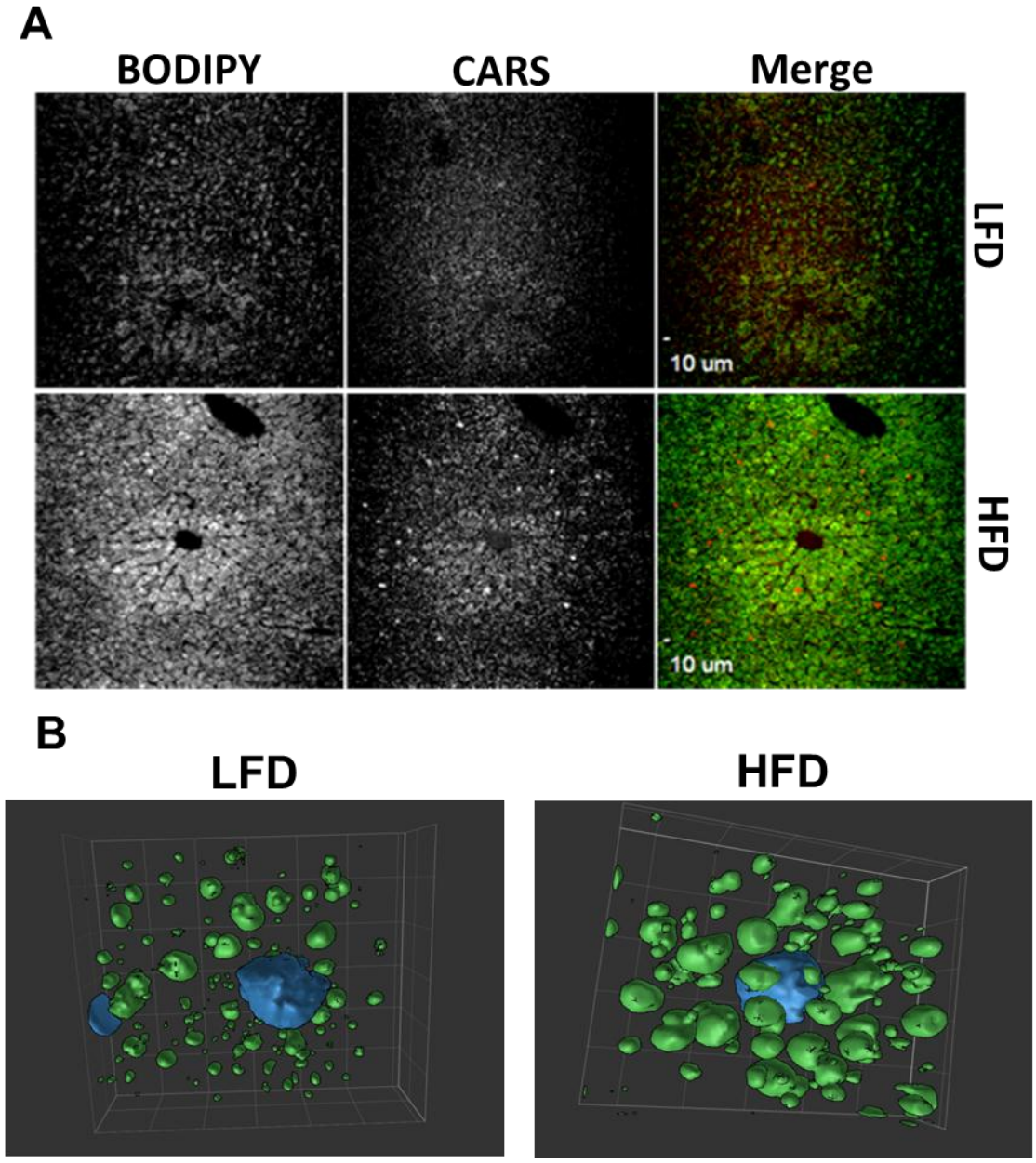

Figure III.2 Diet Effects on Hepatic Lipid Storage
(A) Representative images of frozen liver sections from LF- and HF-refed male stained with BODIPY and imaged by laser confocal (BODIPY) and CARS microscopy (200X magnification). Asterisks indicate central veins. (B) Representative surface-view of 3D projection images of single cells within liver sections from LF (LFD)- and HF (HFD) -refed mice obtained at 600X magnification. Nuclei are shown in blue.

from liver extracts by multiple rounds of floatation through sucrose. This method was previously documented showing that CLD isolated by this procedure are free of membrane structures and other organelles [61]. Figure III.3A shows that the CLD fraction is enriched in specific protein bands that differ significantly from those present in the starting homogenate. In order to demonstrate the enrichment of CLD, I probed the homogenate, post nuclear supernatant (PNS), initial CLD, final wash and final CLD with antibodies to ER (GRP78), CLD (Plin2), peroxisome (PEX3), and mitochondria(VDAC) proteins. Figure III.3B shows that Plin2 was detected in the final CLD fraction, the final wash supernatant, and the initial CLD fraction, but not in the homogenate or PNS. I did not detect VDAC or PEX3, in the CLD-enriched fraction despite the presence of both these markers in the homogenate, PNS and initial CLD. I detected GRP78 in all of the fractions, with the highest intensity in the initial CLD fraction, and the lowest in the final CLD enriched fraction. The presences of GRP78 on the final enriched CLD fraction, yet in much lower abundance than in the initial CLD fraction, is consistent with the idea that GRP78 is closely associated to the CLD, and has been reported for CLD from other cell types [71, 90]. The presence of GRP78 on highly enriched CLD fraction is consistent with evidence that CLD originate at the ER [21] and can be found in close contact withER membranes [91]. Furthermore, the presence of GRP78 in the final wash fraction at a staining intensity that is similar to that of the final enriched-CLD fraction, suggests that GRP78 undergoes relatively slow dissociation from CLD during wash and that further washing would continue to remove only small fractions of the protein from the CLD. These results are consistent with GRP78 having moderate affinity for CLD and provide evidence that mechanisms exist that selectively control CLD-protein interactions.

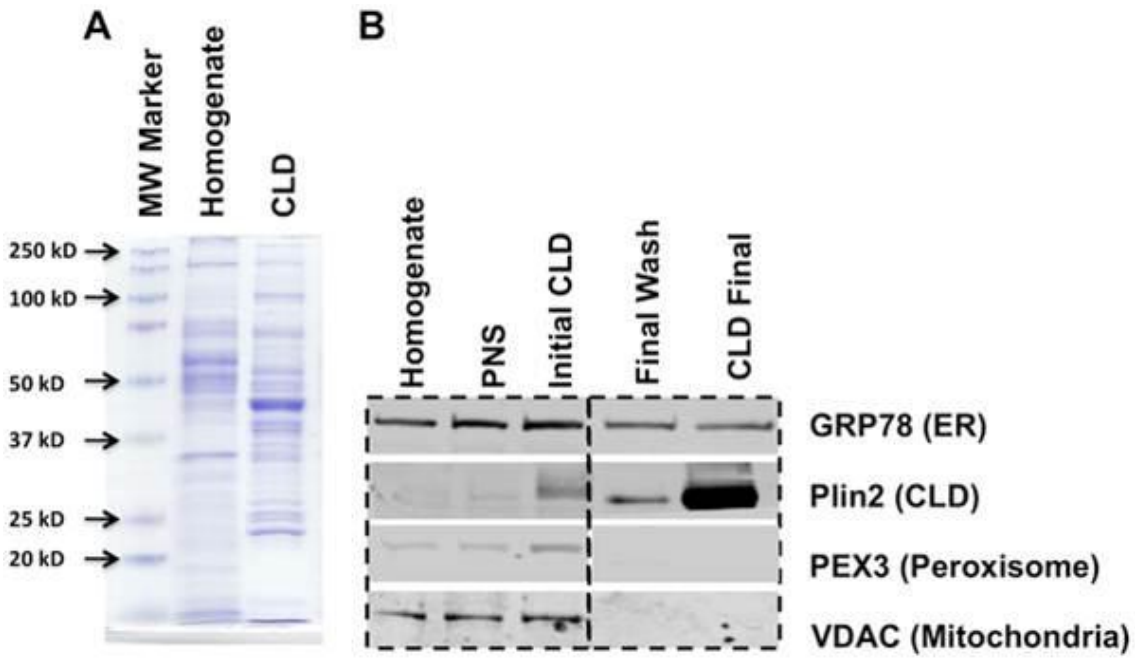

Figure III.3 Unique Protein Patterns of Isolated Hepatic CLD
A) Coomassie blue staining profiles of proteins in liver homogenates and isolated CLD. B) Immunoblot analyses of equal amounts (25μg) of protein from liver homogenate, PNS, initial CLD, final CLD wash, and final enriched CLD fractions reacted with antibodies to GRP78, Plin2, PEX3, and VDAC.

These results are consistent with GRP78 having moderate affinity for CLD and provide evidence that mechanisms exist that selectively control CLD - protein interactions.

Liver Specific- and Common-CLD Proteins

I used LC-MS/MS analysis of trypsin digests of CLD protein extracts as a non-biased "shotgun" approach for identifying the proteomes of LF- and HF-CLD. Only those proteins with two or more unique peptides, and that were found in repeat analyses of isolated CLD from duplicate fasting-re-feeding experiments, were accepted as valid identifications. Overall, I identified 125 proteins on CLD from mice refed the LF diet, and 134 proteins on CLD from mice refed the HF diet. The identified proteins, their

biological functions according to Uniprot and gene ontology (GO) database descriptions, and their relative abundance averages are shown in the Table III.1

Of the proteins found on either LF- or HF-CLD, 54 (36%) were identified previously on CLD from other mammalian sources (Table III.2) and appear to represent a common CLD proteome; whereas 98 proteins (64%) were not previously detected on CLD, and thus potentially represent liver specific CLD associated proteins (Table III.3). The functional categories of the common- and liver-specific CLD proteins are shown in Table III.2. Proteins involved in lipid metabolism (22%), redox/detoxification (17%) and chaperone functions (15%) accounted for over half of the common-CLD proteins, whereas enzymes of amino acid (27%) and carbohydrate metabolism (16%), and redox/detoxification (15%) pathways made up the majority of the liver-specific CLD proteins. I next used the STRING 9.0 program to examine the extent to which the identified proteins exhibited possible functional connections. As shown in Figure III.4B, liver-specific CLD proteins are organized into a series of discrete, interacting nodes, suggesting the existence of multiple functional linkages between nodes, and between proteins within a given node. Common-CLD proteins on the other hand appear to be less functionally related. I found that common-CLD proteins comprised only two non-interacting nodes; one related to protein processing, and another related to glycolysis.

I used the KEGG pathway database to define potential functional interactions among common- and liver-specific CLD proteins (Table III.4). I identified significant enrichment of common-CLD proteins in nine KEGG pathways using a false discovery rate (FDR) value of $p<0.05$. The majority of the pathways are related to carbohydrate (4)

Table III.1 Effects of High- and Low - Fat Re-feeding Diets on the Hepatic CLD Proteome

	Gene	Uniprot ID	**LFD**	**HFD**	Source
Amino Acid Metabolism (GO:0006520)					
Carbonic anhydrase 3	Ca3	P16015	0.121%	0.080%	[80]
Carbamoyl-phosphate synthase [ammonia], mitochondrial	Cps1	Q8C196	0.015%		[79, 80]
Betaine--homocysteine S-methyltransferase 1	Bhmt	O35490	0.140%	0.144%	
Aspartate aminotransferase, cytoplasmic	Got1	P05201	0.094%	0.094%	
Aspartate aminotransferase, mitochondrial	Got2	P05202	0.196%	0.220%	
Glutamine synthetase	Glul	P15105	0.347%	0.250%	
Phenylalanine-4-hydroxylase	Pah	P16331	0.130%	0.092%	
Argininosuccinate synthase	Ass1	P16460	0.041%	0.140%	
Histidine ammonia-lyase	Hal	P35492	0.054%	0.055%	
Fumarylacetoacetase	Fah	P35505	0.009%		
4-hydroxyphenylpyruvate dioxygenase	Hpd	P49429	0.085%	0.067%	
Arginase-1	Arg1	Q61176	0.048%	0.043%	
Sepiapterin reductase	Spr	Q64105	0.060%	0.042%	
Alanine aminotransferase 1	Gpt	Q8QZR5	0.121%	0.087%	
Urocanate hydratase	Uroc1	Q8VC12	0.049%	0.044%	
Cystathionine gamma-lyase	Cth	Q8VCN5	0.005%		
S-adenosylmethionine synthase isoform type-1	Mat1a	Q91X83		0.009%	
Formimidoyltransferase-cyclodeaminase	Ftcd	Q91XD4	0.012%	0.004%	
Argininosuccinate lyase	Asl	Q91YI0	0.003%		
C-1-tetrahydrofolate synthase, cytoplasmic	Mthfd1	Q922D8	0.021%		
Cytosol aminopeptidase	Lap3	Q9CPY7	0.039%	0.042%	
Dihydropyrimidinase	Dpys	Q9EQF5	0.009%	0.019%	
4-trimethylaminobutyraldehyde dehydrogenase	Aldh9a1	Q9JLJ2	0.099%	0.106%	
Glycine N-methyltransferase	Gnmt	Q9QXF8		0.007%	

Table III.1 Effects of High- and Low - Fat Re-feeding Diets on the Hepatic CLD Proteome

Maleylacetoacetate isomerase	Gstz1	Q9WVL0	0.028%	0.049%	
L-serine dehydratase/L-threonine deaminase	Sds	Q8VBT2		0.009%	
Adenosylhomocysteinase	Ahcy	P50247	0.006%	0.004%	
Homogentisate 1,2-dioxygenase	Hgd	O09173	0.041%	0.028%	
Protein Metabolism (GO:0044267)					
(Chaperones)					
Endoplasmin	Hsp90b1	P08113	0.072%	0.041%	[42, 61, 78, 80-82, 92, 93]
Heat shock protein HSP 90-beta	Hsp90ab1	P11499		0.009%	[75, 78, 82, 92, 93]
78 kDa glucose-regulated protein	Hspa5	P20029	0.022%	0.108%	[42, 74-78, 80, 81, 92, 93]
Heat shock cognate 71 kDa protein	Hspa8	P63017	0.093%	0.072%	[78, 80, 82, 92, 93]
Protein disulfide-isomerase	P4hb	P09103	0.019%	0.030%	[74, 75, 78, 80, 81, 92, 93]
Protein disulfide-isomerase A3	Pdia3	P27773	0.018%		[42, 75, 80, 92, 93]
Protein disulfide-isomerase A6	Pdia6	Q922R8	0.013%	0.003%	[42, 74, 75, 80, 82, 92, 93]
Peptidyl-prolyl cis-trans isomerase A	Ppia	P17742		0.037%	[74, 75]
Phenazine biosynthesis-like domain-containing protein 1	Pbld1	Q9DCG6	0.075%	0.048%	
Carbohydrate Meatbolism (GO:0005975)					
Isocitrate dehydrogenase [NADP] cytoplasmic	Idh1	O88844	0.016%	0.018%	
Fructose-bisphosphate aldolase B	Aldob	Q91Y97	0.250%	0.193%	[93]
Alpha-enolase	Eno1	P17182	0.007%		[80, 93]
Malate dehydrogenase, cytoplasmic	Mdh1	P14152	0.081%	0.056%	[79, 80]

Table III.1 Effects of High- and Low - Fat Re-feeding Diets on the Hepatic CLD Proteome

Phosphoglycerate kinase 1	Pgk1	P09411	0.034%	0.062%	[93]
Triosephosphate isomerase	Tpi1	P17751	0.130%	0.142%	[92]
Pancreatic alpha-amylase	Amy2	P00688	0.003%	0.022%	
L-lactate dehydrogenase A chain	Ldha	P06151	0.051%	0.042%	
Cytoplasmic aconitate hydratase	Aco1	P28271	0.009%		
Transketolase	Tkt	P40142	0.020%	0.033%	
Pyruvate kinase isozymes R/L	Pklr	P53657	0.032%	0.020%	
Ketohexokinase	Khk	P97328	0.004%		
Sorbitol dehydrogenase	Sord	Q64442	0.011%	0.041%	
Bifunctional ATP-dependent dihydroxyacetone kinase/FAD-AMP lyase (cyclizing)	Dak	Q8VC30		0.010%	
UTP--glucose-1-phosphate uridylyltransferase	Ugp2	Q91ZJ5	0.028%	0.009%	
Phosphoglucomutase-1	Pgm1	Q9D0F9	0.034%	0.012%	
1,4-alpha-glucan-branching enzyme	Gbe1	Q9D6Y9	0.082%	0.098%	
Phosphoglycerate mutase 1	Pgam1	Q9DBJ1	0.014%	0.009%	
Glycogen phosphorylase, liver form	Pygl	Q9ET01	0.026%	0.032%	
Fructose-1,6-bisphosphatase 1	Fbp1	Q9QXD6	0.022%		
Glutathione Metabolism (GO:0006749)					
Glutathione S-transferase P 1	Gstp1	P19157	0.009%		[92]
Glutathione peroxidase 1	Gpx1	P11352	0.048%	0.043%	
Glutathione S-transferase A3	Gsta3	P30115	0.085%	0.059%	
Lactoylglutathione lyase	Glo1	Q9CPU0	0.120%	0.109%	
Glutathione S-transferase Mu 1	Gstm1	P10649	0.138%	0.156%	
Lipid Metabolism (GO:0006629)					
Peroxiredoxin-6	Prdx6	O08709		0.005%	

Table III.1 Effects of High- and Low - Fat Re-feeding Diets on the Hepatic CLD Proteome

CGI58	Abhd5	Q9DBL9		0.008%	[61, 74-78, 81, 92, 93]
3-ketoacyl-CoA thiolase A, peroxisomal	Acaa1a	Q921H8	0.026%	0.048%	[93]
Acetyl-CoA acetyltransferase, cytosolic	Acat2	Q8CAY6	0.004%	0.006%	[93]
Long-chain-fatty-acid--CoA ligase 1	Acsl1	P41216		0.006%	[61, 74, 80, 81]
Estradiol 17 beta-dehydrogenase 5	Akr1c6	P70694	0.005%	0.011%	[82]
ATP synthase subunit alpha, mitochondrial	Atp5a1	Q03265	0.015%		[80]
ATP synthase subunit beta, mitochondrial	Atp5b	P56480	0.016%	0.029%	[80, 93]
Carboxylesterase 3	Ces1d	Q8VCT4	0.022%	0.045%	[80]
Cytochrome b5	Cyb5a	P56395	0.055%	0.035%	[80, 93]
NADH-cytochrome b5 reductase 3	Cyb5r3	Q9DCN2		0.023%	[42, 74, 75, 77-79, 81, 92, 93]
Fatty acid synthase	Fasn	P19096	0.003%	0.024%	[92, 93]
Monoglyceride lipase	Mgll	O35678	0.032%	0.059%	[79-81, 93]
Epoxide hydrolase 2	Ephx2	P34914	0.007%	0.022%	
Very long-chain specific acyl-CoA dehydrogenase	Acadvl	P50544	0.018%	0.080%	
Hydroxymethylglutaryl-CoA synthase	Hmgcs2	P54869	0.010%	0.011%	
ATP-binding cassette sub-family D member 3	Abcd3	P55096	0.028%	0.056%	
Cytochrome P450 2E1	Cyp2e1	Q05421	0.057%	0.046%	
3-ketoacyl-CoA thiolase B, peroxisomal	Acaa1b	Q8VCH0	0.143%	0.041%	
ATP-citrate synthase	Acly	Q91V92		0.018%	
Inorganic pyrophosphatase	Ppa1	Q9D819		0.018%	
Peroxisomal bifunctional enzyme	Ehhadh	Q9DBM2	0.015%	0.034%	
Estradiol 17-beta-dehydrogenase 11	Hsd17b11	Q9EQ06		0.011%	
Peroxisomal acyl-coenzyme A oxidase 1	Acox1	Q9R0H0	0.003%	0.009%	

Table III.1 Effects of High- and Low - Fat Re-feeding Diets on the Hepatic CLD Proteome

Phosphoenolpyruvate carboxykinase, cytosolic [GTP]	Pck1	Q9Z2V4	0.070%	0.062%	
Lipid Transport (GO:0006869)					
Apolipoprotein E	Apoe	P08226		0.023%	[80, 81, 93]
Apolipoprotein A-I	Apoa1	Q00623	0.007%	0.025%	[80, 81]
Perilipin-2	Plin2	P43883	0.132%	0.133%	[93]
Non-specific lipid-transfer protein	Scp2	P32020	0.077%	0.297%	[42, 82, 93]
Fatty acid-binding protein, liver	Fabp1	P12710	0.016%	0.048%	
Nucleotide Metabolism (GO:0006975)					
Nicotinate phosphoribosyltransferase	Naprt1	Q8CC86	0.072%	0.143%	
Putative L-aspartate dehydrogenase	Aspdh	Q9DCQ2	0.280%	0.170%	
3-hydroxyanthranilate 3,4-dioxygenase	Haao	Q78JT3		0.017%	
			0.060%	0.068%	
Other			0.019%	0.093%	
Actin, cytoplasmic 1	Actb	P60710	0.039%	0.047%	[75, 78, 80, 81, 92, 93]
Serum albumin	Alb	P07724	0.019%	0.054%	[61, 80, 81, 93]
Annexin A5	Anxa5	P48036	0.049%	0.045%	[80]
Clathrin heavy chain 1	Cltc	Q68FD5	0.047%	0.046%	[42, 77-82]
Elongation factor 1-alpha 1	Eef1a1	P10126	0.024%	0.018%	[75, 81, 93]
Histone H2A type 1	Hist1h2ab	P22752	0.016%	0.009%	[93]
Methyltransferase-like protein 7B	Mettl7b	Q9DD20	0.054%	0.048%	[78, 79, 93]
Myosin light polypeptide 6	Myl6	Q60605		0.006%	[93]
Protein NDRG2	Ndrg2	Q9QYG0	0.053%	0.076%	[75, 93]
Ras-related protein Rab-14	Rab14	Q91V41	0.010%	0.044%	[74, 77, 78, 82, 93]

Table III.1 Effects of High- and Low - Fat Re-feeding Diets on the Hepatic CLD Proteome

Tubulin alpha-1C chain	Tuba1c	P68373		0.009%	[75, 80, 93]
Alpha-1-antitrypsin 1	Serpina1a	P07758	0.007%	0.016%	
Serine protease inhibitor A3K	Serpina3k	P07759	0.009%		
Histone H2B type 1-F/J/L	Hist1h2bf	P10853		0.008%	
Ferritin light chain 1	Ftl1	P29391	0.107%	0.131%	
Ribonuclease UK114	Hrsp12	P52760	0.027%	0.027%	
Elongation factor 2	Eef2	P58252	0.004%		
Tubulin beta-4B chain	Tubb4b	P68372	0.020%	0.015%	
Selenide, water dikinase 2	Sephs2	P97364		0.007%	
Liver carboxylesterase 31	Ces3a	Q63880	0.003%		
Regucalcin	Rgn	Q64374	0.063%	0.060%	
Tetratricopeptide repeat protein	Ttc36	Q8VBW8	0.074%	0.062%	
Myosin-9	Myh9	Q8VDD5			
SEC14-like protein 2	Sec142	Q99J08			
Parathymosin	Ptms	Q9D0J8	0.123%	0.082%	
Interferon-inducible GTPase 1	Iigp1	Q9QZ85	0.018%	0.009%	
D-dopachrome decarboxylase	Ddt	O35215	0.110%	0.098%	
			0.200%	0.197%	
Redox/Detox (GO:0055114/ GO:0006805)				0.013%	
Aldehyde dehydrogenase, mitochondrial	Aldh2	P47738	0.055%	0.050%	[75, 93]
Catalase	Cat	P24270	0.022%	0.031%	[75, 80]
Dehydrogenase/reductase SDR family member 1	Dhrs1	Q99L04	0.041%	0.036%	[74-77, 92, 93]
Glyceraldehyde-3-phosphate dehydrogenase	Gapdh	P16858	0.003%		[92]
L-gulonolactone oxidase	Gulo	P58710		0.008%	[79]
17-beta-hydroxysteroid dehydrogenase 13	Hsd17b13	Q8VCR2		0.014%	[80]
3 beta-hydroxysteroid dehydrogenase	Hsd3b3	P26150	0.046%	0.120%	[92]

Table III.1 Effects of High- and Low - Fat Re-feeding Diets on the Hepatic CLD Proteome

Peroxiredoxin-1	Prdx1	P35700	0.110%	0.079%	[75]
Peroxiredoxin-5, mitochondrial	Prdx5	P99029		0.010%	[92]
Cytochrome P450 4A14	Cyp4a14	O35728		0.024%	
Alcohol dehydrogenase 1	Adh1	P00329	0.025%	0.137%	
NADP-dependent malic enzyme	Me1	P06801		0.025%	
Superoxide dismutase [Cu-Zn]	Sod1	P08228	0.035%	0.007%	
Cytochrome P450 2D9	Cyp2d9	P11714	0.026%	0.017%	
Cytochrome P450 2D10	Cyp2d10	P24456	0.143%	0.140%	
Retinal dehydrogenase 1	Aldh1a1	P24549	0.009%	0.007%	
Cytochrome P450 2F2	Cyp2f2	P33267	0.067%	0.008%	
Pterin-4-alpha-carbinolamine dehydratase	Pcbd1	P61458		0.006%	
UDP-glucuronosyltransferase 1-1	Ugt1a1	Q63886			
Aldehyde dehydrogenase family 8 member A1	Aldh8a1	Q8BH00			
Glyoxylate reductase/hydroxypyruvate reductase	Grhpr	Q91Z53	0.007%	0.011%	
Alcohol dehydrogenase [NADP+]	Akr1a1	Q9JII6	0.022%	0.013%	
Cytosolic 10-formyltetrahydrofolate dehydrogenase	Aldh1l1	Q8R0Y6	0.109%	0.144%	
			0.003%	0.014%	
Transport (GO:0006810)			0.016%	0.024%	
Major urinary protein 6	Mup6	P02762			
Serotransferrin	Tf	Q921I1			[61]
Transitional endoplasmic reticulum ATPase	Vcp	Q01853	0.004%	0.008%	[61, 75, 82]
Major urinary protein 20	Mup20	Q5FW60	0.052%	0.017%	
Selenium-binding protein 2	Selenbp2	Q63836	0.003%		

Table III.2 Common CLD Associated Proteins

Table III.2 Common CLD Associated Proteins

Protein Name	Gene	Uniprot ID
Amino Acid Metabolism (GO:0006520)		
Carbonic anhydrase 3	Ca3	P16015
Carbamoyl-phosphate synthase [ammonia], mitochondrial	Cps1	Q8C196
Protein Metabolism (GO:0044267)		
(Chaperones)		
Endoplasmin	Hsp90b1	P08113
Heat shock protein HSP 90-beta	Hsp90ab1	P11499
78 kDa glucose-regulated protein	Hspa5	P20029
Heat shock cognate 71 kDa protein	Hspa8	P63017
Protein disulfide-isomerase	P4hb	P09103
Protein disulfide-isomerase A3	Pdia3	P27773
Protein disulfide-isomerase A6	Pdia6	Q922R8
Peptidyl-prolyl cis-trans isomerase A	Ppia	P17742
Carbohydrate Meatbolism (GO:0005975)		
Fructose-bisphosphate aldolase B	Aldob	Q91Y97
Alpha-enolase	Eno1	P17182
Malate dehydrogenase, cytoplasmic	Mdh1	P14152
Phosphoglycerate kinase 1	Pgk1	P09411
Triosephosphate isomerase	Tpi1	P17751
Glutathione Metabolism (GO:0006749)		
Glutathione S-transferase P 1	Gstp1	P19157

Table III.2 Common CLD Associated Proteins

Lipid Metabolism (GO:0006629)		
CGI58	Abhd5	Q9DBL9
3-ketoacyl-CoA thiolase A, peroxisomal	Acaa1a	Q921H8
Acetyl-CoA acetyltransferase, cytosolic	Acat2	Q8CAY6
Long-chain-fatty-acid--CoA ligase 1	Acsl1	P41216
Estradiol 17 beta-dehydrogenase 5	Akr1c6	P70694
ATP synthase subunit alpha, mitochondrial	Atp5a1	Q03265
ATP synthase subunit beta, mitochondrial	Atp5b	P56480
Carboxylesterase 3	Ces1d	Q8VCT4
Cytochrome b5	Cyb5a	P56395
NADH-cytochrome b5 reductase 3	Cyb5r3	Q9DCN2
Fatty acid synthase	Fasn	P19096
Monoglyceride lipase	Mgll	O35678
Lipid Transport (GO:0006869)		
Apolipoprotein E	Apoe	P08226
Apolipoprotein A-I	Apoa1	Q00623
Perilipin-2	Plin2	P43883
Non-specific lipid-transfer protein	Scp2	P32020
Other		
Actin, cytoplasmic 1	Actb	P60710
Serum albumin	Alb	P07724
Annexin A5	Anxa5	P48036
Clathrin heavy chain 1	Cltc	Q68FD5
Elongation factor 1-alpha 1	Eef1a1	P10126

Table III.2 Common CLD Associated Proteins

Histone H2A type 1	Hist1h2ab	P22752
Methyltransferase-like protein 7B	Mettl7b	Q9DD20
Myosin light polypeptide 6	Myl6	Q60605
Protein NDRG2	Ndrg2	Q9QYG0
Ras-related protein Rab-14	Rab14	Q91V41
Tubulin alpha-1C chain	Tuba1c	P68373
Redox/Detox (GO:0055114/ GO:0006805)		
Aldehyde dehydrogenase, mitochondrial	Aldh2	P47738
Catalase	Cat	P24270
Dehydrogenase/reductase SDR family member 1	Dhrs1	Q99L04
Glyceraldehyde-3-phosphate dehydrogenase	Gapdh	P16858
L-gulonolactone oxidase	Gulo	P58710
17-beta-hydroxysteroid dehydrogenase 13	Hsd17b13	Q8VCR2
3 beta-hydroxysteroid dehydrogenase	Hsd3b3	P26150
Peroxiredoxin-1	Prdx1	P35700
Peroxiredoxin-5, mitochondrial	Prdx5	P99029
Transport (GO:0006810)		
Serotransferrin	Tf	Q921I1
Transitional endoplasmic reticulum ATPase	Vcp	Q01853

Table III.3 Liver Specific CLD Associated Proteins

Protein Name	Gene	Uniprot ID
Amino Acid Metabolism (GO:0006520)		
Adenosylhomocysteinase	Ahcy	P50247
4-trimethylaminobutyraldehyde dehydrogenase	Aldh9a1	Q9JLJ2
Arginase-1	Arg1	Q61176
Argininosuccinate lyase	Asl	Q91YI0
Argininosuccinate synthase	Ass1	P16460
Betaine--homocysteine S-methyltransferase 1	Bhmt	O35490
Cystathionine gamma-lyase	Cth	Q8VCN5
Dihydropyrimidinase	Dpys	Q9EQF5
Fumarylacetoacetase	Fah	P35505
Formimidoyltransferase-cyclodeaminase	Ftcd	Q91XD4
Glutamine synthetase	Glul	P15105
Glycine N-methyltransferase	Gnmt	Q9QXF8
Aspartate aminotransferase, cytoplasmic	Got1	P05201
Aspartate aminotransferase, mitochondrial	Got2	P05202
Alanine aminotransferase 1	Gpt	Q8QZR5
Maleylacetoacetate isomerase	Gstz1	Q9WVL0
Histidine ammonia-lyase	Hal	P35492
4-hydroxyphenylpyruvate dioxygenase	Hpd	P49429
Cytosol aminopeptidase	Lap3	Q9CPY7
S-adenosylmethionine synthase isoform type-1	Mat1a	Q91X83
C-1-tetrahydrofolate synthase, cytoplasmic	Mthfd1	Q922D8
Phenylalanine-4-hydroxylase	Pah	P16331
L-serine dehydratase/L-threonine deaminase	Sds	Q8VBT2

Table III.3 Liver Specific CLD Associated Proteins

Sepiapterin reductase	Spr	Q64105
Urocanate hydratase	Uroc1	Q8VC12
Homogentisate 1,2-dioxygenase	Hgd	O09173
Protein Metabolism (GO:0044267)		
(Chaperones)		
Phenazine biosynthesis-like domain-containing protein 1	Pbld1	Q9DCG6
Carbohydrate Meatbolism (GO:0005975)		
Isocitrate dehydrogenase [NADP] cytoplasmic	Idh1	O88844
Cytoplasmic aconitate hydratase	Aco1	P28271
Pancreatic alpha-amylase	Amy2	P00688
Bifunctional ATP-dependent dihydroxyacetone kinase /FAD-AMP lyase (cyclizing)	Dak	Q8VC30
Fructose-1,6-bisphosphatase 1	Fbp1	Q9QXD6
1,4-alpha-glucan-branching enzyme	Gbe1	Q9D6Y9
Ketohexokinase	Khk	P97328
L-lactate dehydrogenase A chain	Ldha	P06151
Phosphoglycerate mutase 1	Pgam1	Q9DBJ1
Phosphoglucomutase-1	Pgm1	Q9D0F9
Pyruvate kinase isozymes R/L	Pklr	P53657
Glycogen phosphorylase, liver form	Pygl	Q9ET01
Sorbitol dehydrogenase	Sord	Q64442
Transketolase	Tkt	P40142
UTP--glucose-1-phosphate uridylyltransferase	Ugp2	Q91ZJ5
Glutathione Metabolism (GO:0006749)		

Table III.3 Liver Specific CLD Associated Proteins

Lactoylglutathione lyase	Glo1	Q9CPU0
Glutathione peroxidase 1	Gpx1	P11352
Glutathione S-transferase A3	Gsta3	P30115
Glutathione S-transferase Mu 1	Gstm1	P10649
Lipid Metabolism (GO:0006629)		
Peroxiredoxin-6	Prdx6	O08709
ATP-binding cassette sub-family D member 3	Abcd3	P55096
3-ketoacyl-CoA thiolase B, peroxisomal	Acaa1b	Q8VCH0
Very long-chain specific acyl-CoA dehydrogenase	Acadvl	P50544
ATP-citrate synthase	Acly	Q91V92
Peroxisomal acyl-coenzyme A oxidase 1	Acox1	Q9R0H0
Cytochrome P450 2E1	Cyp2e1	Q05421
Peroxisomal bifunctional enzyme	Ehhadh	Q9DBM2
Epoxide hydrolase 2	Ephx2	P34914
Hydroxymethylglutaryl-CoA synthase	Hmgcs2	P54869
Estradiol 17-beta-dehydrogenase 11	Hsd17b11	Q9EQ06
Phosphoenolpyruvate carboxykinase, cytosolic [GTP]	Pck1	Q9Z2V4
Inorganic pyrophosphatase	Ppa1	Q9D819
Lipid Transport (GO:0006869)		
Fatty acid-binding protein, liver	Fabp1	P12710
Nucleotide Metabolism (GO:0006975)		
Putative L-aspartate dehydrogenase	Aspdh	Q9DCQ2
Nicotinate phosphoribosyltransferase	Naprt1	Q8CC86
3-hydroxyanthranilate 3,4-dioxygenase	Haao	Q78JT3

Table III.3 Liver Specific CLD Associated Proteins

Other		
Liver carboxylesterase 31	Ces3a	Q63880
Elongation factor 2	Eef2	P58252
Ferritin light chain 1	Ftl1	P29391
Histone H2B type 1-F/J/L	Hist1h2bf	P10853
Ribonuclease UK114	Hrsp12	P52760
Interferon-inducible GTPase 1	Iigp1	Q9QZ85
Myosin-9	Myh9	Q8VDD5
Parathymosin	Ptms	Q9D0J8
Regucalcin	Rgn	Q64374
SEC14-like protein 2	Sec142	Q99J08
Selenide, water dikinase 2	Sephs2	P97364
Alpha-1-antitrypsin 1	Serpina1a	P07758
Serine protease inhibitor A3K	Serpina3k	P07759
Tetratricopeptide repeat protein	Ttc36	Q8VBW8
Tubulin beta-4B chain	Tubb4b	P68372
D-dopachrome decarboxylase	Ddt	O35215
Redox/Detox (GO:0055114/ GO:0006805)		
Alcohol dehydrogenase 1	Adh1	P00329
Alcohol dehydrogenase [NADP+]	Akr1a1	Q9JII6
Retinal dehydrogenase 1	Aldh1a1	P24549
Aldehyde dehydrogenase family 8 member A1	Aldh8a1	Q8BH00
Cytochrome P450 2D10	Cyp2d10	P24456
Cytochrome P450 2D9	Cyp2d9	P11714

Table III.3 Liver Specific CLD Associated Proteins

Cytochrome P450 2F2	Cyp2f2	P33267
Cytochrome P450 4A14	Cyp4a14	O35728
Glyoxylate reductase/hydroxypyruvate reductase	Grhpr	Q91Z53
NADP-dependent malic enzyme	Me1	P06801
Pterin-4-alpha-carbinolamine dehydratase	Pcbd1	P61458
Superoxide dismutase [Cu-Zn]	Sod1	P08228
UDP-glucuronosyltransferase 1-1	Ugt1a1	Q63886
Cytosolic 10-formyltetrahydrofolate dehydrogenase	Aldh1l1	Q8R0Y6
Transport (GO:0006810)		
Major urinary protein 6	Mup6	P02762
Major urinary protein 20	Mup20	Q5FW60
Selenium-binding protein 2	Selenbp2	Q63836

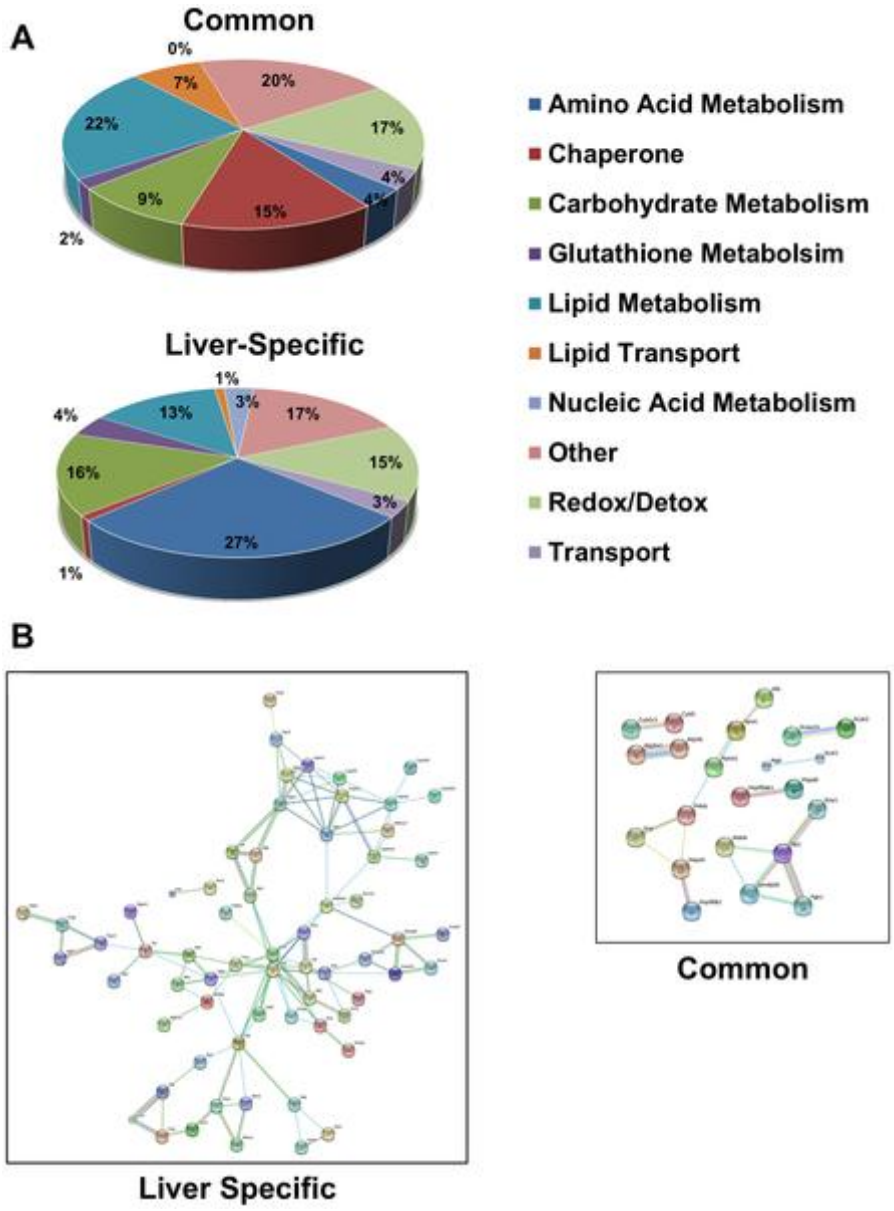

Figure III.4 Hepatic CLD Differs from Other Core CLD Proteomes

(A) Functional categories of common- and liver-specific proteins categorized according to gene ontology (GO) annotations. (B) Association networks of common- and liver-specific CLD associated proteins predicted by the STRING 9.0 program with a confidence level of 0.8. Network edges represent predicted functional associations with different line colors standing for various types of evidence used in establishing the level of confidence. Red, fusion evidence; green, neighborhood evidence; blue, co-occurrence evidence; purple, experimental evidence; yellow, text-mining evidence; black, co-expression evidence. Non-network proteins are not shown.

and fatty acid metabolism (3), the others were related to amino acid metabolism (1) and protein processing (1). For liver-specific CLD proteins, I found significant enrichment in 26 KEGG pathway categories. Of these, 12 were related to amino acid metabolism, 6 were related to carbohydrate metabolism, 4 were related to fatty acid metabolism, 3 were related to xenobiotic metabolism and 1 was related to glutathione metabolism. Among the identified enzymes, several corresponded to large portions of the glycolysis/gluconeogenesis and cysteine/methionine pathways.

Low- and High- Fat Specific CLD Proteins

The functional classes of proteins that were uniquely associated with LF- and HF-CLD exhibited distinct patterns (Figure III.5). The majority of the proteins uniquely associated with LF-CLD are involved in amino acid (29%) and carbohydrate (23%) metabolism. Whereas, most of the uniquely associated proteins on HF-CLD are related to lipid metabolism and redox/detoxification processes. Using the STRING 9.0 program to probe for functionally interactions between LF- and HF-CLD specific proteins, I found that LF-CLD specific proteins formed a single high stringency interaction node connecting enzymes involved in amino acid and acetate metabolism. Whereas, HF-CLD specific proteins formed a high stringency node related to redox/detoxification processes and two sets of individual connections between pyruvate and carbohydrate metabolism, and between methionine/cysteine and dicarboxylic acid metabolism (Figure III.5B). Among the 17 proteins specifically found on LF-CLD, I did not detect significant enrichment in any KEGG pathway. However, among the 26 proteins specifically found on HF-CLD, there was enrichment in 5 KEGG pathways with FDR values < 0.05, PPAR signaling, ascorbate metabolism, pyruvate metabolism, fatty acid metabolism and

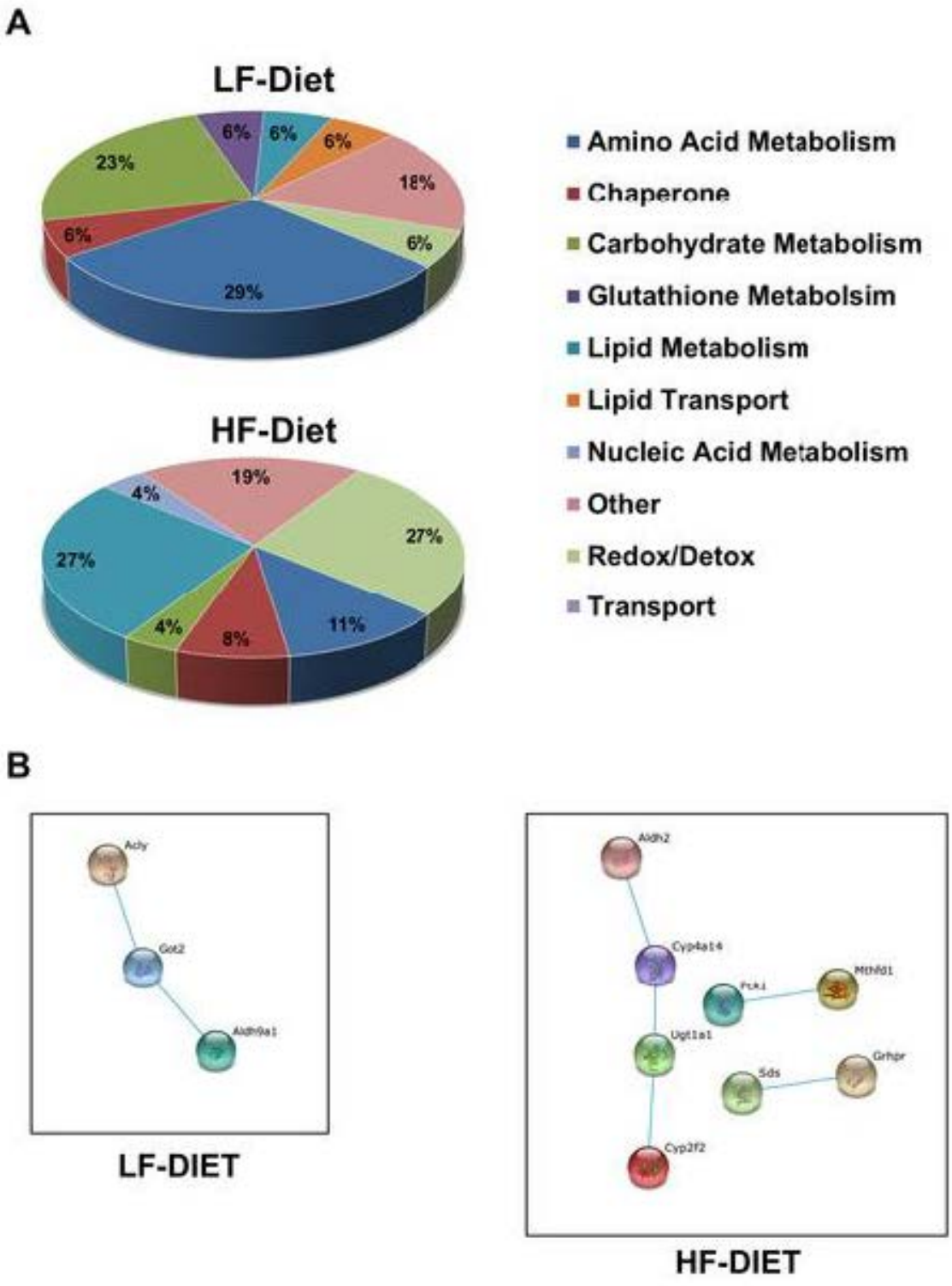

Figure III.5 HFD Induces Expression of Proteins from Different Pathways
(A) Functional categories of LF- and HF-specific CLD associated proteins categorized according to gene ontology (GO) annotations. (B) Association networks of LF- and HF-specific CLD associated proteins predicted by the STRING 9.0 program with a confidence level of 0.8. Color codes are as described in the legend to Figure III.3

glyoxylate metabolism. The identities of the HF-CLD proteins found in enriched KEGG pathways are shown in Table III.5

Diet Affects Plin2 CLD Levels

In addition to finding qualitative differences in the protein compositions of LF- and HF-CLD, I also found that for some proteins LF and HF diets appeared to influence the relative abundance, as suggested by percent spectra (Table III.2). One of the proteins exhibiting a relative large change in apparent abundance was Plin2. To determine if differences of Plin2 reflected actual differences in its abundance on CLD, I investigated Plin2 in hepatic tissue by immunofluorescence (IF) microscopy, and in isolated CLD by quantitative immunoblot analysis (Figure III.6). IF analysis showed significant Plin2 immunostaining in both LF- and HF-refed livers, with increased Plin2 staining intensity in livers of HF-refed livers in the central vein region (Figure III.6A). I next determined the relative amounts Plin2 on isolated CLD by quantitative immunoblot analysis. When compared to total CLD protein (Figure III.6B), or to total CLD TG (Figure III.6C), I found that HF-re-feeding increased the average amount of Plin2 associated with CLD by approximately 4-fold over that found for LF-refed animals.

Fasting and HF diets are reported to increase hepatic Plin2 transcript levels [94]. Thus, I was interested in determining whether the enrichment of Plin2 on CLD in HF refed mice corresponded to enhanced Plin2 mRNA expression. As shown in Figure

Table III.4 Liver Specific- and Common-CLD Protein KEGG Pathways

Liver Specific CLD associated proteins

KEGG ID	Pathway	Number Genes	Of P-value fdr
mmu00270	Cysteine and methionine metabolism	8	8.54E-07
mmu00350	Tyrosine metabolism	7	1.44E-05
mmu00330	Arginine and proline metabolism	8	1.73E-05

Table III.4 Liver Specific- and Common-CLD Protein KEGG Pathways

Liver Specific CLD associated proteins

KEGG ID	Pathway	Number Of Genes	P-value fdr
mmu00010	Glycolysis/Gluconeogenesis	9	2.25E-05
mmu00620	Pyruvate metabolism	7	2.25E-05
mmu00360	Phenylalanine metabolism	5	2.26E-05
mmu00071	Fatty acid metabolism	7	2.26E-05
mmu00250	Alanine, aspartate and glutamate metabolism	6	3.61E-05
mmu00982	Drug metabolism – cytochrome P450	8	9.24E-05
mmu03320	PPAR signaling pathway	8	9.24E-05
mmu00400	Phenylalanine, tyrosine and tryptophan biosynthesis	3	1.37E-04
mmu00980	Metabolism of xenobiotics by cytochrome P450	7	3.10E-04
mmu00480	Glutathione metabolism	6	6.03E-04
mmu04146	Peroxisome	7	6.03E-04
mmu00500	Starch and sucrose metabolism	5	9.90E-04
mmu00450	Selenoamino acid metabolism	4	2.10E-03
mmu00020	Citrate cycle (TCA cycle)	4	6.50E-03
mmu00260	Glycine, serine and threonine metabolism	4	7.84E-03
mmu00630	Glyoxylate and dicarboxylate metabolism	3	1.20E-02
mmu00410	beta-Alanine metabolism	3	2.05E-02
mmu00910	Nitrogen metabolism	3	2.05E-02
mmu00280	Valine, leucine and isoleucine degradation	4	2.45E-02
mmu00340	Histidine metabolism	3	2.78E-02
mmu00030	Pentose phosphate pathway	3	4.16E-02
mmu00903	Limonene and pinene degradation	2	4.24E-02
mmu00640	Propanoate metabolism	3	4.24E-02
Common CLD associated proteins			
mmu04146	Peroxisome	6	8.95E-04
mmu00010	Glycolysis/Gluconeogenesis	6	8.95E-04
mmu00071	Fatty acid metabolism	4	9.00E-03
mmu03320	PPAR signaling pathway	4	4.64E-02
mmu00051	Fructose and mannose metabolism	3	4.64E-02
mmu00650	Butanoate metabolism	3	4.64E-02
mmu00380	Tryptophan metabolism	3	4.64E-02
mmu00620	Pyruvate metabolism	3	4.64E-02
mmu04612	Antigen processing and presentation	4	4.64E-02

Table III.5 Specific HFD CLD Protein KEGG Pathways

KEGG ID	Pathway	P-value (fdr)	Gene
mmu00053	Ascorbate and aldarate metabolism	2.13E-03	Gulo
			Aldh2
			Ugt1a1
mmu03320	PPAR signaling pathway	7.47E-03	Apoa1
			Hmgcs2
			Pck1
			Cyp4a14
mmu00620	Pyruvate metabolism	1.37E-02	Grhpr
			Pck1
			Aldh2
mmu00071	Fatty acid metabolism	1.37E-02	Acadvl
			Aldh2
			Cyp4a14
mmu00630	Glyoxylate and dicarboxylate metabolism	4.73E-02	Mthfd1
			Grhpr

III.6D, I found that Plin2 transcript levels in total hepatic RNA were similar for HF- and LF-refed mice. The data in Figure III.6D also show that hepatic Plin2 transcript levels are several folds greater than those of other PLIN family members, and that hepatic transcript expression of other PLIN family genes also are not influenced by the content of fat in the re-feeding diet. Collectively these data suggest that the HF diet increases the association of Plin2 with CLD, elevating its relative CLD abundance, and that this effect is not related to Plin2 expression levels.

High Fat Feeding Increases Plin2 Surface Density on CLD

As a CLD surface associated protein, an increase in the relative amount of Plin2 on CLD could be due to loss of other CLD-associated proteins, or absolute increases in its surface density. To distinguish between these two mechanisms, I quantified the effects

of HF exposure on the surface density of Plin2 by electron microscopy after immuno-gold labeling. For these experiments I used a cell line that constitutively expresses recombinant mouse Plin2 under control of the CMV promoter [95] to avoid potential effects of fat exposure on Plin2 expression. Figure III.6 shows that CLD in these cells increased in size following feeding with 100 μM oleic acid (OA), and that the number of anti-Plin2 conjugated-gold particles on the surface of individual CLD increased as a function of time in OA-supplemented media. The average surface densities of anti-Plin2 conjugated-gold particles on CLD in cells incubated in control media without OA supplementation (T 0hr), and cells supplemented with OA for 4 or 24 hrs are shown in the graph in Figure III.6E. The CLD surface density of Plin2 increased following incubation in OA supplemented medium by about 2-fold over the T0 density after 4 hrs ($p<0.01$) and 6-fold after 24 hrs ($p<0.001$). These data provide direct evidence that the surface density of Plin2 on CLD is dynamically regulated and increased under conditions of high fat exposure.

Endoplasmic Reticulum Chaperone Proteins Localize to Hepatic CLD

ER proteins, including several with chaperone function, have been identified on isolated CLD from various mammalian cells and tissues [61, 74, 76, 78, 93], as well as from drosophila larvae [73]. I detected GRP78 in highly enriched hepatic CLD by immunoblotanalysis (Figure III.8), and I found GRP78 and numerous other chaperone-related proteins on LF- and HF-CLD by proteomic analysis (Table III.1). Hepatic GRP78 expression is upregulated in response to ER stress [96], and elements of the ER stress pathway are known to play crucial roles in regulating hepatic lipid metabolism, including lipogenesis [97]. To assess possible LF- and HF-diet re-feeding effects on

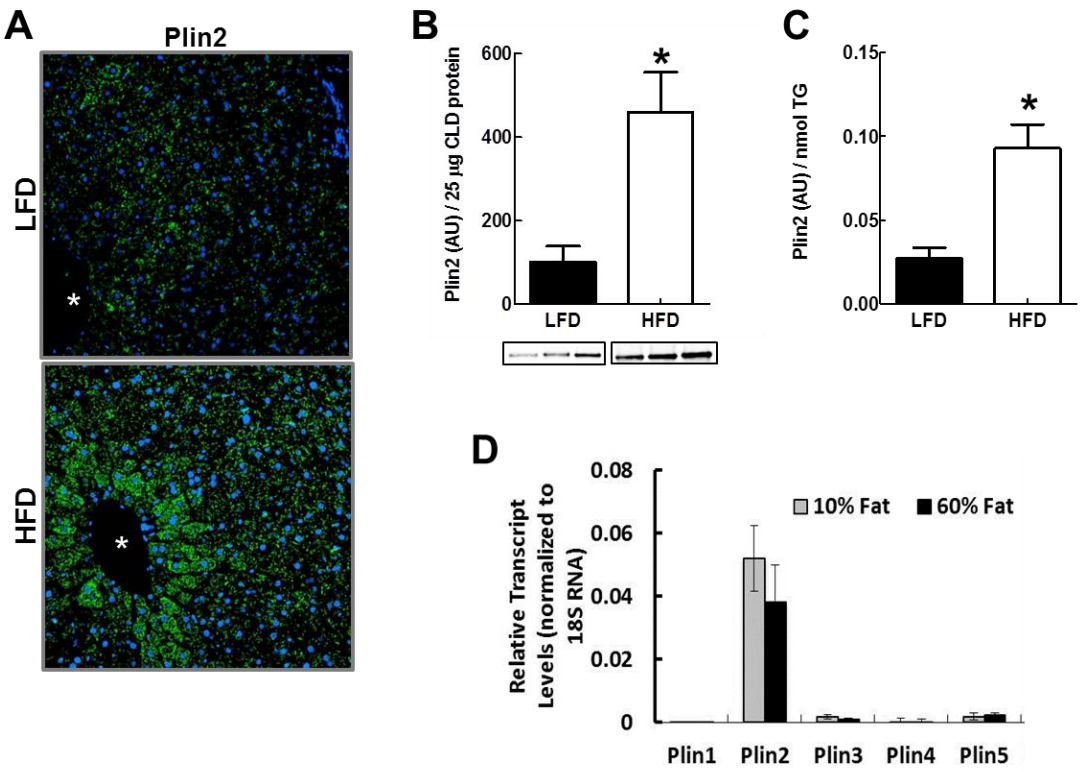

Figure III.6 Diet Effects Plin2 on CLD

(A) Representative confocal Plin2 immunofluorescence (green) images of liver sections from fasted male mice refed with LF (LFD) – and HF (HFD)-diets and stained with antibodies to Plin2. Nuclei (blue) were stained with DAPI. Asterisks indicate central veins. (B) Quantitative immunoblot analysis of Plin2 levels in enriched CLD protein extracts from fast-fed male mice on LF (LFD)- or HF(HFD)-diets. Insets show immunoblots of 25 µg of CLD protein from 3 mice. The graph shows the average (± SD) Plin2 levels normalized to 25 µg of total CLD protein from LF (N = 3) and HF (N = 3) mice. (C) CLD Plin2 levels normalized to CLD TG content. Values are means (± SD) for LF (N = 3) and HF (N = 3) refed animals. Asterisks in B and C indicate HFD values differ from LFD values ($p<0.0001$). (D) Transcript levels of PLIN family members in livers of fasted and refed mice on LFD and HFD quantified by qRT-PCR using primers listed in Table II.1. Values are means± SD normalized to 18S RNA. Asterisks indicate Plin2 transcript levels are significantly elevated over transcript levels for Plins 1,3,4, and 5.

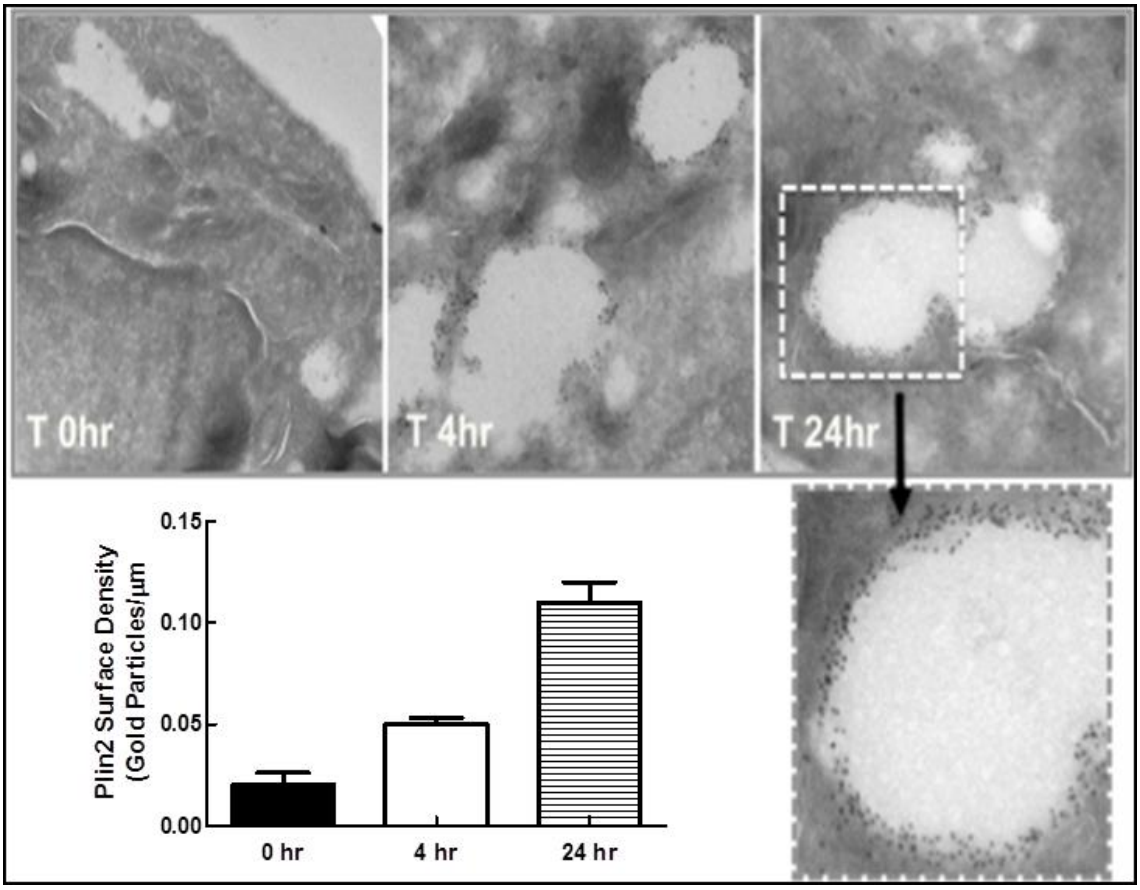

Figure III.7 Diet Effects Plin2 Surface Density on CLD
Effects of HF feeding on Plin2 surface density in HEK293 cells stably expressing Plin2-VSV. Images are representative electron micrographs of anti-PLIN2-gold particle labeled cells that were cultured in oleic acid-supplemented media for 0h, 4h or 24h. An enlarged micrograph of a CLD at 24h is shown. Average (± SD) Plin2 surface densities on CLD at each time point are shown for 50–75 CLD from triplicate cultures. The experiment was repeated twice with similar results. Asterisks indicate statistically significant differences from T = 0 time point, double dagger indicates statistically significant differences between 4h and 24h time points

chaperone-CLD interactions in the liver, and better understand the nature of these interactions, I quantified CLD-GRP78 levels in response to LF- and HF-re-feeding, and directly investigated the association of GRP78 with CLD in hepatic tissue by IF analysis (III.8D). The levels of GRP78 in liver homogenates of LF- and HF-refed mice did not differ significantly from each other, or from GRP78 levels found in livers of non-fasted mice, which suggests that hepatic CLD responses are not associated with obvious ER stress. Furthermore, I did not find significant differences in the amount of CLD-associated GRP78 in LF- and HF-refed livers, demonstrating that unlike the Plin2 response, CLD levels of GRP78 are not influenced by diet.

Evidence of direct association between GRP78 and CLD in intact cells has been obtained in adipocytes [98]. To verify that GRP78 directly associates with CLD in intact hepatocytes, I visualized liver sections from fasted mice that were refed with the HF diet and immunostained for Plin2 and GRP78 with laser confocal microscopy (Figure III.8D). GRP78 immunostaining was detected in the ER network of hepatocytes and on the surface of their CLD. In contrast to the relatively uniform staining intensity of Plin2 on CLD, GRP78 localized as discrete patches on the CLD surface, in a pattern similar to that described for CLD in adipocytes [98].Protein disulfide isomerase (PDI) is another

prominent ER chaperone protein that I identified by proteomic analysis of hepatic CLD from LF-and HF-refed mice (Table III.1). I validated the association of PDI with isolated CLD by immunoblot analysis, and confirmed its CLD localization by laser confocal imaging of immunostained stained liver sections (Figure III.8E). Similar to GRP78, PDI localized as discrete patches on the surface of Plin2-positive CLD. Collectively, the GRP78 and PDI immunostaining data validate proteomic evidence of

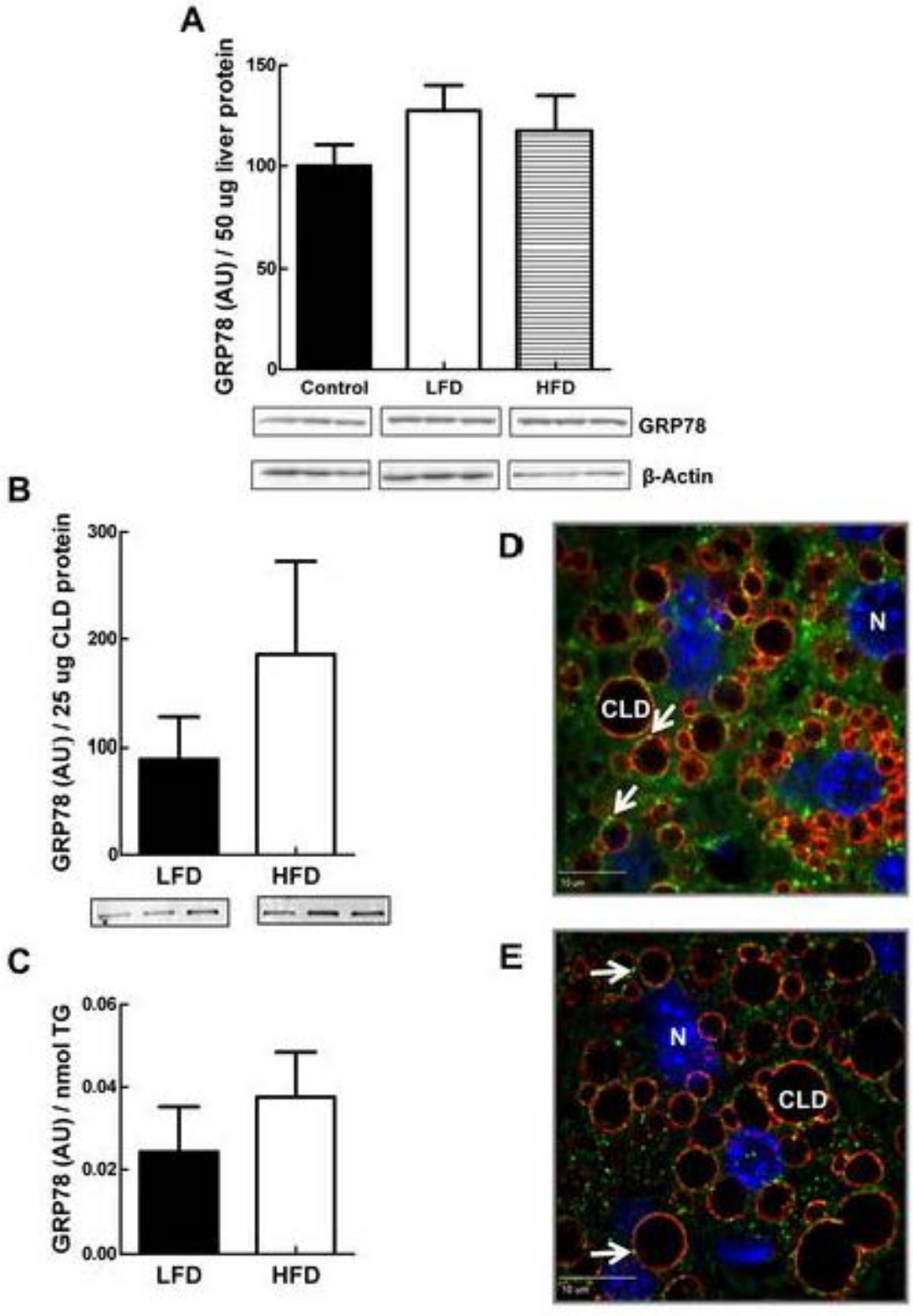

Figure III.8 ER Proteins are Associated with CLD

Figure III.8 ER Proteins are Associated with CLD

(A) Quantitative immunoblot analysis of GRP78 levels in liver extracts from non-fasted male mice (Control) and fast-fed male mice on LF- or HF-diets. Insets show immunoblots of 50 μg of total liver homogenate protein from 3 mice probed with antibodies to GRP78 or β-actin. The graph shows the average (± SD) GRP78 levels normalized to β-actin from Control (3), LF- (LFD) (N = 3) and HF- (HFD) (N = 3) refed mice. (B) Quantitative immunoblot analysis of GRP78 levels in enriched CLD protein extracts from fast-fed male mice on LF- or HF-diets. Insets show immunoblots of 25 μg of CLD protein from 3 mice. The graph shows the average (± SD) GRP78 levels normalized to 25 μg of CLD protein from LF- (LFD) (N = 3) and HF- (HFD) (N = 3) refed mice. (C) CLD GRP78 levels normalized to CLD TG content. Values are means (± SD) for LFD (N = 3) and HFD (N = 3) refed animals. (D) Representative confocal immunofluorescence images of liver sections from HF refed mice stained with antibodies to Plin2 (red) and GRP78 (green). (E) Representative confocal immunofluorescence images of liver sections from HF refed mice stained with antibodies to Plin2 (red) and PDI (green). Nuclei in images in D and E (blue) were stained with DAPI. Arrows in D and E indicate localization of GRP78 or PDI on CLD. Bar is 10 μm.

ER chaperone protein-CLD association and suggest that chaperones exhibit distinct organizational patterns on the CLD surface.

LF and HF Re-feeding Differentially Affect CLD Levels of the Methionine-Metabolizing Enzyme BHMT

Pathway analysis, revealed significant enrichment of enzymes associated with the cysteine-homocysteine-methionine pathway on liver-CLD (Table VII.1). Figure III.9A, shows the relationship between the identified proteins and specific steps of the cysteine-methionine metabolism pathway. Betaine homocysteine S-methyltransferase (BHMT), a critical regulatory enzyme of this pathway [99], is an abundant liver protein and one of the top proteomic hits on CLD from LF- and HF-fed mice. In mice, loss of BHMT hasbeen shown to induce hepatosteatosis [100], and high fat feeding has been shown to increase hepatic BHMT transcript levels [101]. I was thus interested in determining if diet affected the amount of BHMT associated with CLD. Figure III.9B shows that BHMT levels in whole liver extracts from LF- and HF-refed animals were significantly (77% and 128% respectively) higher than those of non-fasted control animals. Although hepatic BHMT levels in animals re-fed the HF-diet tended to be higher than those of LF-refed animals, the differences did not reach statistical significance. In contrast, levels of BHMT associated LF-CLD were about 3-times higher than that found associated with HF-CLD when normalized to either total CLD protein, or to CLD-TG content (Figure III.9 C and D). These results provide direct evidence for the presence of BHMT on CLD, and demonstrate that its CLD association is altered by diet.

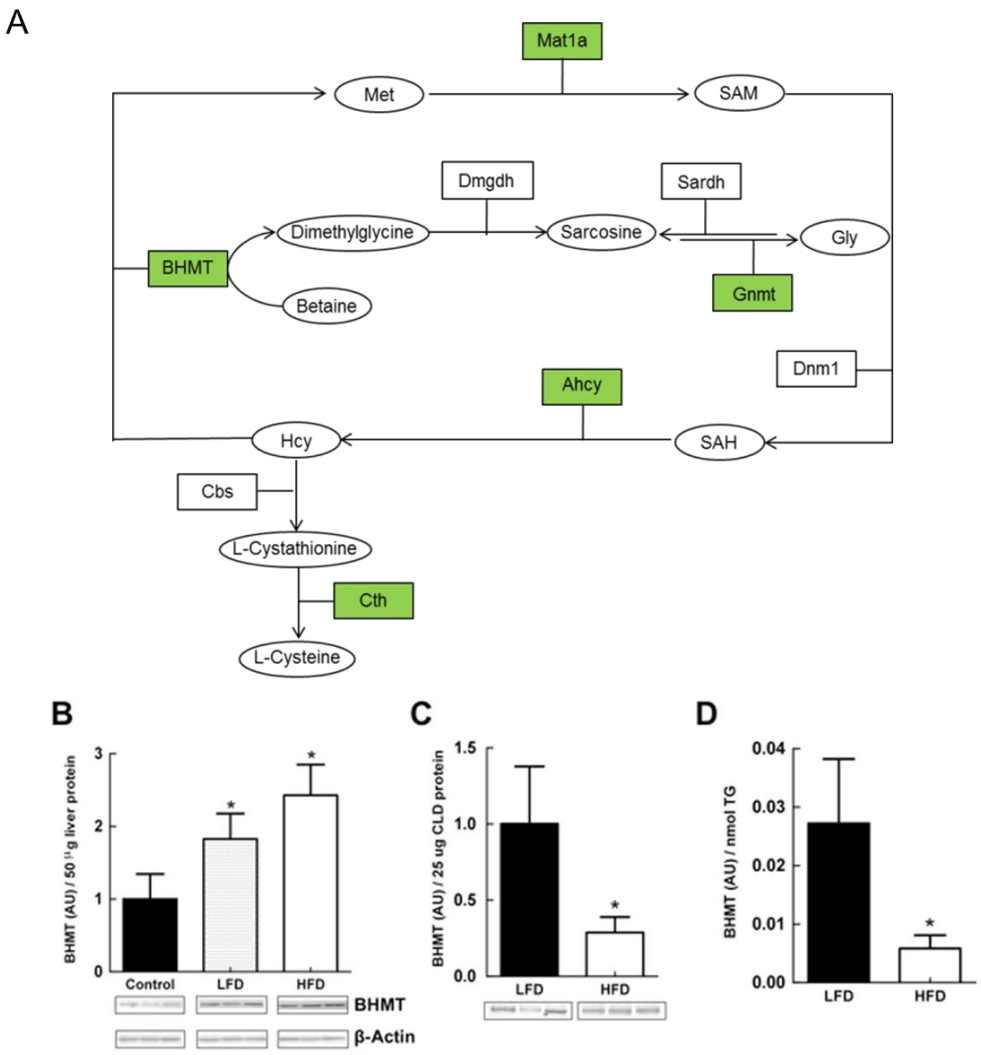

Figure III.9 Methionine-Cysteine Pathway Proteins Associated with CLD
(A) Schematic diagram representing the methionine/cysteine pathway. Boxes represent proteins, circles represent metabolites. Green colored boxes indicate proteins identified on hepatic CLD. (B) Quantitative immunoblot analysis of BHMT levels in liver extracts from non-fasted male mice (Control) and refed male mice on LF- or HF-diets. Insets show immunoblots of 50 µg of total liver homogenate protein from 3 mice probed with antibodies to BHMT or β-actin. The graph shows the average (± SD) BHMT levels normalized to β-actin from Control (3), LFD (N = 3) and HFD (N = 3) refed mice. Asterisks indicate LFD and HFD values differ from Control values ($p<0.005$). (C) Quantitative immunoblot analysis of BHMT levels in CLD protein extracts from refed male mice on LF- or HF-diets. Insets show immunoblots of 25 µg of CLD protein from 3 mice. The graph shows the average (± SD) BHMT levels normalized to 25 µg of CLD protein from LFD (N = 3) and HFD (N = 3) mice. (D) CLD BHMT levels normalized to CLD TG content. Values are means (± SD) for LFD (N = 3) and HFD (N = 3) refed animals. Asterisks in C and D indicate HFD values differ from LFD values ($p<0.001$).

Discussion

Neutral lipid accumulation in the liver, a critical determinant of hepatic lipid homeostasis and liver health [85, 102, 103], is affected by diet and alterations in metabolic function [104, 105]. CLD are responsible for storage and mobilization of neutral lipid stores through the actions of specific surface associated proteins. Although earlier studies have identified proteins associated with hepatic CLD from mice [61, 80], the data presented here provide the first comprehensive non-biased description of the mouse hepatic CLD proteome. The novel findings of this study are that the hepatic CLD protein composition appears to be distinct from that of CLD from other sources; enzymes of multiple metabolic pathways are present on hepatic CLD; and the protein composition of hepatic CLD from fasted and refed mice is qualitatively and quantitatively influenced by dietary fat content, and corresponds to alterations in hepatic metabolic properties.Together, these findings provide evidence that CLD properties are dynamically regulated by the metabolic status of the liver, and that CLD may function in coordinating diverse metabolic activities within liver cells.

Metabolic Functions of Hepatic CLD

The primary biological function of CLD is generally understood to be neutral lipid storage, which is thought to involve the integrated actions of ER enzymes and specific CLD-associated proteins [106]. In agreement with this concept, multiple proteomic studies have consistently detected various ER proteins, lipid metabolism enzymes and members of the PLIN family of CLD-associated proteins on isolated CLD from multiple mammalian sources [42, 61, 74-82, 92, 93]. There is also growing evidence that CLD may sequester proteins, thereby indirectly contributing to other

cellular functions [107]. My study provides evidence that, at least within the liver, CLD may also function as a platform for coordinating metabolic functions by bringing together elements of specific metabolic pathways. Although additional work is needed to formally establish this concept, I found that the hepatic CLD protein composition is significantly enriched in enzymes composing KEGG pathways related to amino acid, carbohydrate, lipid and xenobiotic metabolism. Further, the identified proteins comprised multiple networks of functionally linked enzymes that, in some cases, correspond to intact portions of metabolic pathways. While I cannot rule out that some of the identified proteins represent adventitious associations of abundant liver proteins with CLD resulting from tissue disruption, the presence of multiple, metabolically related, enzymes on isolated CLD indicate that their CLD association is not simply an accident of isolation. For instance, this conclusion is supported by the observation that CLD levels of BHMT, an abundant cytoplasmic liver enzyme [108], are differentially affected by dietary fat content, thereby suggesting that the association is physiologically regulated. Additionally, my observations that the ER chaperone proteins GRP78 and PDI localize to the CLD surface provide direct *in situ* evidence that proteins from other cellular compartments can be detected on CLD in intact hepatocytes. Although functions for CLD-associated GRP78 and PDI have not been identified, the presence of chaperone proteins provides a mechanism for achieving correct folding of proteins on the CLD surface. Collectively these data argue that protein composition of hepatic CLD represent *bone fide* interactions that are related to the physiological functions of the liver.

CLD Properties Reflect Differences in Liver Metabolism

My data indicate that the differential effects of LF- and HF-diet on hepatic CLD protein compositions reflect, in part, differences in hepatic metabolic properties. Indirect calorimetry measurements documented that LF- and HF-re-feeding differentially affected the energy metabolism of fasted mice, inducing lipogenesis and the use of carbohydrates for fuel in LF-refed animals, while stimulating the use of fat for fuel in HF-refed animals. Consistent with these metabolic differences, I found a selective enrichment of enzymes involved in amino acid and carbohydrate metabolism, and *de novo* fatty acid synthesis on LF-CLD. In contrast, enzymes and proteins involved in fatty acid metabolism and lipid transport were enriched on HF-CLD. Additional studies are required to assess the functional significances of these differences. However, it is likely that protein composition differences will reflect subtle modulations of CLD activity, rather than overt changes in their function, since I did not detect large qualitative differences in the protein compositions of LF- and HF-CLD.

This concept is supported by observations that CLD binding of BHMT, a key enzyme in cysteine-methionine metabolism, is differentially affected by dietary fat content and metabolic status of the liver, and is independent of total tissue BHMT levels. In conjunction with evidence that multiple members of the cysteine-methionine metabolic pathway are present on hepatic CLD, the ability of diet to influence CLD-BHMT interactions raises the possibility that CLD may contribute to hepatic metabolic functions by helping to coordinate cysteine-methionine metabolism by providing a platform for cytosolic enzymatic reactions.

Diet Induces Alterations in CLD Surface Organization

Diet effects on liver metabolic properties, including transcript expression and protein profiles, have been identified in both long-term and fasting-re-feeding studies [83, 84, 109, 110]. There is also increasing recognition that diet influences the molecular properties of hepatic organelles, including mitochondria and ER [111, 112]. My data expand the effects of diet to include hepatic CLD, documenting directly that the amount of dietary fat affects their molecular properties. The observed effects include alterations in CLD-associated levels of Plin2 and BHMT, both of which are functionally linked to fatty liver formation in mice [4, 100]. Plin2 is a structural CLD-associated protein [113] that plays an essential role in the effects of HF diet on hepatic lipid accumulation [37, 38]. The finding that HF re-feeding increases the CLD surface density of Plin2 provides evidence that its surface organization is dynamically regulated and those alterations in the surface properties of Plin2 may contribute to its lipid storage functions. As yet, it is unclear how diet-induced changes in Plin2 surface density affect hepatic CLD properties. However, the observations that increased Plin2 surface density appears to be associated with larger CLD raise the possibility that Plin2 surface properties may contribute to the regulation of CLD size, which in the liver appears to be influenced by dietary fat content. Consistent with these data in the liver, the McManaman laboratory previously demonstrated that loss of Plin2 was associated with a decrease in the size of CLD in mammary glands of pregnant mice [39]. Additional work is needed to determine how Plin2 regulates hepatic CLD size.

In summary, my study has described the mouse hepatic CLD proteome, and demonstrated that it is markedly different from that of CLD in other cells and tissues. I have also shown that the hepatic CLD proteome is dynamically influenced by dietary fat

content, and related to differences in liver metabolic properties. The proteins found on hepatic CLD are enriched in enzymes with extensive functional connections known to be important for liver metabolism. These findings are consistent with growing evidence that CLD protein compositions are influenced by cellular function, metabolic disorders and/or the physical properties of CLD [59, 69, 76], and they provide support for an expanded role for CLD in regulating cellular metabolic properties beyond that of lipid storage. These data should allow new hypotheses and insights into the cellular mechanism by which the liver response to metabolic changes and challenges.

CHAPTER IV

PERILIPIN-2 FUNCTIONS AS A SCAFFOLDING PROTEIN TO REGULATE HEPATIC LIPID ACCUMULATION AND CYTOPLASMIC LIPID DROPLET

Introduction

As a major regulator of energy homeostasis, the liver is a primary target of obesity-associated metabolic alterations [102], and disruption of hepatic lipid metabolism is proposed to play a fundamental role in the initiation and progression of many metabolic diseases [114, 115]. As incidences of diseases associated with hepatic lipid dysregulation rise, understanding of the mechanisms that regulate lipid synthesis, accumulation, and secretion in liver cells, is important towards understanding how these dysfunctions contribute to disease.

Multiple PLIN family members are found in hepatic tissue [59, 69]. Depending on physiological status, genotype, and species, Plins 1-3 have been detected on CLD in hepatocytes and stellate cells of human, mouse, and bovine liver [44, 59, 69], while Plin5 has been detected on hepatocyte CLD in livers of Plin2-null mice after prolonged high fat (HF) diet feeding [40]. Information about the precise roles of PLIN family members in regulating hepatic lipid metabolism, however, is still relatively limited. In mice, PLINs 2 and 3 have both been shown to be important for hepatic lipid accumulation in response to chronic HF diet feeding [37, 38, 40, 44]. However, their mechanisms of action appear to differ, since the presence of one does not appear to fully compensate for loss of the other [37, 38, 40, 44].

In rodents, fasting and re-feeding is associated with hepatic lipid accumulation [40], and up-regulation of genes associated with lipid synthesis and storage, including

Plin2 [83, 84, 94]. In chapter III, I demonstrated that differences in the hepatic lipid content, and the properties and protein compositions of CLD, in fasted mice that were re-fed with high or low fat diets were associated with differences in CLD Plin2 levels [40]. In the work presented here, I tested the hypothesis that Plin2 is a primary determinant of acute hepatic lipid accumulation and CLD properties in fasted and re-fed mice, and that its expression differentially affects how these properties are influenced by dietary fat content.

Results

Food Intake and Metabolic Activities of Fasted and Re-fed Mice

Fasting and diet composition are known to influence food intake, liver metabolism, and hepatic lipid storage in mice [87, 88, 116]. Previously, long-term HF diet feeding studies in mice revealed that loss of Plin2 was associated with reduced food intake and decreased amounts of adipose relative to WT mice [40]. Therefore, to understand how Plin2 affects hepatic lipid responses to fasting and re-feeding with HF- or LF-diets it was necessary first to establish whether its loss affected food intake or the metabolic responses in this model. Figure IV.1A shows that body weights of fasted WT and D5KO mice re-fed with LF- or HF-diets were similar. In agreement with my previous report [116], I found greater food consumption in fasted WT mice re-fed the HF diet compared to those re-fed the LF diet (Figure IV.1B). However, there was no difference in food consumption of fasted D5KO mice re-fed either the LF- or the HF-diet. I also found no significant differences in liver weights of fasted WT and D5KO animals re-fed LF- or HF-diets (Figure IV.1C), although liver weights of D5KO mice re-fed the HF diet tended to be lower than those of WT mice re-fed this diet. Figure IV.1D shows

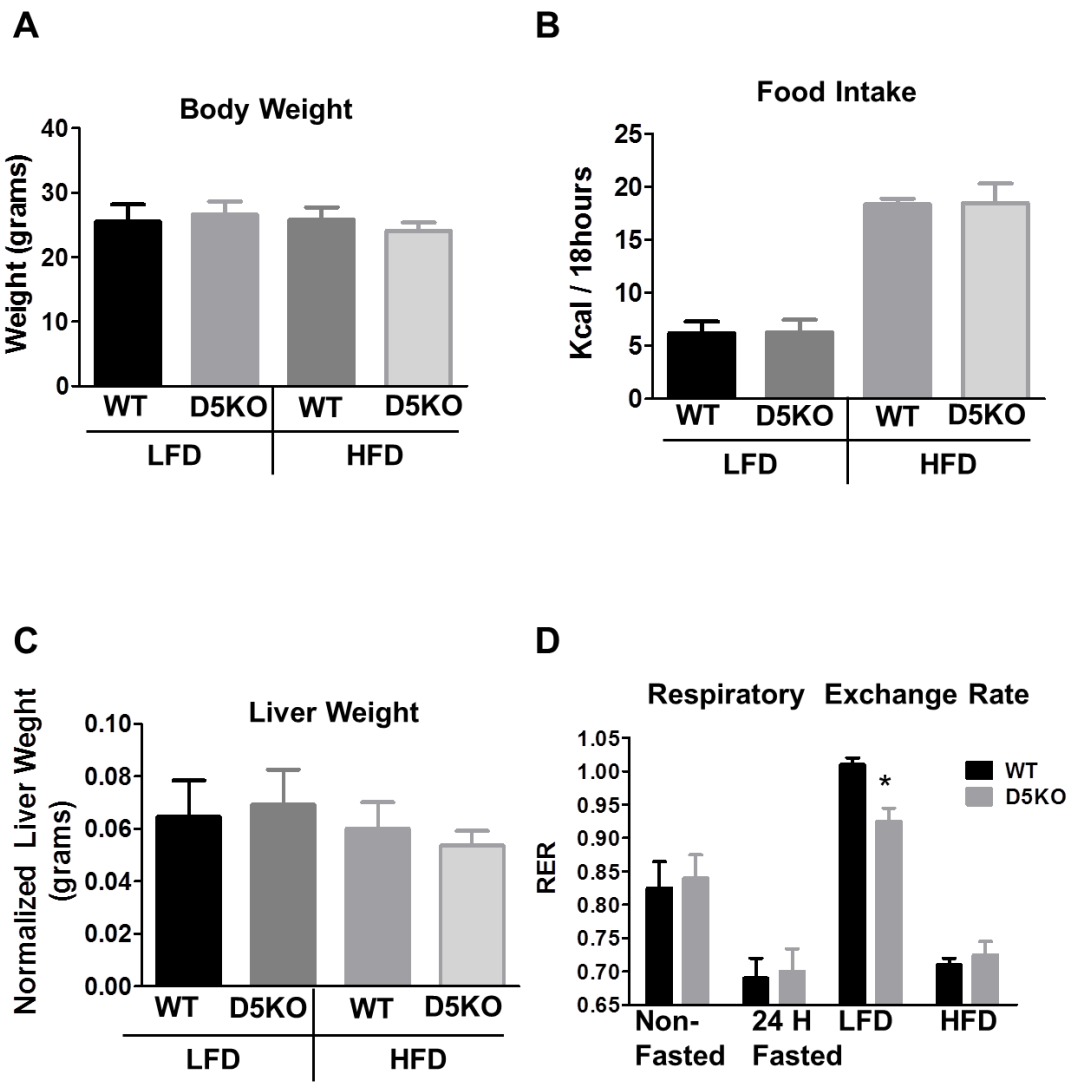

Figure IV.1 Physiological Effects of Fasting and Re-feeding on WT and D5KO Mice

Effects of LF- and HF-re-feeding on body weight (A), food intake (B) and liver weights (C) in fasted male mice. Values are means (± SD) for 3 animals in each group. (D) Respiratory exchange ratios (RER) of non-fasted, 24 hour fasted (24 Hrs) and 24 hour fasted mice that were re-fed with LF (LFD) or HF (HFD) diets. Non-fasted and fasted values correspond to averages (± SD) of 8 animals obtained prior to re-feeding. LF- and HF-re-feeding values correspond to averages (± SD) for 3 animals in each group. The asterisk indicates significance at $p<0.05$ compared to WT mice (Figure IV.1B).

respiratory exchange ratios (RER) for WT and D5KO mice prior to fasting, following a 24 hour period of fast, and after re-feeding with LF- or HF-diets. Prior to fasting, RER values of both WT and D5KO mice were approximately 0.8, as fuel use reflected the broad mixture of carbohydrate, fat, and protein in their diets. During fasting, RER values dropped to approximately 0.7 in both WT and D5KO mice, indicating a switch to fat as the primary source of energy. These data documented that loss of Plin2 was not associated with significant effects on basal metabolic properties prior to or during fasting. Re-feeding on a LF diet resulted in RER values that were close to 1.0 in WT animals, reflecting the preferential use of carbohydrate for energy production, and the likelihood that *de novo* lipogenesis was induced under these conditions [117]. RER values of LF diet re-fed D5KO mice were closer to 0.9, which was significantly less than that of WT mice on this diet, and suggests that loss of Plin2 was associated with decreased use of carbohydrates for energy in these animals. RER values for both WT and D5KO mice re-fed the HF diet were close to 0.7, indicating that they were utilizing fat for energy, and that loss of Plin2 does not affect this response .

Effects of Plin2 Loss on Hepatic Lipid Accumulation in Fasted and Re-fed Mice

Observations that Plin2 deficiency prevents fatty liver induced by long-term HF feeding in murine models of obesity, suggest that it may be a physiological determinant of hepatic lipid accumulation [37, 38]. However, Plin2 deletion was also associated with decreased food intake and reduction in adipose content in HF re-fed mice [40], raising the possibility that impaired hepatic lipid accumulation in Plin2 deficient mice was secondary to more general metabolic alterations. To address this possibility, I estimated the effects of Plin2 loss on acute hepatic lipid accumulation in the fasting and re-feeding

model by staining frozen liver sections with BODIPY to specifically label neutral lipids within cells [116, 118]. Representative fluorescence images of BODIPY stained neutral lipids in liver sections of fasted WT and D5KO mice re-fed with HF- or LF-diets are shown in Figure IV.2A. In agreement with my previous studies [116], I found more extensive lipid accumulation in livers of WT mice re-fed the HF diet compared to those re-fed the LF diet. In contrast, lipid accumulation in livers of D5KO mice re-fed the HF diet appeared to be similar to those re-fed the LF diet, and less than that found in livers of WT mice on comparable diets. To confirm these observations, I quantified the amount of BODIPY staining in multiple liver sections from cohorts of fasted and re-fed WT and D5KO mice (Figure IV.2B). The level of BODIPY staining in livers of WT animals re-fed the HF diet were nearly five times that found in livers of WT mice re-fed the LF diet or in D5KO mice re-fed HF- or LF-fat diets. In Plin2-DK5O mice, BODIPY staining levels were similar for livers of HF- or LF- diet re-fed animals and comparable to that found in LF re-fed WT mice.

Hepatocyte metabolic properties, including lipid and glucose metabolism, and lipid accumulation, vary between the periportal (zone 1) and centralobular (zone 3) zones [119-122]. In non-fasted mice chronically re-fed a HF diet, Plin2 positive CLD accumulation initially begins in zone 3 after about one week and becomes more prominent in zone 2 by 3 weeks [59]. To determine if hepatic lipid accumulation following fasting and re-feeding exhibits zone specificity, and if zone specificity of lipid accumulation is affected by dietary fat content and Plin2 expression, I quantified the zonal distribution of BODIPY stained lipid in hepatic sections from fasted and re-fed WT and D5KO mice (Figure IV.3). There was a trend to greater relative amounts of lipid in

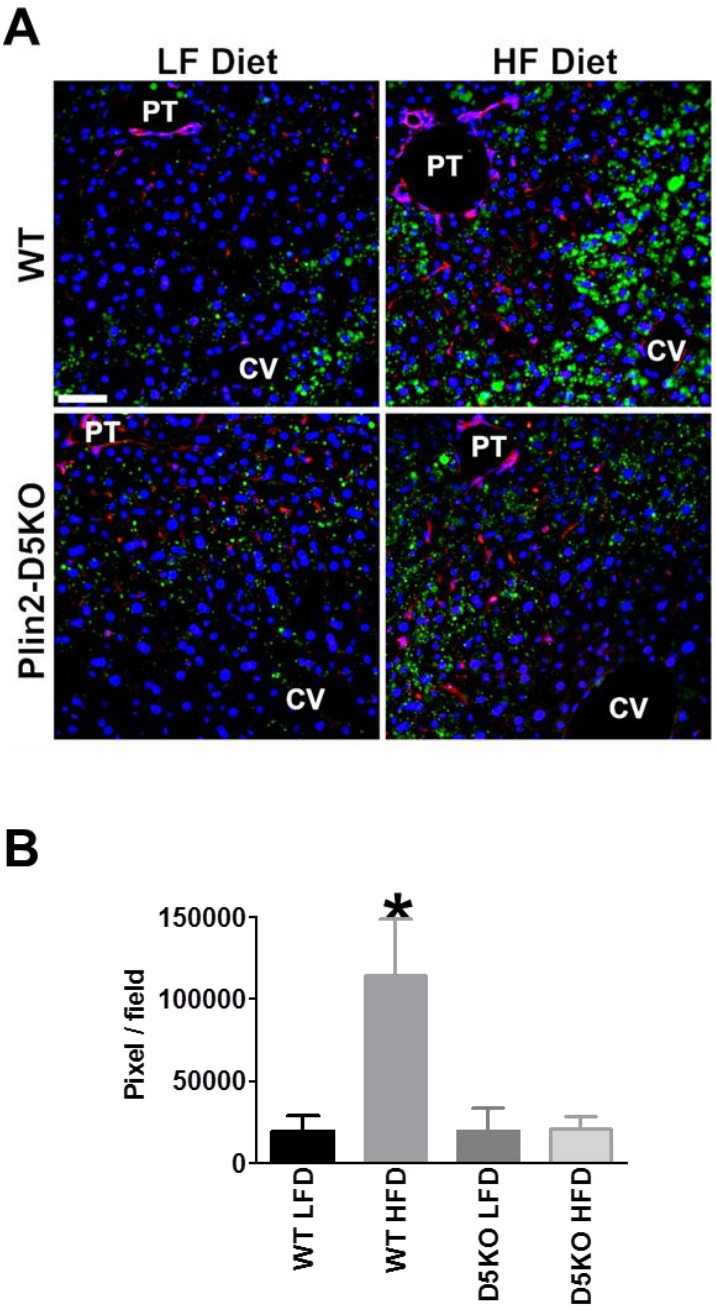

Figure IV.2 Loss of Plin2 Decreases Hepatic Accumulation

(A) Hepatic lipid accumulation from representative liver sections from WT and D5KO mice on LFD and HFD. (B) Quantitative measurements of total lipid accumulation from BODIPY stained liver sections. Values are means (± SD) for 3 animals in each group. Asterisk indicate WT-HFD values differ from WT-LFD, D5KO-LFD, and D5KO-HFD values ($p<0.0001$).

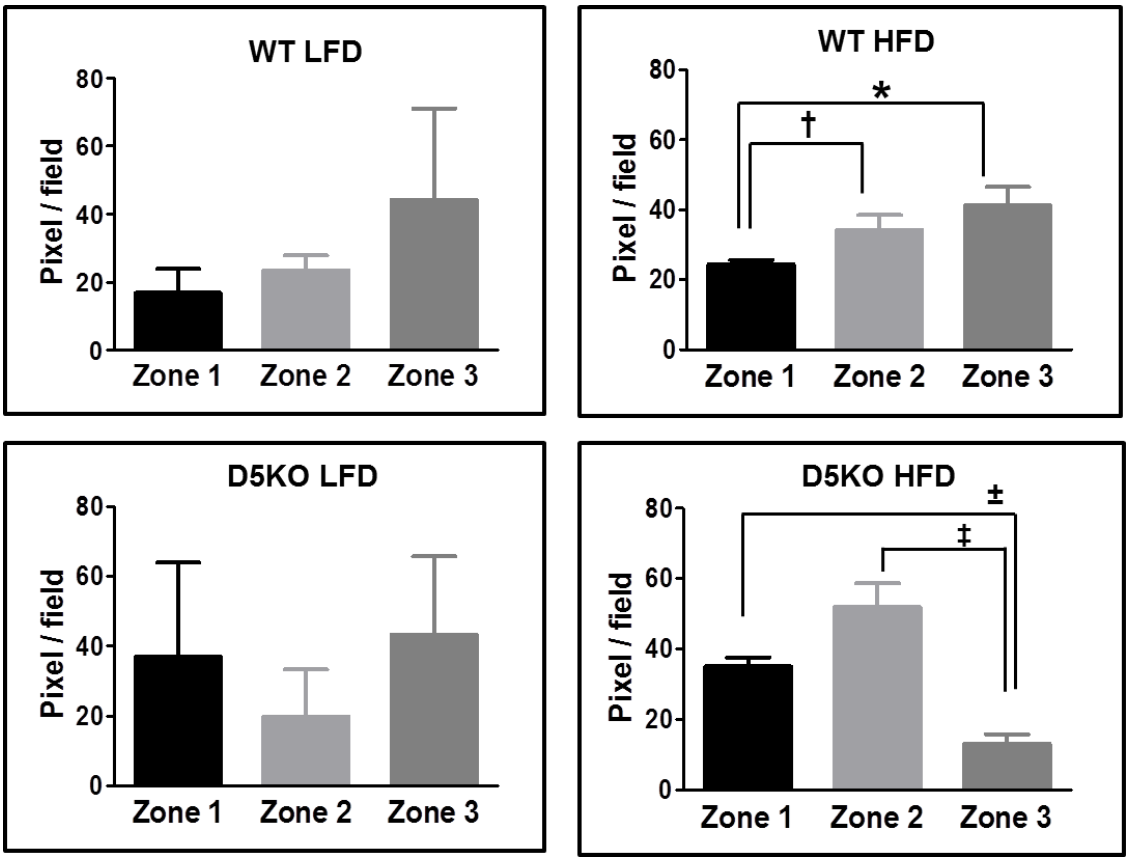

Figure IV.3 Loss of Plin2 Decreases Hepatic CLD Distribution

Quantitative measurements of total lipid accumulation in zones 1-3 as determined by BODIPY-stained liver sections. Values are means (± SD) for 3 animals in each group, with 3 sections for each zone. Asterisks indicate WT-HFD values of zone 1 differ in values from WT-HFD zone 2 ($p<0.05$), dagger indicates WT-HFD values of zone 1 differ in values from WT-HFD zone 3 ($p<0.05$). Plus/minus sign indicate D5KO-HFD values of zone 3 differ in values from D5KO-HFD zone 1, double dagger indicate D5KO-HFD values of zone 3 differ in values from D5KO-HFD of zone 2($p<0.05$). Neutral lipids were imaged from frozen liver sections using BODIPY (green) and nuclei were identified with DAPI (blue). 3i Marianas Inverted Spinning Disk was used for imaging and Slidebook 5.5 software was used for quantitation.

zone 3 compared to zones 1 or 2 in livers of WT mice re-fed the LF diet, but it did not reach significance. However, in WT mice fed the HF diet, relative lipid levels in zone 3 were significantly greater than zones 1 or 2, and relative lipid levels in zone 2 were significantly greater than zone 1 levels. I did not detect zonal differences in relative lipid accumulation in D5KO mice re-fed the LF diet. Surprisingly, I found that relative lipid accumulation was significantly increased in zones 1 and 2 compared to zone 3 in D5KO mice re-fed the HF diet. Collectively, these results indicate that Plin2 selectively contributes to hepatic lipid accumulation associated with re-feeding fasted animals a HF diet, and that it plays a role in establishing the zone dependence of this process.

The Effects of Dietary Fat Content and Plin2 Expression on CLD Lipid Content

CLD size corresponds to the quantity of stored lipid, and possibly reflects other aspects of their function [123]. To determine if dietary fat levels and Plin2 expression affect lipid storage in individual CLD, I quantified CLD size distributions in livers of HF- and LF-re-fed WT and D5KO mice (Figure IV.4). 3D-projection images of BODIPY stained CLD in hepatocytes of HF- and LF-re-fed WT and D5KO mice (Figure IV.4A), reveal significant differences in the number and size of their CLD; with hepatocytes from HF re-fed WT mice having greater numbers of CLD, and a greater percentage of large CLD, than hepatocytes from LF-re-fed WT mice or from HF- or LF-re-fed D5KO mice.

Quantification of CLD size distribution (Table IV.1 and Figure IV.4B) shows that in livers of fasted WT mice re-fed the HF diet, the distribution of CLD sizes conforms to a Gaussian curve ($P=0.016$) with CLD diameters ranging from very small (< 1 um) to relative larger (> 5 um) sizes, and a median of 2.16 μm. The CLD size distributions in hepatocytes of fasted WT animals re-fed the LF diet ($P=0.49$), or in hepatocytes of fasted

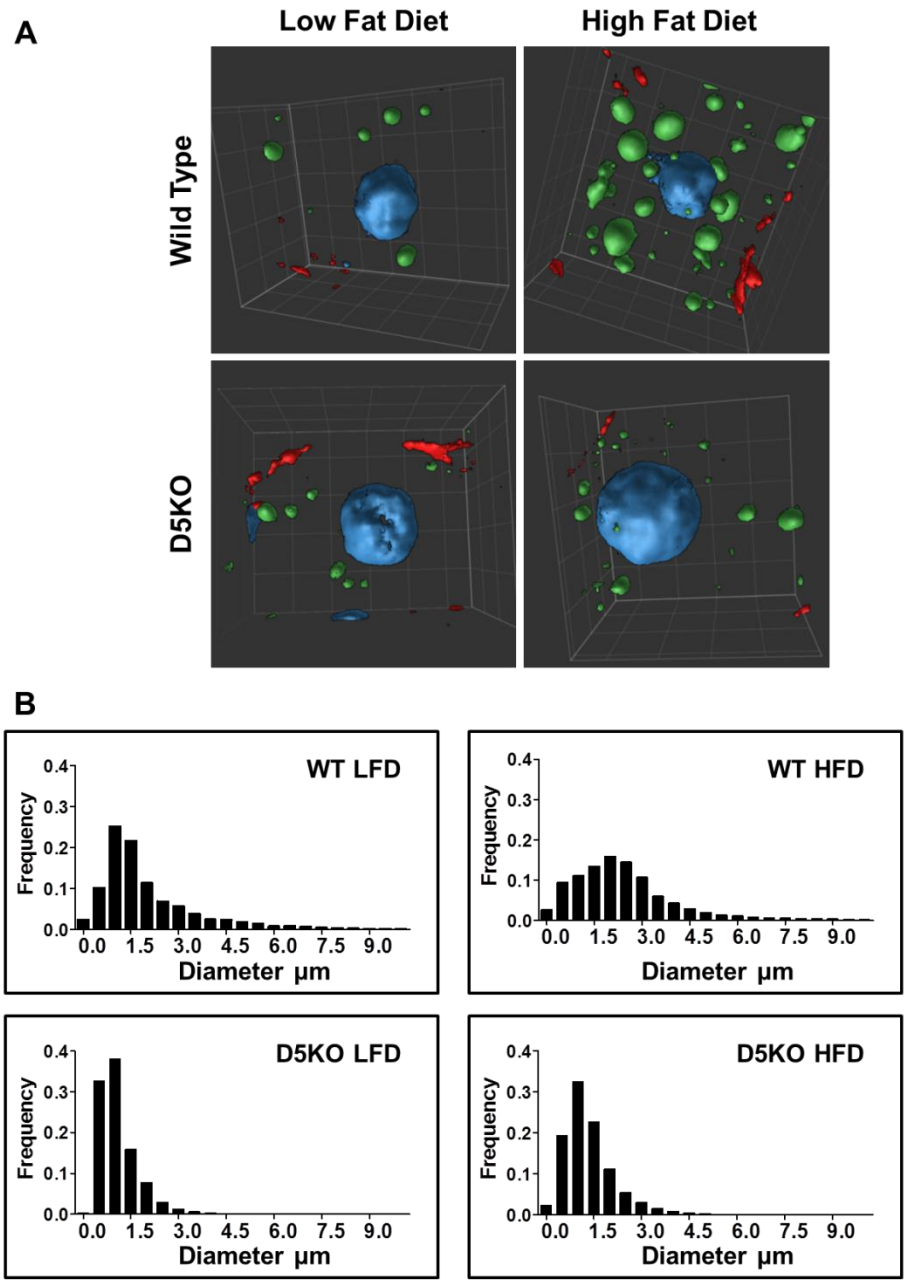

Figure IV.4 The Loss of Plin2 and Diet Decreases the Size of Hepatic CLD
The loss of Plin2 decreases the size of the CLD as determined from BODIPY imaging. (A) Representative surface-view of 3D projection images of single cells within liver sections from LF (LFD)- and HF (HFD) -re-fed WT and D5KO mice obtained at 600X magnification. Neutral lipids were imaged from frozen liver sections using BODIPY (green) and nuclei were identified with DAPI (blue). (B) Histogram analysis of size distribution from liver sections from LF (LFD)- and HF (HFD) –re-fed WT and D5KO mice. Values are for 3 animals in each group, 25 images per animal.

Table IV.1 CLD Size Properties				
	WT LFD	WT HFD	D5KO LFD	D5KO HFD
Gaussian (P-value) (D'Agostino & Person omnibus)	0.49	0.016	0.06	0.87
Median (min to max)	1.5 (0.21 – 9.970)	2.16 (0.21 – 9.98)	0.945 (0.21 – 7.56)	1.2 (0.21- 9.970)
Mann-Whitney U (two tailed)		P- Value	P- Value	P- Value
WT LFD		<0.001	<0.001	<0.001
WT HFD			<0.001	<0.001
D5KO LFD				<0.001
D5KO HFD				
Kruskal-Wallis test	P <0.001			

D5KO mice re-fed the LF (P= 0.06) or HF-diets (P=0.87)) were significantly narrower and did not conform to a normal Gaussian distribution [124] (Figure IV.4B). The median diameter of CLD in hepatocytes of fasted WT LF-re-fed animals (1.5 um), D5KO LF-re-fed (0.945 um), and D5KO HF-re-fed (1.2 um) were significantly less than that of the HF re-fed WT mice. These data demonstrate that lipid storage within individual hepatic CLD is increased by HF re-feeding relative to that of CLD in livers of LF re-fed mice, and that Plin2 deletion appears to interfere with this function.

Plin3 and Plin5 Localize to Hepatic CLD in Fasted and Re-fed D5KO

Plin3 has been shown to function in regulating hepatic lipid accumulation in WT mice following prolonged HF diet feeding [44], and there is cell culture evidence that it

compensates for the loss of Plin2 in regulating CLD accumulation in some cell types [125]. However, in livers of D5KO mice re-fed a HF diet for 12 weeks, Plin5 was found to selectively coat the few CLD present in their hepatocytes, whereas Plin3 coated CLD in stellate cells [40]. To define how Plin2 deletion affects the PLIN composition of CLD in hepatocytes in the fasting and re-feeding model, I immunostained livers sections of D5KO mice that were fasted and re-fed the HF diet with antibodies to Plins 1, 3, 4, and5. Figure IV.5A shows that many hepatocyte CLD were positive for both Plin 3 and Plin5 (white arrow), whereas others stained for Plin3 (red, large white arrowhead) or Plin5 (green, small white arrowhead) but not both.

Differences in the amount of Plin2 on hepatic CLD from fasted WT mice re-fed LF- or HF diets suggest that its CLD surface density is regulated by diet, and that differences in Plin2 CLD surface density may contribute to its physiological functions [116]. To determine if hepatic CLD levels of other PLIN family members are regulated by diet, I quantified the levels of Plin3 and Plin5 on isolated hepatic CLD from fasted D5KO mice following re-feeding with LF- or HF-diets. Figure IV.5B shows that the amount of Plin3 associated with CLD isolated from livers of HF re-fed animals was significantly less than that found on CLD from LF diet re-fed animals. In contrast, the amount of Plin5 on isolated CLD was not affected by dietary fat content.

Hepatic Plin5 transcript levels are increased by fasting [45], whereas Plin3 transcript levels are increased by prolonged HF diet feeding [44]. Consequently, I was interested in determining if the effects of diet on relative differences in hepatic CLD levels Plin3 and Plin5 are related to differences in their transcript levels. Figure IV.5C shows relative hepatic transcript levels for PLIN family members in livers of fasted WT

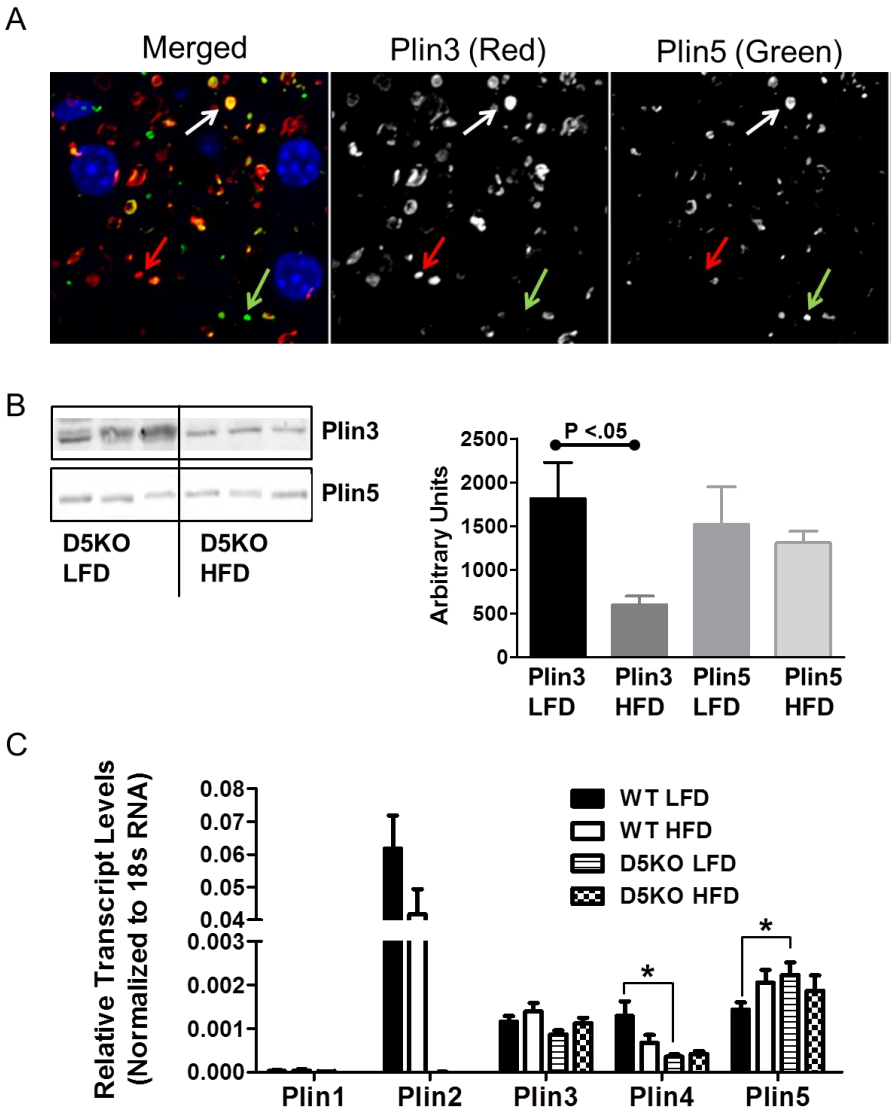

Figure IV.5 The Loss of D5KO Mice Express Hepatic Plin3 and Plin5
(A) Representative confocal immunofluorescence images of liver sections from HF re-fed D5KO mice stained with antibodies to Plin3 (green) and Plin5 (red). Nuclei in images in D and E (blue) were stained with DAPI. Arrows (white) localization of Plin3 and Plin5, (red) Plin5 and (green) Plin3. (B) Quantitative immunoblot analysis of Plin3 and Plin5 levels in enriched CLD protein extracts from fast-re-fed male D5KO mice on LF (LFD) - or HF (HFD)-diets. Insets show immunoblots of 25 μg of CLD protein from 3 mice. The graph shows the average (± SD) Plin3 or Plin5 levels normalized to 25 μg of total CLD protein from LF (N = 3) and HF (N = 3) mice. (C) Transcript levels of PLIN family members in livers of fasted and re-fed WT and D5KO mice on LFD and HFD quantified by qRT-PCR. Values are means± SD normalized to 18S RNA from 4 animals in each group. Asterisks indicate significance P <0.05.

and D5KO mice re-fed with the LF or the HF diet. With the exception of Plin1, transcripts for other PLIN family members were detected in livers of fasted mice on either of the re-feeding diets. Plin2 transcripts levels in WT livers are 30- to 50-times greater than transcript levels of PLINs 3-5, and were not affected by the content of fat in the re-feeding diet. Hepatic Plin3 transcript levels in livers of WT or D5KO mice were also not affected by dietary fat content. On the other hand, Plin5 transcript levels in livers of WT mice re-fed the LF diet were significantly decreased over those D5KO re-fed LF diet, whereas they were similar between diets in livers of D5KO and WT mice. Interestingly, I found that Plin4 transcript levels in livers of LF D5KO mice were significantly increased above those in livers of WT LF re-fed mice. However, the type of diet did not affect Plin4 transcript levels in either WT or D5KO mice. These data indicate that in previously fasted mice the effects of dietary fat on hepatic CLD levels of Plins 2, 3, or 5 are mediated by translational or post-translational mechanisms, and not by effects of fat content on their respective transcript levels.

Diet Effects on Hepatic CLD Protein Composition

The effects of Plin2 loss on hepatic lipid accumulation and zonal distribution, CLD size, and Plin3 and Plin5 associations with CLD suggest that it may be a primary determinant of hepatic CLD properties. To test this hypothesis, I used LC-MS/MS analysis of trypsin digests of CLD protein extracts to define the protein composition profiles of hepatic CLD from WT and D5KO mice re-fed with LF- or HF- diets. For these experiments, I analyzed three biological replicates from each group in triplicate. Only those proteins present in all three biological replicates, and in each of the triplicate runs, were considered for further analysis. Proteins with two or more unique peptides

Table IV.2 Isolated Hepatic CLD Proteome from WT and D5KO Mice

Amino Acid Metabolism (GO:0006520)	**Gene names**	**Accession**	**WT LFD**		**WT HFD**		**D5KO LFD**		**D5KO HFD**	
			Mean	**SD**	**Mean**	**SD**	**Mean**	**SD**	**Mean**	**SD**
Adenosyl-homocysteinase	Ahcy	P50247	0.27%	0.17%			0.43%	0.01%	0.44%	0.02%
Arginase-1	Arg1	Q61176	0.27%	0.15%			0.51%	0.02%	0.52%	0.04%
Argininosuccinate lyase	Asl	Q91YI0					0.40%	0.02%	0.53%	0.03%
Argininosuccinate synthase	Ass1	P16460	0.42%	0.28%	0.14%	0.05%	0.49%	0.05%	0.61%	0.12%
Betaine--homocysteine S-methyltransferase 1	Bhmt	O35490	0.89%	0.53%	0.31%	0.08%	0.75%	0.20%	1.03%	0.24%
Carbonic anhydrase 3	Ca3	P16015	0.31%	0.19%			0.40%	0.16%	0.45%	0.03%
Carbamoyl-phosphate synthase [ammonia], mitochondrial	Cps1	Q8C196	0.91%	0.61%	0.07%	0.03%	0.20%	0.15%	1.00%	0.43%
Cystathionine gamma-lyase	Cth	Q8VCN5					0.10%	0.01%	0.14%	0.02%
Dihydropyrimidinase	Dpys	Q9EQF5							0.10%	0.01%
Fumarylacetoacetase	Fah	P35505					0.19%	0.05%	0.23%	0.03%
Formimidoyltransferase cyclodeaminase	Ftcd	Q91XD4							0.15%	0.06%
Glutamine synthetase	Glul	P15105					0.24%	0.11%	0.26%	0.05%
Glycine N-methyltransferase	Gnmt	Q9QXF8	0.19%	0.06%	0.13%	0.05%	0.28%	0.01%	0.35%	0.02%
Aspartate aminotransferase, cytoplasmic	Got1	P05201					0.22%	0.01%	0.27%	0.03%
Alanine aminotransferase 1	Gpt	Q8QZR5							0.12%	0.04%
Homogentisate 1,2-dioxygenase	Hgd	O09173							0.10%	0.01%
4-hydroxyphenylpyruvate dioxygenase	Hpd	P49429					0.17%	0.03%	0.33%	0.00%
Cytosol aminopeptidase	Lap3	Q9CPY7					0.05%	0.03%	0.11%	0.01%
S-adenosylmethionine synthase isoform type-1	Mat1a	Q91X83	0.14%	0.03%			0.30%	0.09%	0.31%	0.10%
Phenylalanine 4 hydroxylase	Pah	P16331					0.13%	0.02%	0.22%	0.05%

Table IV.2 Isolated Hepatic CLD Proteome from WT and D5KO Mice

Urocanate hydratase	Uroc1	Q8VC12				0.06% 0.03%
Protein Metabolism (GO:0044267)						
Chaperones						
78 kDa glucose-regulated protein	Grp78	P20029	0.21% 0.01%	0.15% 0.06%	0.21% 0.07%	0.31% 0.15%
Heat shock protein HSP 90-alpha	Hsp90aa1	P07901			0.07% 0.03%	0.12% 0.02%
Heat shock protein HSP 90-beta	Hsp90ab1	P11499		0.10% 0.06%	0.47% 0.05%	0.55% 0.10%
Endoplasmin	Hsp90b1	P08113		0.06% 0.00%		0.09% 0.06%
Heat shock cognate 71 kDa protein	Hspa8	P63017	0.30% 0.11%	0.21% 0.11%	0.57% 0.07%	0.59% 0.04%
Protein disulfide-isomerase	P4hb	P09103	0.29% 0.11%	0.14% 0.11%	0.14% 0.07%	0.22% 0.06%
Protein disulfide-isomerase A3	Pdia3	P27773	0.11% 0.03%	0.11% 0.09%	0.05% 0.01%	0.08% 0.03%
Protein disulfide-isomerase A6	Pdia6	Q922R8	0.06% 0.01%	0.98% 0.13%		0.08% 0.02%
Peptidyl-prolyl cis-trans isomerase A	Ppia	P17742				0.15% 0.02%
Uricase	Uox	P25688	0.12% 0.05%	0.31% 0.02%		
Carbohydrate Meatbolism (GO:0005975)						
Fructose-bisphosphate aldolase B	Aldob	Q91Y97	0.57% 0.21%	0.08% 0.03%	0.55% 0.03%	0.50% 0.04%
Bifunctional ATP-dependent dihydroxyacetone kinase/FAD-AMP lyase (cyclizing)	Dak	Q8VC30			0.24% 0.06%	0.21% 0.04%
Alpha-enolase	Eno1	P17182	0.16% 0.08%		0.29% 0.02%	0.32% 0.05%
Fructose-1,6-bisphosphatase 1	Fbp1	Q9QXD6	0.26% 0.17%		0.37% 0.12%	0.47% 0.01%
Glyceraldehyde-3-phosphate dehydrogenase	Gapdh	P16858	0.26% 0.11%		0.30% 0.02%	0.33% 0.02%
Glycerol-3-phosphate dehydrogenase [NAD(+)], cytoplasmic	Gpd1	P13707				0.06% 0.02%

Table IV.2 Isolated Hepatic CLD Proteome from WT and D5KO Mice

Isocitrate dehydrogenase [NADP] cytoplasmic	Idh1	O88844					0.20%	0.08%	0.30%	0.02%
L-lactate dehydrogenase A chain	Ldha	P06151					0.17%	0.03%	0.20%	0.02%
Malate dehydrogenase, cytoplasmic	Mdh1	P14152	0.09%	0.06%			0.13%	0.02%	0.17%	0.01%
Phosphoglycerate kinase 1	Pgk1	P09411					0.14%	0.05%	0.17%	0.07%
Phosphoglucomutase-1	Pgm1	Q9D0F9							0.08%	0.02%
Glycogen phosphorylase, liver	Pygl	Q9ET01							0.08%	0.01%
Sorbitol dehydrogenase	Sord	Q64442					0.18%	0.02%	0.24%	0.01%
Transketolase	Tkt	P40142							0.11%	0.02%
Maleylacetoacetate isomerase	Gstz1	Q9WVL0					0.06%	0.01%	0.07%	0.05%
Triosephosphate isomerase	Tpi1	P17751					0.17%	0.02%	0.18%	0.01%
Glutathione Metabolism (GO:0006749)										
Glutathione peroxidase 1	Gpx1	P11352	0.06%	0.02%			0.17%	0.03%	0.23%	0.04%
Glutathione S-transferase A3	Gsta3	P30115	0.14%	0.05%			0.17%	0.02%	0.21%	0.04%
Glutathione S-transferase Mu 1	Gstm1	P10649	0.27%	0.01%	0.13%	0.05%	0.51%	0.11%	0.46%	0.05%
Glutathione S-transferase P 1	Gstp1	P19157	0.32%	0.11%	0.28%	0.10%	0.29%	0.07%	0.37%	0.02%
Microsomal glutathione S-transferase 1	Mgst1	Q91VS7			0.09%	0.03%			0.05%	0.02%
Lipid Metabolism (GO:0006629)										
ATP-binding cassette sub-family D member 3	Abcd3	P55096	0.08%	0.02%	0.24%	0.14%				
CGI58	Abhd5	Q9DBL9					0.22%	0.01%	0.10%	0.01%
3-ketoacyl-CoA thiolase B, peroxisomal	Acaa1b	Q8VCH0	0.14%	0.05%						

Table IV.2 Isolated Hepatic CLD Proteome from WT and D5KO Mice

3-ketoacyl-CoA thiolase, mitochondrial	Acaa2	Q8BWT1	0.12%	0.08%	0.63%	0.32%						
Very long-chain specific acyl-CoA dehydrogenase	Acadvl	P50544			0.04%	0.02%						
ATP-citrate synthase	Acly	Q91V92					0.20%	0.05%				
Peroxisomal acyl-coenzyme A oxidase 1	Acox1	Q9R0H0	0.16%	0.02%	0.15%	0.03%			0.14%	0.02%		
Long-chain-fatty-acid--CoA ligase 1	Acsl1	P41216	0.41%	0.12%	1.60%	0.26%	0.43%	0.20%	0.25%	0.02%		
Estradiol 17 beta-dehydrogenase 5	Atp5a1	Q03265	0.21%	0.14%	0.14%	0.06%						
ATP synthase subunit alpha, mitochondrial	Atp5b	P56480	0.27%	0.10%	0.49%	0.11%			0.22%	0.08%		
ATP synthase subunit beta, mitochondrial	Ces1d	Q8VCT4	0.10%	0.02%	0.08%	0.02%						
Carboxylesterase 3	Ces3a	Q63880	0.18%	0.07%	0.09%	0.02%	0.15%	0.05%	0.22%	0.04%		
Cytochrome b5	Cyb5a	P56395			0.10%	0.06%	0.11%	0.01%				
NADH-cytochrome b5 reductase 3	Cyb5r3	Q9DCN2	0.87%	0.31%	0.86%	0.07%	0.30%	0.04%	0.17%	0.04%		
Cytochrome P450 2E1	Cyp2e1	Q05421	0.12%	0.03%	0.14%	0.03%						
Peroxisomal bifunctional enzyme	Ehhadh	Q9DBM2	0.21%	0.08%	0.52%	0.08%	0.06%	0.01%	0.21%	0.08%		
Epoxide hydrolase 2	Ephx2	P34914	0.20%	0.14%			0.08%	0.06%	0.21%	0.06%		
Fatty acid synthase	Fabp1	P12710	0.33%	0.14%	0.14%	0.06%	0.33%	0.05%	0.35%	0.02%		
Hydroxymethylglutaryl-CoA synthase	Fasn	P19096	0.22%	0.15%			0.95%	0.04%				
Estradiol 17-beta-dehydrogenase 11	Hmgcs2	P54869	0.16%	0.06%	0.13%	0.08%			0.23%	0.09%		
Corticosteroid 11-beta-dehydrogenase isozyme	Hsd11b1	P50172			0.09%	0.06%						
Estradiol 17-beta-dehydrogenase 11	Hsd17b11	Q9EQ06	0.35%	0.06%	0.11%	0.02%	0.23%	0.03%	0.05%	0.00%		
17-beta-hydroxysteroid dehydrogenase 13	Hsd17b13	Q8VCR2	0.87%	0.25%	0.08%	0.05%	0.69%	0.10%	0.31%	0.02%		
Peroxisomal multifunctional enzyme type 2	Hsd17b4	P51660	0.05%	0.02%	0.14%	0.06%						
Estradiol 17 beta-dehydrogenase 5	Hsd17b5	P70694					0.23%	0.05%	0.24%	0.03%		

Table IV.2 Isolated Hepatic CLD Proteome from WT and D5KO Mice

3-keto-steroid reductase	Hsd17b7	O88736					0.19%	0.02%				
Lanosterol synthase	Lss	Q8BLN5	0.07%	0.02%	0.06%	0.04%	0.24%	0.06%				
Monoglyceride lipase	Mgll	O35678	0.29%	0.10%	0.07%	0.04%	0.10%	0.06%				
Sterol-4-alpha-carboxylate 3-dehydrogenase	Nsdhl	Q9R1J0	0.18%	0.07%	0.06%	0.02%	0.22%	0.04%				
Peroxiredoxin-6	Prdx6	O08709	0.12%	0.07%			0.24%	0.06%	0.27%	0.03%		
Phosphoenolpyruvate carboxykinase, cytosolic [GTP]	Pepck	Q9Z2V4							0.15%	0.03%		
Very long-chain acyl-CoA synthetase	Slc27a2	O35488	0.06%	0.02%	0.17%	0.05%						
Lipid Transport (GO:0006869)												
Apolipoprotein A-I	Apoa1	Q00623			0.11%	0.01%	0.08%	0.03%	0.13%	0.06%		
	Apoa4	P06728			0.10%	0.04%						
Apolipoprotein E	Apoe	P08226	0.26%	0.25%	0.22%	0.05%	0.23%	0.04%	0.18%	0.02%		
	Pgrmc1	O55022			0.05%	0.02%						
Perilipin-2	Plin2	P43883	1.93%	0.72%	0.09%	0.01%						
Perilipin-3	Plin3	Q9DBG5			0.05%	0.01%	0.48%	0.08%				
Perilipin-5	Plin5	Q8BVZ1					0.19%	0.13%				
Non-specific lipid-transfer protein	Scp2	P32020	0.09%	0.04%	0.23%	0.06%	0.11%	0.06%	0.22%	0.02%		
SEC14-like protein 2	Sec14l2	Q99J08							0.11%	0.05%		
PCTP-like protein	Stard10	Q9JMD3							0.07%	0.02%		
Nucleotide Metabolism (GO:0006975)												
Nucleoside diphosphate kinase B	Nme2	Q01768							0.08%	0.01%		
Other												

Table IV.2 Isolated Hepatic CLD Proteome from WT and D5KO Mice

D-dopachrome decarboxylase	Ddt	O35215	0.04%	0.02%			0.14%	0.02%	0.18%	0.02%
Cell death activator CIDE-B	Cideb	O70303			0.06%	0.03%	0.10%	0.02%		
Catechol O-methyltransferase	Comt	O88587					0.07%	0.02%	0.12%	0.02%
Major urinary protein 6	Mup6	P02762	0.09%	0.06%	0.37%	0.13%			0.14%	0.08%
Serine protease inhibitor A3K	Serpina3k	P07759	0.04%	0.02%			0.17%	0.05%	0.19%	0.01%
Polyubiquitin-B	Ubb	P0CG49					0.12%	0.01%	0.10%	0.02%
Elongation factor 1-alpha 1	Eef1a1	P10126	0.19%	0.11%	0.10%	0.06%	0.24%	0.06%	0.25%	0.01%
Alpha-1-antitrypsin 1-2	Serpina1b	P22599			0.07%	0.02%	0.18%	0.05%	0.17%	0.02%
Ribonuclease UK114	Hrsp12	P52760	0.13%	0.08%			0.25%	0.08%	0.33%	0.02%
Alpha-actinin-4	Actn4	P57780							0.04%	0.02%
Elongation factor 2	Eef2	P58252							0.16%	0.10%
Eukaryotic initiation factor 4A-	Eif4a1	P60843							0.07%	0.01%
Heterogeneous nuclear ribonucleoprotein K	Hnrnpk	P61979							0.05%	0.01%
14-3-3 protein epsilon	Ywhae	P62259							0.11%	0.02%
Profilin-1	Pfn1	P62962							0.07%	0.03%
14-3-3 protein zeta/delta	Ywhaz	P63101					0.16%	0.06%	0.19%	0.02%
Phosphatidylethanolamine-binding protein 1	Pebp1	P70296							0.08%	0.01%
Regucalcin	Rgn	Q64374	0.20%	0.12%			0.32%	0.10%	0.34%	0.04%
Inorganic pyrophosphatase	Ppa1	Q9D819					0.09%	0.01%	0.11%	0.01%
Phenazine biosynthesis-like domain-containing protein 1	Pbld1	Q9DCG6							0.04%	0.01%
Methyltransferase-like protein 7B	Mettl7b	Q9DD20	0.86%	0.34%	0.28%	0.05%	0.69%	0.02%	0.33%	0.03%
Bile salt export pump	Abcb11	Q9QY30			0.05%	0.01%				
Interferon-inducible GTPase 1	Iigp1	Q9QZ85	0.17%	0.08%	0.08%	0.02%				

Table IV.2 Isolated Hepatic CLD Proteome from WT and D5KO Mice

Redox/Detox (GO:0055114/ GO:0006805)												
Alcohol dehydrogenase [NADP+] dehydrogenase 1	Adh1	P00329	0.31%	0.23%			0.32%	0.05%	0.26%	0.03%
Apoptosis-inducing factor 2	Aifm2	Q8BUE4	0.08%	0.02%	0.07%	0.03%				
Retinal dehydrogenase 1	Aldh1a1	P24549	0.31%	0.19%			0.37%	0.07%		
Cytosolic 10-formyltetrahydrofolate dehydrogenase	Aldh1l1	Q8R0Y6	0.28%	0.13%			0.45%	0.07%	0.55%	0.07%
Fatty aldehyde dehydrogenase	Aldh3a2	P47740	0.07%	0.02%						
Cytochrome P450 2D10	Cyp2d10	P24456	0.14%	0.09%	0.20%	0.11%				
Cytochrome P450 2D26	Cyp2d26	Q8CIM7	0.06%	0.03%	0.99%	0.10%				
Cytochrome P450 2D9	Cyp2d9	P11714							0.04%	0.01%
Cytochrome P450 2F2	Cyp2f2	P33267	0.08%	0.03%	0.09%	0.03%				
Cytochrome P450 4A14	Cyp4a14	O35728			0.05%	0.01%				
Dehydrogenase/ reductase SDR family member 1	Dhrs1	Q99L04	1.09%	0.29%	0.20%	0.09%	0.78%	0.09%	0.34%	0.05%
Dehydrogenase/reductase SDR family member on chromosome X homolog	Dhrsx	Q8VBZ0					0.05%	0.03%		
Dimethylaniline monooxygenase [N-oxide-forming] 5	Fmo5	P97872			0.23%	0.15%				
Glyoxylate reductase/ hydroxypyruvate reductase	Grhpr	Q91Z53							0.10%	0.01%
L-gulonolactone oxidase	Gulo	P58710	0.79%	0.15%	0.21%	0.07%	0.66%	0.16%	0.14%	0.04%
3-hydroxyanthranilate 3,4-dioxygenase	Haao	Q78JT3					0.06%	0.03%	0.08%	0.01%
3 beta-hydroxysteroid dehydrogenase	Hsd3b3	P26150	0.30%	0.14%	0.16%	0.03%	0.31%	0.06%	0.08%	0.02%
3 beta-hydroxysteroid dehydrogenase type 7	Hsd3b7	Q9EQC1	0.14%	0.07%	0.09%	0.03%	0.17%	0.05%		
NADP-dependent malic enzyme	Me1	P06801					0.09%	0.01%		
Peroxiredoxin-1	Prdx1	P35700	0.27%	0.08%	0.54%	0.05%	0.29%	0.07%	0.28%	0.06%

Table IV.2 Isolated Hepatic CLD Proteome from WT and D5KO Mice

Peroxiredoxin-5, mitochondrial	Prdx5	P99029					0.08%	0.01%
Retinol dehydrogenase 7	Rdh7	O88451	0.07%	0.04%	0.12%	0.07%		
UDP-glucose 6-dehydrogenase	Ugdh	O70475					0.06%	0.03%
UDP-glucuronosyltransferase 1-1	Ugt1a1	Q63886	0.09%	0.04%	0.05%	0.04%		
UDP-glucuronosyltransferase 2A3	Ugt2a3	Q8BWQ1			0.09%	0.01%		
UDP-glucuronosyltransferase 2B17	Ugt2b17	P17717			0.04%	0.03%		
Superoxide dismutase [Cu-Zn]	Sod1	P08228					0.11%	0.07%
Catalase	Cat	P24270	0.25%	0.05%	0.19%	0.09%	0.18% 0.06%	0.28% 0.06%
Transport (GO:0006810)								
Serum albumin	Alb	P07724	0.67%	0.16%	0.35%	0.03%	1.30%	0.26%
Ferritin light chain 1	Ftl1	P29391					0.17%	0.05%
Ras-related protein Rab-11B	Rab11b	P46638			0.09%	0.02%	0.10%	0.02%
Ras-related protein Rab-14	Rab14	Q91V41	0.12%	0.10%	0.16%	0.06%		
Ras-related protein Rab-18	Rab18	P35293			0.09%	0.06%		
Ras-related protein Rab-1B	Rab1b	Q9D1G1			0.05%	0.04%		
Ras-related protein Rab-2A	Rab2a	P53994			0.10%	0.03%		
Ras-related protein Rab-7A	Rab7a	P51150	0.10%	0.00%	0.06%	0.02%		
Selenium-binding protein 2	Selenbp2	Q63836	0.37%	0.21%	0.21%	0.04%	0.65%	0.05%
Serotransferrin	Tf Trf	Q921I1					0.24%	0.12%
Transitional endoplasmic reticulum ATPase	Vcp	Q01853					0.22%	0.05% 0.20% 0.01%

and two or more unique spectra were accepted as valid identifications. Using these criteria, I identified respectively 77 and 78 proteins on CLD from WT mice, and 116 and 93 proteins on CLD from D5KO mice re-fed the HF and LF diets. The identified proteins, their Uniprot identification numbers, and estimates of their relative abundance as determined by their percentage of total spectra for WT and D5KO mice, are shown in Table IV.2. The identified proteins are organized according to Gene Ontology (GO) molecular function categories [126].

Effects of Plin2 Loss on Gene Ontology (GO) Categories of CLD Proteins

To identify possible functional interactions between Plin2 and the fat content of the re-feeding diet, I compared the number of proteins within specific GO molecular function and sub-cellular localization categories on D5KO CLD to that of WT CLD for each diet (Figure IV.6). Within GO molecular function categories (Figure IV.6A), I found that carbohydrate and amino acid metabolism enzymes were enriched, and lipid metabolism and redox/detox enzymes were depleted, on D5KO CLD relative to WT CLD for both LF- and HF-re-fed mice. I also found that lipid transport proteins were enriched on D5KO CLD relative to WT CLD in LF re-fed mice, whereas in HF fed mice there was a depletion of general transport, and lipid transport proteins on D5KO CLD compared to WT CLD.

With respect to GO sub-cellular localization categories (Figure IV.6B), I found that loss of Plin2 was associated with CLD enrichment in cytoplasmic and nuclear proteins. In the case of cytoplasmic proteins, the magnitude the enrichment was markedly greater for CLD from HF diet re-fed animals. I also found that proteins classified as ER or peroxisomal, were depleted on CLD from LF- or HF-diet re-fed

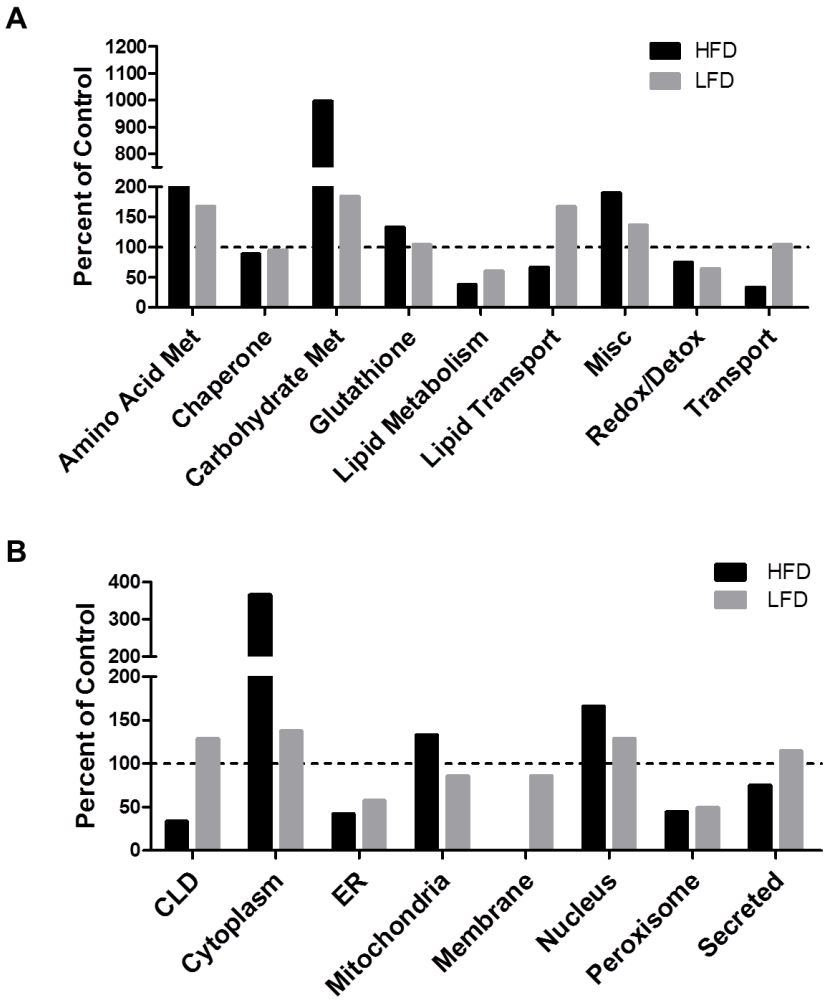

Figure IV.6 Loss of Plin2 Alters Proteins Associated with Specific Functions and Subcellular Localization

Loss of Plin2 changes CLD proteome based on (A) function and (B) subcellular localization according to gene ontology (GO) annotations. Percent of control was calculated from the number of proteins from each category for D5KO normalized to the number of proteins from each category from WT on the same diet. Dotted line represents 100% indicating no change in either direction.

D5KO mice compared to CLD from WT mice re-fed these diets. In addition, I found a marked depletion of proteins classified as CLD-associated on CLD isolated from HFD re-fed D5KO mice relative to CLD from WT mice re-fed this diet.

KEGG Pathway Interactions of WT and D5KO CLD Proteins

I previously detected enzymes associated with multiple metabolic pathways on hepatic CLD from fasted and re-fed WT mice, and found that the fat content of the re-feeding diet produced metabolic pathway-specific alterations in enzyme composition [116]. To determine how Plin2 loss affects the organization and composition of CLD-associated metabolic pathways, I mapped CLD-associated proteins from LF- and HF-re-fed WT and D5KO mice onto metabolic pathways using KEGG pathway analysis algorithms [127]. Initially, I combined the CLD proteomic results from LF- and HF-re-fed animals to simplify analysis, and define how Plin2 loss affects metabolic pathway organization on CLD independent of potential diet influences. As shown in Figure IV.7, enzymes found on hepatic WT and D5KO CLD (indicated by individual colored dots; green are common to WT and D5KO CLD, blue are specific to WT CLD and red are specific to D5KO CLD) correspond to specific, and interacting, metabolic networks (indicated by correspondingly colored lines). Enzymes composing intact fatty acid synthesis and elongation pathways were present on CLD from WT mice (green and blue dots and lines). WT CLD also contained enzymes composing components of other pathways, including specialized lipid and methionine-homocysteine metabolism pathways. The fatty acid metabolism pathway is also represented on D5KO CLD, but enzymes needed for fatty acid elongation are missing from these CLD, as indicated by the blue (WT specific) dots and lines in this pathway. However, D5KO CLD possesses

intact portions of carbohydrate, amino acid, and nucleotide metabolism pathways, including the TCA and urea cycles, which are not found on WT CLD (red dots and lines). Tables IV.3 – IV.5 contains the list of specific metabolic KEGG pathways and the proteins that were identified within each of these pathways from WT, D5KO, and the proteins shared between the WT and D5KO proteome.

Plin2 E3ffects on CLD Protein Abundance

Because a number of enzymes were common to WT and D5KO CLD (green dots, Figure IV.7), I was interested next in whether Plin2 loss might alter CLD function by influencing their relative abundance on the CLD surface. To investigate this possibility, I estimated the effects of Plin2 loss on the relative abundance of the common proteins by determining the ratio of their spectral count values for D5KO CLD to that of WT CLD for each diet. The average spectral count ratio of each protein for animals re-fed the LF- or HF-diets is shown in Table IV.5. Complete lists of these values for LF- and HF-re-fed are shown in Tables IV.6 and IV.7 respectively. Volcano plots of these data used to identify significant effects of Plin2 loss and diet on the average relative abundances of individual proteins (Figure IV.8). Differences were considered significant if p-values were less than 0.05, and relative abundance changes corresponded to a 100% or greater increase, or a 50% or greater decrease relative to WT CLD values as indicate by values lying above the lines and outside the shaded regions in Figures IV.8A and IV.8B. Relative few CLD proteins from livers of D5KO mice re-fed the LF diet had abundances that differed significantly from those of WT mice on this diet (Figure IV.8A). Among those that did, were three enzymes with abundances that were more than 3.5 fold over

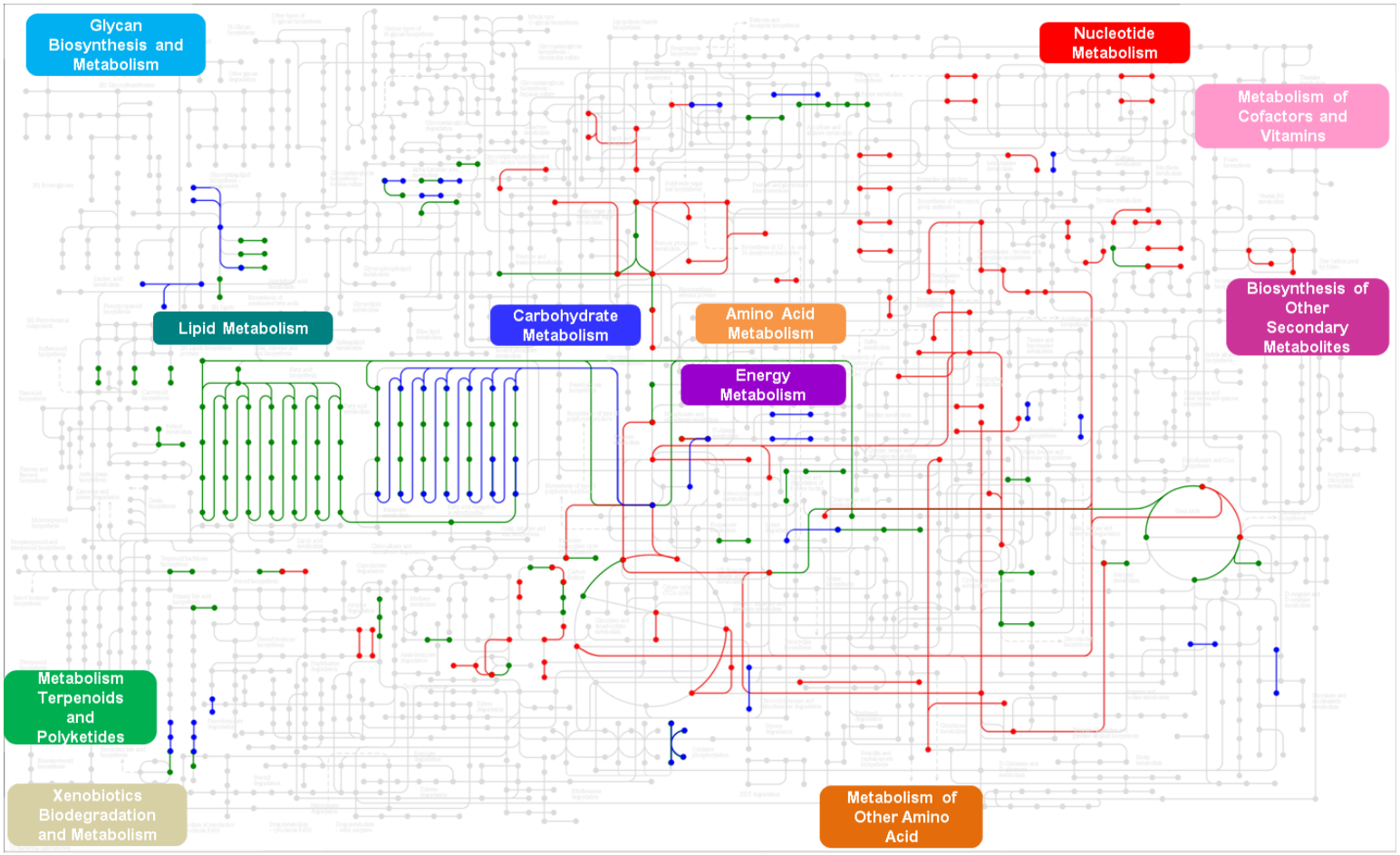

Figure IV.7 . Loss of Plin2 Alters Protein Association from Specific Pathways
KEGG analysis was used to determine proteins in the metabolic pathways specific to D5KO (red), WT (Blue) or both (green).

Table IV.3 KEGG Identities of Proteins on Hepatic CLD of WT and D5KO Mice

KEGG Pathway ID	*Gene*	*KEGG Enzyme ID*
	Metabolic pathways (mmu: 01100)	
mmu:101502	Hsd3b7	EC:1.1.1.181)
mmu:11430	Acox1	EC:1.3.3.6)
mmu:11522	Adh1	EC:1.1.1.1)
mmu:11668	Aldh1a1	EC:1.2.1.36)
mmu:11720	Mat1a	EC:2.5.1.6)
mmu:11758	Prdx6	EC:1.11.1.9 1.11.1.15)
mmu:11846	Arg1	EC:3.5.3.1)
mmu:11898	Ass1	EC:6.3.4.5)
mmu:11947	Atp5b	EC:3.6.3.14)
mmu:12116	Bhmt	EC:2.1.1.5)
mmu:13850	Ephx2	EC:3.3.2.10 3.1.3.76)
mmu:14081	Acsl1	EC:6.2.1.3)
mmu:14104	Fasn	EC:2.3.1.85 2.3.1.38 2.3.1.39 2.3.1.41 3.1.2.14 1.3.1.10 4.2.1.59 1.1.1.100)
mmu:14121	Fbp1	EC:3.1.3.11)
mmu:14433	Gapdh	EC:1.2.1.12)
mmu:15360	Hmgcs2	EC:2.3.3.10)
mmu:16987	Lss	EC:5.4.99.7)
mmu:17449	Mdh1	EC:1.1.1.37)
mmu:18194	Nsdhl	EC:1.1.1.170)
mmu:19733	Rgn	EC:3.1.1.17)
mmu:20280	Scp2	EC:2.3.1.176)
mmu:227231	Cps1	EC:6.3.4.16)
mmu:230163	Aldob	EC:4.1.2.13)
mmu:23945	Mgll	EC:3.1.1.23)
mmu:268756	Gulo	EC:1.1.3.8)
mmu:269378	Ahcy	EC:3.3.1.1)
mmu:433182	Gm5506	
mmu:74147	Ehhadh	EC:1.1.1.35 5.3.3.8 4.2.1.17)
	Peroxisome (mmu: 04146)	
mmu:11430	Acox1	EC:1.3.3.6)
mmu:12359	Cat	EC:1.11.1.6)
mmu:13850	Ephx2	EC:3.3.2.10 3.1.3.76)
mmu:14081	Acsl1	EC:6.2.1.3)
mmu:18477	Prdx1	EC:1.11.1.15)
mmu:20280	Scp2	EC:2.3.1.176)
mmu:74147	Ehhadh	EC:1.1.1.35 5.3.3.8 4.2.1.17)

Table IV.3 KEGG Identities of Proteins on Hepatic CLD of WT and D5KO Mice

	Carbon Metabolism (mmu: 01200)	
mmu:14121	Fbp1	EC:3.1.3.11)
mmu:14433	Gapdh	EC:1.2.1.12)
mmu:17449	Mdh1	EC:1.1.1.37)
mmu:19733	Rgn	EC:3.1.1.17)
mmu:227231	Cps1	EC:6.3.4.16)
mmu:230163	Aldob	EC:4.1.2.13)
mmu:433182	Gm5506	
	PPAR signaling (mmu: 03320)	
mmu:11430	Acox1	EC:1.3.3.6)
mmu:11806	Apoa1	
mmu:14080	Fabp1	
mmu:14081	Acsl1	EC:6.2.1.3)
mmu:15360	Hmgcs2	EC:2.3.3.10)
mmu:20280	Scp2	EC:2.3.1.176)
mmu:74147	Ehhadh	EC:1.1.1.35 5.3.3.8 4.2.1.17)
	Biosynthesis of amino acids (mmu:01230)	
mmu:11846	Arg1	EC:3.5.3.1)
mmu:11898	Ass1	EC:6.3.4.5)
mmu:14433	Gapdh	EC:1.2.1.12)
mmu:227231	Cps1	EC:6.3.4.16)
mmu:230163	Aldob	EC:4.1.2.13)
mmu:433182	Gm5506	
	Glutathione Metabolism (mmu:00480)	
mmu:14775	Gpx1	EC:1.11.1.9)
mmu:14859	Gsta3	EC:2.5.1.18)
mmu:14862	Gstm1	EC:2.5.1.18)
mmu:14870	Gstp1	EC:2.5.1.18)
mmu:56615	Mgst1	EC:2.5.1.18)
	Metabolism of xenobiotics by cytochrome P450 (mmu: 00980)	
mmu:11522	Adh1	EC:1.1.1.1)
mmu:14859	Gsta3	EC:2.5.1.18)
mmu:14862	Gstm1	EC:2.5.1.18)
mmu:14870	Gstp1	EC:2.5.1.18)
mmu:56615	Mgst1	EC:2.5.1.18)

Table IV.3 KEGG Identities of Proteins on Hepatic CLD of WT and D5KO Mice

Drug metabolism by cytochrome P450 (mmu: 00982)		
mmu:11522	Adh1	EC:1.1.1.1)
mmu:14859	Gsta3	EC:2.5.1.18)
mmu:14862	Gstm1	EC:2.5.1.18)
mmu:14870	Gstp1	EC:2.5.1.18)
mmu:56615	Mgst1	EC:2.5.1.18)
Glycolysis/Gluconeogenesis (mmu: 00010)		
mmu:11522	Adh1	EC:1.1.1.1)
mmu:14121	Fbp1	EC:3.1.3.11)
mmu:14433	Gapdh	EC:1.2.1.12)
mmu:230163	Aldob	EC:4.1.2.13)
mmu:433182	Gm5506	
Fatty acid metabolism (mmu: 00071)		
mmu:11430	Acox1	EC:1.3.3.6)
mmu:11522	Adh1	EC:1.1.1.1)
mmu:14081	Acsl1	EC:6.2.1.3)
mmu:74147	Ehhadh	EC:1.1.1.35 5.3.3.8 4.2.1.17)
Pentose Phosphate Pathway (mmu: 00030)		
mmu:14121	Fbp1	EC:3.1.3.11)
mmu:19733	Rgn	EC:3.1.1.17)
mmu:230163	Aldob	EC:4.1.2.13)
Arginine and Proline Metabolism (mmu:00330)		
mmu:11846	Arg1	EC:3.5.3.1)
mmu:11898	Ass1	EC:6.3.4.5)
mmu:227231	Cps1	EC:6.3.4.16)
Cysteine and Methionine (mmu: 00270)		
mmu:11720	Mat1a	EC:2.5.1.6)
mmu:12116	Bhmt	EC:2.1.1.5)
mmu:269378	Ahcy	EC:3.3.1.1)
Fat digestion and absorption (mmu: 04975)		
mmu:11806	Apoa1	
mmu:14080	Fabp1	
Tryptophan Metabolism (mmu: 00380)		
mmu:12359	Cat	EC:1.11.1.6)

Table IV.3 KEGG Identities of Proteins on Hepatic CLD of WT and D5KO Mice

mmu:74147	Ehhadh	EC:1.1.1.35 5.3.3.8 4.2.1.17)
	Primary bile acid biosynthesis (mmu:00120)	
mmu:101502	Hsd3b7	EC:1.1.1.181)
mmu:20280	Scp2	EC:2.3.1.176)
	Butanoate metabolism (mmu: 00650)	
mmu:15360	Hmgcs2	EC:2.3.3.10)
mmu:74147	Ehhadh	EC:1.1.1.35 5.3.3.8 4.2.1.17)
	Arachidonic acid metabolism (mmu: 00590)	
mmu:13850	Ephx2	EC:3.3.2.10 3.1.3.76)
mmu:14775	Gpx1	EC:1.11.1.9)
	Retinol metabolism (mmu:00830)	
mmu:11522	Adh1	EC:1.1.1.1)
mmu:11668	Aldh1a1	EC:1.2.1.36)
	HIF-1 Signaling (mmu: 04066)	
mmu:14433	Gapdh	EC:1.2.1.12)
mmu:433182	Gm5506	
	Fructose and mannose metabolism (mmu: 00051)	
mmu:14121	Fbp1	EC:3.1.3.11)
mmu:230163	Aldob	EC:4.1.2.13)
	Valine, leucine and isoleucine degradation (mmu: 00280)	
mmu:15360	Hmgcs2	EC:2.3.3.10)
mmu:74147	Ehhadh	EC:1.1.1.35 5.3.3.8 4.2.1.17)
	Insulin signaling pathway (mmu:04910)	
mmu:14104	Fasn	EC:2.3.1.85 2.3.1.38 2.3.1.39 2.3.1.41 3.1.2.14 1.3.1.10 4.2.1.59 1.1.1.100)
mmu:14121	Fbp1	EC:3.1.3.11)
	Ascorbate and aldarate metabolism (mmu: 00053)	
mmu:19733	Rgn	EC:3.1.1.17)
mmu:268756	Gulo	EC:1.1.3.8)
	Steroid hormone biosynthesis (mmu: 00140)	
mmu:16987	Lss	EC:5.4.99.7)

Table IV.3 KEGG Identities of Proteins on Hepatic CLD of WT and D5KO Mice

mmu:18194	Nsdhl	P) dependent steroid dehydrogenase-like
	Glyoxylate and dicarboxylate metabolism (mmu: 00630)	
mmu:12359	Cat	EC:1.11.1.6)
mmu:17449	Mdh1	EC:1.1.1.37)
	Glycine, serine and threonine metabolism (mmu: 00260)	
mmu:12116	Bhmt	EC:2.1.1.5)
mmu:14711	Gnmt	EC:2.1.1.20)
	Alanine, aspartate and glutamate metabolism (mmu: 00250)	
mmu:11898	Ass1	EC:6.3.4.5)
mmu:227231	Cps1	EC:6.3.4.16)
	Nitrogen metabolism (mmu: 00910)	
mmu:12350	Car3	EC:4.2.1.1)
mmu:227231	Cps1	EC:6.3.4.16)
	Oxidative phosphorylation (mmu:00190)	
mmu:11947	Atp5b	EC:3.6.3.14)
	beta-Alanine metabolism (mmu: 00410)	
mmu:74147	Ehhadh	EC:1.1.1.35 5.3.3.8 4.2.1.17)
	Phenylalanine Metabolism (mmu: 00360)	
mmu:11758	Prdx6	EC:1.11.1.9 1.11.1.15)
	Biosynthesis of unsaturated fatty acids (mmu: 01040)	
mmu:11430	Acox1	EC:1.3.3.6)
	Retrograde endocannabinoid signaling (mmu: 04723)	
mmu:23945	Mgll	EC:3.1.1.23)
	Amino sugar and nucleotide sugar metabolism (mmu: 00520)	
mmu:109754	Cyb5r3	EC:1.6.2.2)
	Propanoate metabolism (mmu: 00640)	
mmu:74147	Ehhadh	EC:1.1.1.35 5.3.3.8 4.2.1.17)
	Fatty Acid biosynthesis	
mmu:14104	Fasn	EC:2.3.1.85 2.3.1.38 2.3.1.39 2.3.1.41

Table IV.3 KEGG Identities of Proteins on Hepatic CLD of WT and D5KO Mice

		3.1.2.14 1.3.1.10 4.2.1.59 1.1.1.100)
	Pyruvate metabolism (mmu: 00620)	
mmu:17449	Mdh1	EC:1.1.1.37)
	Vitamin digestion and absorption (mmu: 04977)	
mmu:11806	Apoa1	
	alpha-Linolenic metabolism (mmu: 00592)	
mmu:11430	Acox1	EC:1.3.3.6)
	Adipocytokine signaling pathway (mmu: 4920)	
mmu:14081	Acsl1	EC:6.2.1.3)
	One carbon pool by folate (mmu: 00670)	
mmu:107747	Aldh1l1	EC:1.5.1.6)
	Tyrosine Metabolism (mmu:00350)	
mmu:11522	Adh1	
	Glycerolipid metabolism (mmu: 00561)	
mmu:23945	Mgll	EC:3.1.1.23)
	Lysine degradation (mmu: 00310)	
mmu:74147	Ehhadh	EC:1.1.1.35 5.3.3.8 4.2.1.17)
	Degradation of aromatic compounds (mmu: 01220)	
mmu:19733	Rgn	EC:3.1.1.17)
	Citrate cycle (TCA) (mmu: 00020)	
mmu:17449	Mdh1	EC:1.1.1.37)
	Synthesis and degradation of ketone bodies (mmu: 00072)	
mmu:15360	Hmgcs2	EC:2.3.3.10)

Table IV.4 KEGG Identities of Proteins Unique to Hepatic CLD of WT Mice

KEGG Pathway ID	*Gene*	*KEGG Enzyme ID*
	Metabolic pathways (mmu: 01100)	
mmu:104158	Ces1d	EC:3.1.1.1 3.1.1.67
mmu:11370	Acadvl	EC:1.3.8.9
mmu:11671	Aldh3a2	EC:1.2.1.3
mmu:11946	Atp5a1	
mmu:13106	Cyp2e1	EC:1.14.13.n7
mmu:13119	Cyp4a14	EC:1.14.15.3
mmu:15483	Hsd11b1	EC:1.1.1.146
mmu:15488	Hsd17b4	EC:4.2.1.107 4.2.1.119 1.1.1.n12
mmu:22262	Uox	EC:1.7.3.3
mmu:235674	Acaa1b	EC:2.3.1.16
mmu:394436	Ugt1a1	EC:2.4.1.17
mmu:52538	Acaa2	EC:2.3.1.16
mmu:72094	Ugt2a3	EC:2.4.1.17
	Metabolism of xenobiotics by cytochrome P450 (mmu: 00980)	
mmu:13101	Cyp2d10	EC:1.14.14.1
mmu:13106	Cyp2e1	EC:1.14.13.n7
mmu:13107	Cyp2f2	
mmu:15483	Hsd11b1	EC:1.1.1.146
mmu:394436	Ugt1a1	EC:2.4.1.17
mmu:72094	Ugt2a3	EC:2.4.1.17
mmu:76279	Cyp2d26	EC:1.14.14.1
	Drug metabolism by cytochrome P450 (mmu: 00982)	
mmu:13101	Cyp2d10	EC:1.14.14.1
mmu:13106	Cyp2e1	EC:1.14.13.n7
mmu:14263	Fmo5	EC:1.14.13.8
mmu:394436	Ugt1a1	EC:2.4.1.17
mmu:72094	Ugt2a3	EC:2.4.1.17
mmu:76279	Cyp2d26	EC:1.14.14.1
	Fatty acid metabolism (mmu: 00071)	
mmu:11370	Acadvl	EC:1.3.8.9
mmu:11671	Aldh3a2	EC:1.2.1.3
mmu:13119	Cyp4a14	EC:1.14.15.3
mmu:235674	Acaa1b	EC:2.3.1.16
mmu:52538	Acaa2	EC:2.3.1.16

Table IV.4 KEGG Identities of Proteins Unique to Hepatic CLD of WT Mice

Peroxisome (mmu: 04146)		
mmu:15488	Hsd17b4	EC:4.2.1.107 4.2.1.119 1.1.1.n12
mmu:19299	Abcd3	
mmu:235674	Acaa1b	EC:2.3.1.16
mmu:26458	Slc27a2	EC:6.2.1.3
Pentose and glucuronate interconversion (mmu: 00040)		
mmu:11671	Aldh3a2	EC:1.2.1.3
mmu:394436	Ugt1a1	EC:2.4.1.17
mmu:72094	Ugt2a3	EC:2.4.1.17
Valine, leucine and isoleucine degradation (mmu: 00280)		
mmu:11671	Aldh3a2	EC:1.2.1.3
mmu:235674	Acaa1b	EC:2.3.1.16
mmu:52538	Acaa2	EC:2.3.1.16
Ascorbate and aldarate metabolism (mmu: 00053)		
mmu:11671	Aldh3a2	EC:1.2.1.3
mmu:394436	Ugt1a1	EC:2.4.1.17
mmu:72094	Ugt2a3	EC:2.4.1.17
Steroid hormone biosynthesis (mmu: 00140)		
mmu:15483	Hsd11b1	EC:1.1.1.146
mmu:394436	Ugt1a1	EC:2.4.1.17
mmu:72094	Ugt2a3	EC:2.4.1.17
Drug metabolism (mmu: 00983)		
mmu:104158	Ces1d	EC:3.1.1.1 3.1.1.67
mmu:394436	Ugt1a1	EC:2.4.1.17
mmu:72094	Ugt2a3	EC:2.4.1.17
Retinol metabolism (mmu:00830)		
mmu:13119	Cyp4a14	EC:1.14.15.3
mmu:394436	Ugt1a1	EC:2.4.1.17
mmu:72094	Ugt2a3	EC:2.4.1.17
PPAR signaling (mmu: 03320)		
mmu:13119	Cyp4a14	EC:1.14.15.3
mmu:235674	Acaa1b	EC:2.3.1.16
mmu:26458	Slc27a2	EC:6.2.1.3

Table IV.4 KEGG Identities of Proteins Unique to Hepatic CLD of WT Mice

Starch and sucrose (mmu: 00500)		
mmu:394436	Ugt1a1	EC:2.4.1.17
mmu:72094	Ugt2a3	EC:2.4.1.17
Porphyrin and chlorophyll metabolism (mmu: 00860)		
mmu:394436	Ugt1a1	EC:2.4.1.17
mmu:72094	Ugt2a3	EC:2.4.1.17
Arachidonic acid metabolism (mmu: 00590)		
mmu:13106	Cyp2e1	EC:1.14.13.n7
mmu:13119	Cyp4a14	EC:1.14.15.3
ABC transporters (mmu: 02010)		
mmu:19299	Abcd3	
mmu:27413	Abcb11	
Oxidative phosphorylation (mmu:00190)		
mmu:11946	Atp5a1	
Fat digestion and absorption (mmu: 04975)		
mmu:11808	Apoa4	
Tryptophan Metabolism (mmu: 00380)		
mmu:11671	Aldh3a2	EC:1.2.1.3
Caffeine metabolism (mmu: 00232)		
mmu:22262	Uox	EC:1.7.3.3
beta-Alanine metabolism (mmu: 00410)		
mmu:11671	Aldh3a2	EC:1.2.1.3
Primary bile acid biosynthesis (mmu:00120)		
mmu:15488	Hsd17b4	EC:4.2.1.107 4.2.1.119 1.1.1.n12
Bile secretion (mmu: 04976)		
mmu:27413	Abcb11	
Purine metabolism (mmu:00230)		

Table IV.4 KEGG Identities of Proteins Unique to Hepatic CLD of WT Mice

mmu:22262	Uox	EC:1.7.3.3
	Glycerolipid metabolism (mmu: 00561)	
mmu:11671	Aldh3a2	EC:1.2.1.3
	Biosynthesis of unsaturated fatty acids (mmu: 01040)	
mmu:235674	Acaa1b	EC:2.3.1.16
	Histidine metabolism (mmu: 00340)	
mmu:11671	Aldh3a2	EC:1.2.1.3
	Fatty acid elongation (mmu: 00062)	
mmu:52538	Acaa2	EC:2.3.1.16
	Lysine degradation (mmu: 00310)	
mmu:11671	Aldh3a2	EC:1.2.1.3
	Linoleic acid metabolism (mmu: 00591)	
mmu:13106	Cyp2e1	EC:1.14.13.n7
	Propanoate metabolism (mmu: 00640)	
mmu:11671	Aldh3a2	EC:1.2.1.3
	Glycolysis/Gluconeogenesis (mmu: 00010)	
mmu:11671	Aldh3a2	EC:1.2.1.3
	Pyruvate metabolism (mmu: 00620)	
mmu:11671	Aldh3a2	EC:1.2.1.3
	Vitamin digestion and absorption (mmu: 04977)	
mmu:11808	Apoa4	
	alpha-Linolenic metabolism (mmu: 00592)	
mmu:235674	Acaa1b	EC:2.3.1.16
	Arginine and Proline Metabolism (mmu:00330)	
mmu:11671	Aldh3a2	EC:1.2.1.3

Table IV.5 KEGG Identities of Proteins Unique to Hepatic CLD of D5KO Mice

KEGG Pathway ID	*Gene*	*KEGG Enzyme ID*
	Metabolic pathways (mmu: 01100)	
mmu:104112	Acly	EC:2.3.3.8
mmu:107766	Haao	EC:1.13.11.6
mmu:107869	Cth	EC:4.4.1.1
mmu:109900	Asl	EC:4.3.2.1
mmu:110095	Pygl	EC:2.4.1.1
mmu:12846	Comt	EC:2.1.1.6
mmu:14085	Fah	EC:3.7.1.2
mmu:14317	Ftcd	EC:2.1.2.5 4.3.1.4
mmu:14645	Glul	EC:4.1.1.15 6.3.1.2
mmu:14718	Got1	EC:2.6.1.1
mmu:14874	Gstz1	EC:2.5.1.18 5.2.1.2
mmu:15233	Hgd	EC:1.13.11.5
mmu:15445	Hpd	EC:1.13.11.27
mmu:15490	Hsd17b7	EC:1.1.1.62 1.1.1.270
mmu:15926	Idh1	EC:1.1.1.42
mmu:16828	Ldha	EC:1.1.1.27
mmu:17436	Me1	EC:1.1.1.40
mmu:18103	Nme2	EC:2.7.4.6 2.7.13.3
mmu:18478	Pah	EC:1.14.16.1
mmu:18534	Pck1	EC:4.1.1.32
mmu:18655	Pgk1	EC:2.7.2.3
mmu:20322	Sord	EC:1.1.1.14
mmu:21881	Tkt	EC:2.2.1.1
mmu:21991	Tpi1	EC:5.3.1.1
mmu:22235	Ugdh	EC:1.1.1.22
mmu:225913	Dak	EC:2.7.1.29 4.6.1.15 2.7.1.28
mmu:243537	Uroc1	EC:4.2.1.49
mmu:64705	Dpys	EC:3.5.2.2
mmu:66988	Lap3	EC:3.4.11.5 3.4.11.1
mmu:72157	Pgm2	EC:5.4.2.2
mmu:76238	Grhpr	EC:1.1.1.79 1.1.1.81
mmu:76282	Gpt	EC:2.6.1.2
	Biosynthesis of amino acids (mmu:01230)	
mmu:107869	Cth	EC:4.4.1.1
mmu:109900	Asl	EC:4.3.2.1
mmu:14645	Glul	EC:4.1.1.15 6.3.1.2

Table IV.5 KEGG Identities of Proteins Unique to Hepatic CLD of D5KO Mice

mmu:14718	Got1	EC:2.6.1.1
mmu:15926	Idh1	EC:1.1.1.42
mmu:18478	Pah	EC:1.14.16.1
mmu:18655	Pgk1	EC:2.7.2.3
mmu:21881	Tkt	EC:2.2.1.1
mmu:21991	Tpi1	EC:5.3.1.1
mmu:76282	Gpt	EC:2.6.1.2

Carbon Metabolism (mmu: 01200)

mmu:15926	Idh1	EC:1.1.1.42
mmu:17436	Me1	EC:1.1.1.40
mmu:18655	Pgk1	EC:2.7.2.3
mmu:21881	Tkt	EC:2.2.1.1
mmu:21991	Tpi1	EC:5.3.1.1
mmu:225913	Dak	EC:2.7.1.29 4.6.1.15 2.7.1.28

Tyrosine Metabolism (mmu:00350)

mmu:12846	Comt	EC:2.1.1.6
mmu:14085	Fah	EC:3.7.1.2
mmu:14718	Got1	EC:2.6.1.1
mmu:14874	Gstz1	EC:2.5.1.18 5.2.1.2
mmu:15233	Hgd	EC:1.13.11.5
mmu:15445	Hpd	EC:1.13.11.27

Glycolysis/Gluconeogenesis (mmu: 00010)

mmu:16828	Ldha	EC:1.1.1.27
mmu:18534	Pck1	EC:4.1.1.32
mmu:18655	Pgk1	EC:2.7.2.3
mmu:21991	Tpi1	EC:5.3.1.1
mmu:72157	Pgm2	EC:5.4.2.2

Pyruvate metabolism (mmu: 00620)

mmu:16828	Ldha	EC:1.1.1.27
mmu:17436	Me1	EC:1.1.1.40
mmu:18534	Pck1	EC:4.1.1.32
mmu:76238	Grhpr	EC:1.1.1.79 1.1.1.81

Alanine, aspartate and glutamate metabolism (mmu: 00250)

mmu:109900	Asl	EC:4.3.2.1

Table IV.5 KEGG Identities of Proteins Unique to Hepatic CLD of D5KO Mice

mmu:14645	Glul	EC:4.1.1.15 6.3.1.2
mmu:14718	Got1	EC:2.6.1.1
mmu:76282	Gpt	EC:2.6.1.2

Arginine and Proline Metabolism (mmu:00330)

mmu:109900	Asl	EC:4.3.2.1
mmu:14645	Glul	EC:4.1.1.15 6.3.1.2
mmu:14718	Got1	EC:2.6.1.1
mmu:66988	Lap3	EC:3.4.11.5 3.4.11.1

Phenylalanine Metabolism (mmu: 00360)

mmu:14718	Got1	EC:2.6.1.1
mmu:15445	Hpd	EC:1.13.11.27
mmu:18478	Pah	EC:1.14.16.1

2-Oxocarboxylic acid metabolism (mmu: 01210)

mmu:14718	Got1	EC:2.6.1.1
mmu:15926	Idh1	EC:1.1.1.42
mmu:76282	Gpt	EC:2.6.1.2

Peroxisome (mmu: 04146)

mmu:15926	Idh1	EC:1.1.1.42
mmu:20655	Sod1	EC:1.15.1.1
mmu:54683	Prdx5	EC:1.11.1.15

HIF-1 Signaling (mmu: 04066)

mmu:16828	Ldha	EC:1.1.1.27
mmu:18655	Pgk1	EC:2.7.2.3
mmu:22041	Trf	

Citrate cycle (TCA) (mmu: 00020)

mmu:104112	Acly	EC:2.3.3.8
mmu:15926	Idh1	EC:1.1.1.42
mmu:18534	Pck1	EC:4.1.1.32

Starch and sucrose (mmu: 00500)

mmu:110095	Pygl	EC:2.4.1.1
mmu:22235	Ugdh	EC:1.1.1.22
mmu:72157	Pgm2	EC:5.4.2.2

Table IV.5 KEGG Identities of Proteins Unique to Hepatic CLD of D5KO Mice

Cysteine and Methionine (mmu: 00270)		
mmu:107869	Cth	EC:4.4.1.1
mmu:14718	Got1	EC:2.6.1.1
mmu:16828	Ldha	EC:1.1.1.27
Amino sugar and nucleotide sugar metabolism (mmu: 00520)		
mmu:22235	Ugdh	EC:1.1.1.22
mmu:72157	Pgm2	EC:5.4.2.2
Glutathione Metabolism (mmu:00480)		
mmu:15926	Idh1	EC:1.1.1.42
mmu:66988	Lap3	EC:3.4.11.5 3.4.11.1
Pyrimidine metabolism (mmu:00240)		
mmu:18103	Nme2	EC:2.7.4.6 2.7.13.3
mmu:64705	Dpys	EC:3.5.2.2
Purine metabolism (mmu:00230)		
mmu:18103	Nme2	EC:2.7.4.6 2.7.13.3
mmu:72157	Pgm2	EC:5.4.2.2
Fructose and mannose metabolism (mmu: 00051)		
mmu:20322	Sord	EC:1.1.1.14
mmu:21991	Tpi1	EC:5.3.1.1
Histidine metabolism (mmu: 00340)		
mmu:14317	Ftcd	EC:2.1.2.5 4.3.1.4
mmu:243537	Uroc1	EC:4.2.1.49
Insulin signaling pathway (mmu:04910)		
mmu:110095	Pygl	EC:2.4.1.1
mmu:18534	Pck1	EC:4.1.1.32
Glyoxylate and dicarboxylate metabolism (mmu: 00630)		
mmu:14645	Glul	EC:4.1.1.15 6.3.1.2
mmu:76238	Grhpr	EC:1.1.1.79 1.1.1.81
Steroid hormone biosynthesis (mmu: 00140)		
mmu:12846	Comt	EC:2.1.1.6
mmu:15490	Hsd17b7	EC:1.1.1.62 1.1.1.270

Table IV.5 KEGG Identities of Proteins Unique to Hepatic CLD of D5KO Mice

Glycine, serine and threonine metabolism (mmu: 00260)

mmu:107869	Cth	EC:4.4.1.1
mmu:76238	Grhpr	EC:1.1.1.79 1.1.1.81

Phenylalanine, tyrosine and tryptophan biosynthesis (mmu: 00400)

mmu:14718	Got1	EC:2.6.1.1
mmu:18478	Pah	EC:1.14.16.1

PPAR signaling (mmu: 03320)

mmu:17436	Me1	EC:1.1.1.40
mmu:18534	Pck1	EC:4.1.1.32

Oxidative phosphorylation (mmu:00190)

mmu:67895	Ppa1	EC:3.6.1.1

Tryptophan Metabolism (mmu: 00380)

mmu:107766	Haao	EC:1.13.11.6

beta-Alanine metabolism (mmu: 00410)

mmu:64705	Dpys	EC:3.5.2.2

Pentose and glucuronate interconversion (mmu: 00040)

mmu:22235	Ugdh	EC:1.1.1.22

Galactose metabolism (mmu: 00052)

mmu:72157	Pgm2	EC:5.4.2.2

Glycerophospholipid metabolism (mmu: 00564)

mmu:14555	Gpd1	EC:1.1.1.8

Propanoate metabolism (mmu: 00640)

mmu:16828	Ldha	EC:1.1.1.27

Metabolism of xenobiotics by cytochrome P450 (mmu: 00980)

mmu:13105	Cyp2d9	EC:1.14.14.1

Adipocytokine signaling pathway (mmu: 4920)

mmu:18534	Pck1	EC:4.1.1.32

Table IV.5 KEGG Identities of Proteins Unique to Hepatic CLD of D5KO Mice

Drug metabolism by cytochrome P450 (mmu: 00982)		
mmu:13105	Cyp2d9	EC:1.14.14.1
One carbon pool by folate (mmu: 00670)		
mmu:14317	Ftcd	EC:2.1.2.5 4.3.1.4
Glycerolipid metabolism (mmu: 00561)		
mmu:225913	Dak	EC:2.7.1.29 4.6.1.15 2.7.1.28
Pantothenate and CoA biosynthesis (mmu: 00770)		
mmu:64705	Dpys	EC:3.5.2.2
Ascorbate and aldarate metabolism (mmu: 00053)		
mmu:22235	Ugdh	EC:1.1.1.22
Steroid biosynthesis (mmu: 00100)		
mmu:15490	Hsd17b7	EC:1.1.1.62 1.1.1.270
Inositol phosphate metabolism (mmu:00562)		
mmu:21991	Tpi1	EC:5.3.1.1
Selenocompound metabolism (mmu: 00450)		
mmu:107869	Cth	EC:4.4.1.1
Drug metabolism (mmu: 00983)		
mmu:64705	Dpys	EC:3.5.2.2
Nitrogen metabolism (mmu: 00910)		
mmu:14645	Glul	EC:4.1.1.15 6.3.1.2

Table IV.6 D5KO Proteins Enriched and Depleted on LFD compared to WT

Gene Ontology Category	Gene	Accession Number	Fold Change	P-value
Amino Acid Metabolism (GO:0006520)				
Betaine--homocysteine S-methyltransferase 1	Bhmt	O35490	5.92	0.03
Argininosuccinate synthase	Ass1	P16460	4.38	0.04
Carbamoyl-phosphate synthase [ammonia], mitochondrial	Cps1	Q8C196	1.60	0.36
Glycine N-methyltransferase	Gnmt	Q9QXF8	3.90	0.00
Carbohydrate Meatbolism (GO:0005975)				
Fructose-bisphosphate aldolase B	Aldob	Q91Y97	3.13	0.02
Protein Metabolism (GO:0044267)				
Chaperones				
Endoplasmin	Hsp90b1	P08113	0.96	0.94
Protein disulfide-isomerase	P4hb	P09103	1.02	0.90
Heat shock protein HSP 90-beta	Hsp90ab1	P11499	9.54	0.01
78 kDa glucose-regulated protein	Grp78	P20029	1.11	0.74
Protein disulfide-isomerase A3	Pdia3	P27773	0.53	0.12
Heat shock cognate 71 kDa protein	Hspa8	P63017	2.85	0.02
Protein disulfide-isomerase A6	Pdia6	Q922R8	0.98	0.95
Glutathione Metabolism (GO:0006749)				
Glutathione S-transferase Mu 1	Gstm1	P10649	4.63	0.00
Glutathione S-transferase P 1	Gstp1	P19157	2.60	0.01
Microsomal glutathione S-transferase 1	Mgst1	Q91VS7	0.56	0.03

Table IV.6 D5KO Proteins Enriched and Depleted on LFD compared to WT

Lipid Metabolism (GO:0006629)				
Fatty acid synthase	Fabp1	P12710	2.71	0.01
Long-chain-fatty-acid--CoA ligase 1	Acsl1	P41216	0.46	0.01
Estradiol 17-beta-dehydrogenase 11	Hmgcs2	P54869	1.64	0.14
Cytochrome b5	Cyb5a	P56395	1.25	0.33
ATP synthase subunit alpha, mitochondrial	Atp5b	P56480	0.90	0.74
Carboxylesterase 3	Ces3a	Q63880	1.06	0.70
17-beta-hydroxysteroid dehydrogenase 13	Hsd17b13	Q8VCR2	0.32	0.01
Peroxisomal bifunctional enzyme	Ehhadh	Q9DBM2	1.06	0.79
NADH-cytochrome b5 reductase 3	Cyb5r3	Q9DCN2	0.33	0.02
Estradiol 17-beta-dehydrogenase 11	Hsd17b11	Q9EQ06	0.16	0.02
Peroxisomal acyl-coenzyme A oxidase 1	Acox1	Q9R0H0	1.74	0.15
Lipid Transport (GO:0006869)				
Apolipoprotein E	Apoe	P08226	0.51	0.00
Non-specific lipid-transfer protein	Scp2	P32020	2.01	0.15
Apolipoprotein A-I	Apoa1	Q00623	0.58	0.45
Other				
Major urinary protein 6	Mup6	P02762	1.12	0.22
Elongation factor 1-alpha 1	Eef1a1	P10126	1.75	0.26
Alpha-1-antitrypsin 1-2	Serpina1b	P22599	4.53	0.02
Methyltransferase-like protein 7B	Mettl7b	Q9DD20	0.39	0.01
Redox/Detox (GO:0055114/ GO:0006805)				
Retinol dehydrogenase 7	Rdh7	O88451	0.95	0.86
Catalase	Cat	P24270	1.91	0.08
Cytochrome P450 2D10	Cyp2d10	P24456	1.00	1.00
3 beta-hydroxysteroid dehydrogenase	Hsd3b3	P26150	0.24	0.00
Peroxiredoxin-1	Prdx1	P35700	3.19	0.04
L-gulonolactone oxidase	Gulo	P58710	0.29	0.03
Dehydrogenase/ reductase SDR family member 1	Dhrs1	Q99L04	0.34	0.01
Transport (GO:0006810)				
Serum albumin	Alb	P07724	3.45	0.00
Selenium-binding protein 2	Selenbp2	Q63836	6.65	0.00

Table IV.7 D5KO Proteins Enriched and Depleted on HFD compared to WT

Gene Ontology Category	Gene	Accession Number	Fold Change	P-value
Amino Acid Metabolism (GO:0006520)				
Betaine--homocysteine S-methyltransferase 1	Bhmt	O35490	0.84	0.55
Carbonic anhydrase 3	Ca3	P16015	1.27	0.09
Argininosuccinate synthase	Ass1	P16460	1.17	0.66
Adenosyl-homocysteinase	Ahcy	P50247	1.61	0.26
Arginase-1	Arg1	Q61176	1.85	0.10
Carbamoyl-phosphate synthase [ammonia], mitochondrial	Cps1	Q8C196	0.22	0.21
S-adenosylmethionine synthase isoform type-1	Mat1a	Q91X83	2.12	0.12
Glycine N-methyltransferase	Gnmt	Q9QXF8	1.45	0.17
Carbohydrate Meatbolism (GO:0005975)				
Malate dehydrogenase, cytoplasmic	Mdh1	P14152	1.53	0.35
Glyceraldehyde-3-phosphate dehydrogenase	Gapdh	P16858	1.14	0.55
Alpha-enolase	Eno1	P17182	1.80	0.07
Fructose-bisphosphate aldolase B	Aldob	Q91Y97	0.97	0.90
Fructose-1,6-bisphosphatase 1	Fbp1	Q9QXD6	1.46	0.27
Protein Metabolism (GO:0044267) Chaperones				
Protein disulfide-isomerase	P4hb	P09103	0.49	0.26
78 kDa glucose-regulated protein	Grp78	P20029	1.00	1.00
Protein disulfide-isomerase A3	Pdia3	P27773	0.47	0.04

Table IV.7 D5KO Proteins Enriched and Depleted on HFD compared to WT

Heat shock cognate 71 kDa protein	Hspa8	P63017	1.89	0.03
Glutathione Metabolism (GO:0006749)				
Glutathione S-transferase Mu 1	Gstm1	P10649	1.88	0.06
Glutathione peroxidase 1	Gpx1	P11352	2.67	0.06
Glutathione S-transferase P 1	Gstp1	P19157	0.89	0.69
Glutathione S-transferase A3	Gsta3	P30115	1.16	0.54
Lipid Metabolism (GO:0006629)				
Peroxiredoxin-6	Prdx6	O08709	2.05	0.08
Monoglyceride lipase	Mgll	O35678	0.34	0.17
Fatty acid synthase	Fabp1	P12710	1.00	1.00
Hydroxymethylglutaryl-CoA synthase	Fasn	P19096	4.33	0.01
Epoxide hydrolase 2	Ephx2	P34914	0.40	0.12
Long-chain-fatty-acid--CoA ligase 1	Acsl1	P41216	1.07	0.59
Carboxylesterase 3	Ces3a	Q63880	0.85	0.72
Lanosterol synthase	Lss	Q8BLN5	3.67	0.04
17-beta-hydroxysteroid dehydrogenase 13	Hsd17b13	Q8VCR2	0.79	0.24
Peroxisomal bifunctional enzyme	Ehhadh	Q9DBM2	0.28	0.08
NADH-cytochrome b5 reductase 3	Cyb5r3	Q9DCN2	0.34	0.10
Estradiol 17-beta-dehydrogenase 11	Hsd17b11	Q9EQ06	0.65	0.05
Sterol-4-alpha-carboxylate 3-dehydrogenase	Nsdhl	Q9R1J0	1.26	0.13
Lipid Transport (GO:0006869)				
Apolipoprotein E	Apoe	P08226	0.89	0.83
Non-specific lipid-transfer protein	Scp2	P32020	1.19	0.70
Other				
D-dopachrome decarboxylase	Ddt	O35215	3.94	0.01
Serine protease inhibitor A3K	Serpina3k	P07759	4.25	0.07
Elongation factor 1-alpha 1	Eef1a1	P10126	1.24	0.65
Ribonuclease UK114	Hrsp12	P52760	1.96	0.28
Regucalcin	Rgn	Q64374	1.64	0.13
Methyltransferase-like protein 7B	Mettl7b	Q9DD20	0.81	0.47

Table IV.7 D5KO Proteins Enriched and Depleted on HFD compared to WT

Redox/Detox (GO:0055114/ GO:0006805)				
Alcohol dehydrogenase [NADP+] dehydrogenase 1	Adh1	P00329	1.01	0.99
Catalase	Cat	P24270	0.71	0.16
Retinal dehydrogenase 1	Aldh1a1	P24549	1.18	0.52
3 beta-hydroxysteroid dehydrogenase	Hsd3b3	P26150	1.03	0.92
Peroxiredoxin-1	Prdx1	P35700	1.10	0.02
L-gulonolactone oxidase	Gulo	P58710	0.83	0.28
Cytosolic 10-formyltetrahydrofolate dehydrogenase	Aldh1l1	Q8R0Y6	1.60	0.06
Dehydrogenase/ reductase SDR family member 1	Dhrs1	Q99L04	0.71	0.15
3 beta-hydroxysteroid dehydrogenase type 7	Hsd3b7	Q9EQC1	1.23	0.19
Transport (GO:0006810)				
Serum albumin	Alb	P07724	1.94	0.12
Selenium-binding protein 2	Selenbp2	Q63836	1.76	0.12

WT CLD values, and one that was less than 50% of its WT value. In contrast, I found 22 proteins on hepatic CLD from D5KO mice re-fed that HF diet that differed significantly in abundance from that found on CLD from HF re-fed WT mice (Figure IV.8B). Of these, 9 exhibited significantly decreased relative abundance, and 13 exhibited significantly increased relative abundance. Among the 13 proteins with increased abundance, two were members of the one-carbon metabolism pathway (BHMT and glycine –methyltransferase), and several related to the glutathione pathway. Among the 9 proteins with decreased abundance on D5KO CLD, several were associated with steroid biosynthesis. The identities and KEGG pathway assignments of CLD proteins with significant differences in relative abundances between WT and D5KO CLD on LF- and HF-diets are listed in table IV.6 and table IV.7.

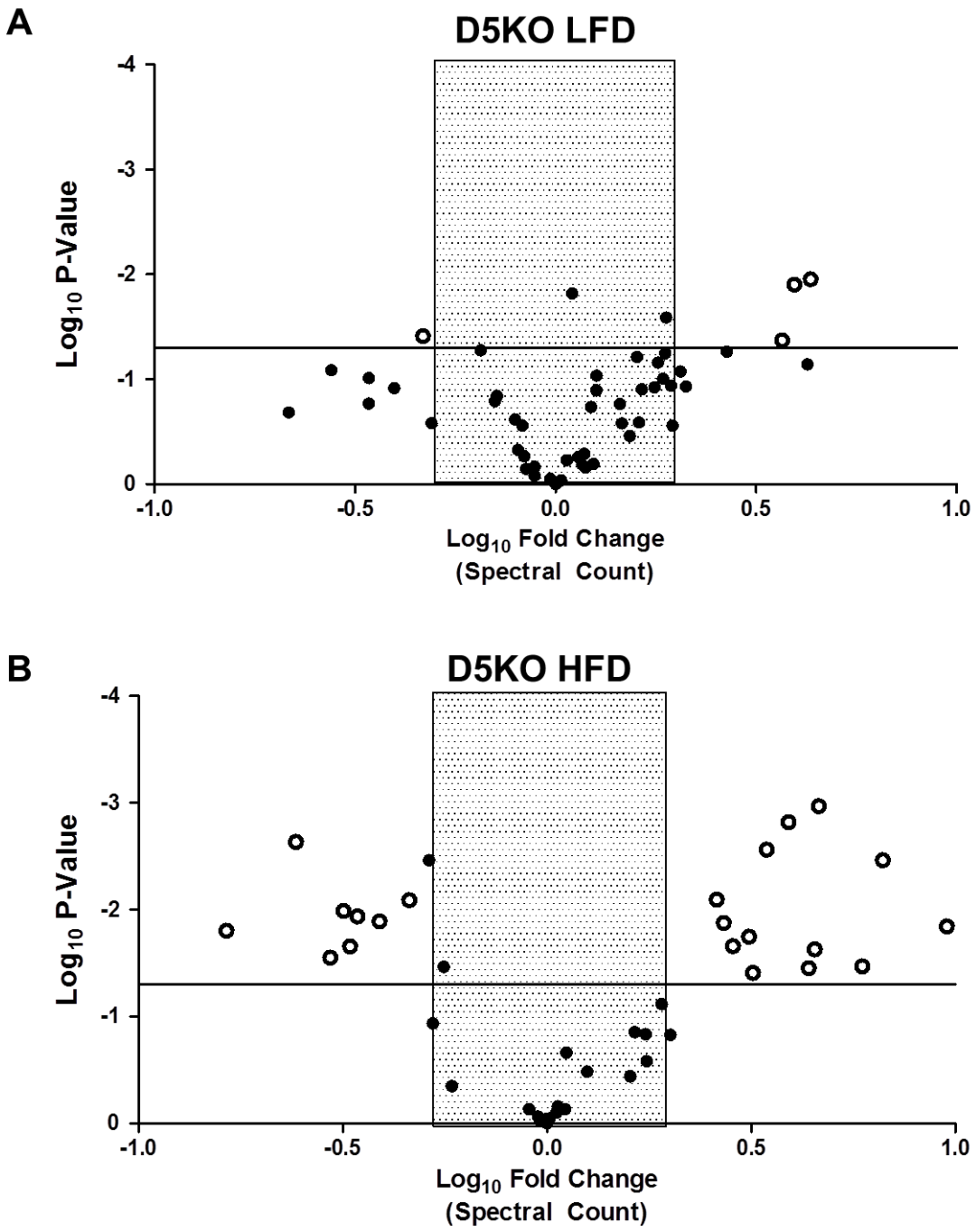

Figure IV.8 . Loss of Plin2 Has Greater Effect with HFD
Volcano plots of D5KO vs. WT on (A) LFD and (B) HFD. Area in the shaded box represent fold changed less than two. Straight line represents P <0.05. Areas outside the shaded box and above the line represent proteins that have more than a twofold change in either direction compared to WT and are have a p value less than 0.05 (open circles). Areas inside the shaded box and below the line represents proteins that have less than a twofold change in either direction, and have p value greater than 0.05 (dark circles).

Effects of Plin2 and Diet on CLD Associated Metabolic Pathways

I used the proteomics data, and volcano plot results to map specific KEGG pathway modifications associated with Plin2 loss following LF- or HF-re-feeding conditions (Figures IV.9 and IV.10). Modifications were classified as enriched (red), depleted (blue), or unchanged (black) relative to WT CLD on each diet. Figure IV.9 shows that in LF-re-fed mice, loss of Plin2 is associated with enrichment of enzymes of the fatty acid synthesis pathway and enzymes that link fatty acid synthesis and fatty acid elongation pathways. There were also increased amounts of enzymes related to amino acid metabolism, as well as portions of the glycolysis, urea and TCA cycles. Conversely, enzymes of the fatty acid elongation pathway and portions of other lipid metabolism and detoxification pathways were depleted by loss of Plin2. Figure IV.10 shows that in HF-re-fed mice, loss of Plin2 is associated with increases in enzymes related to distinct portions of the amino acid, nucleotide and citrate metabolism pathways and the urea cycle, and decreases in enzymes of the fatty acid elongation pathway, and portions of other lipid metabolism and detoxification pathways.

Discussion

Observations that Plin2 deficiency impairs fatty liver formation in mice chronically re-fed a HF diet [37, 38, 40] suggest that Plin2 is a critical regulator of hepatic lipid accumulation. However, physiological adaptations occur during prolonged HF diet feeding [128-131] that may influence phenotypic responses to reduced Pln2 expression, and complicate understanding of its physiological roles. In this study, I used acute fasting and feeding model that avoid adaptive responses to define how Plin2 loss affects hepatic lipid accumulation and CLD properties. The major findings of my study

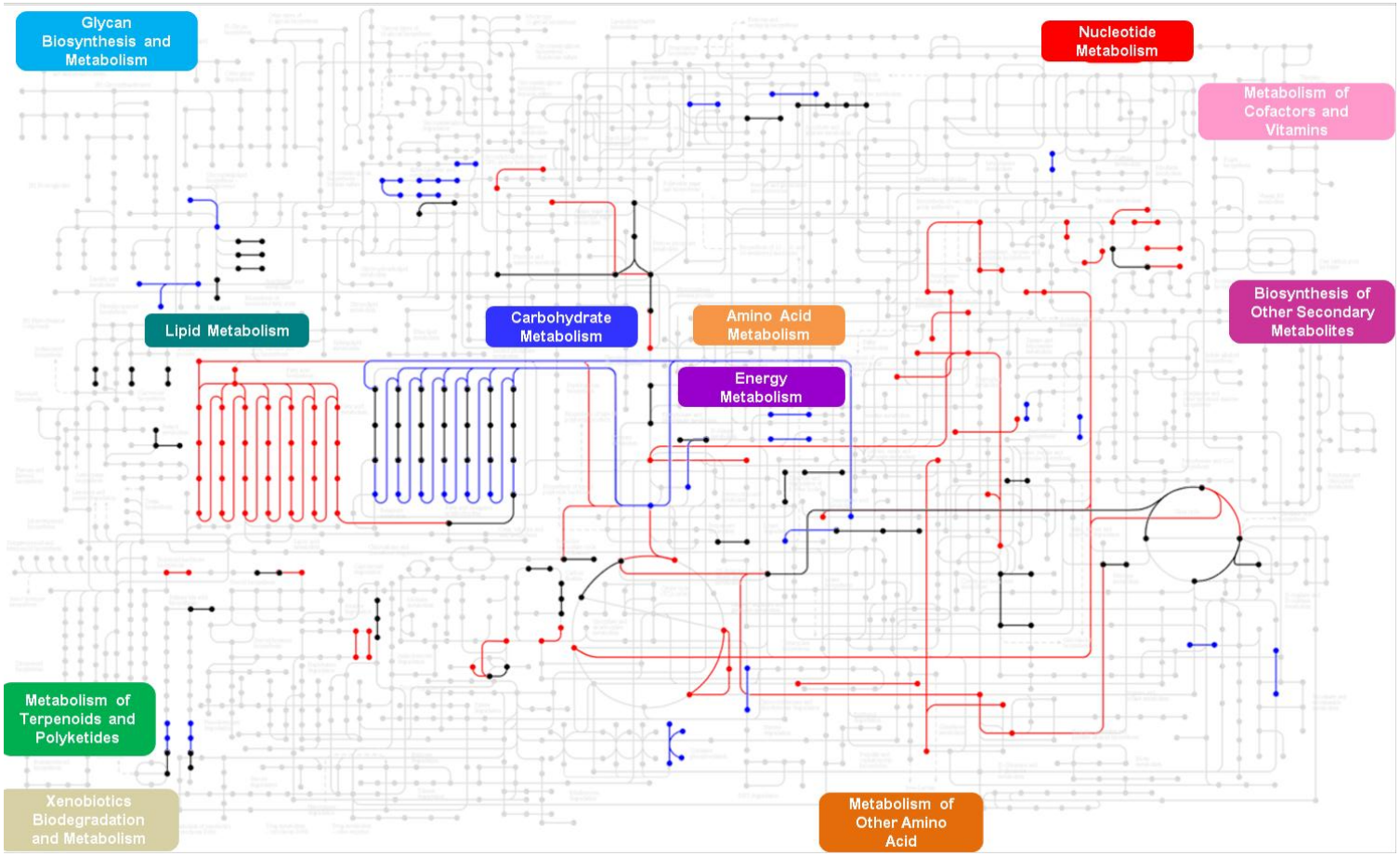

Figure IV.9 . Diet Influences Different Metabolic Pathways on CLD Proteome in D5KO Mice
KEGG analysis was used to determine proteins in the metabolic pathways that were depleted (red), enriched (blue), or unchanged (black) on CLD from LF- re-fed D5KO compared to WT.

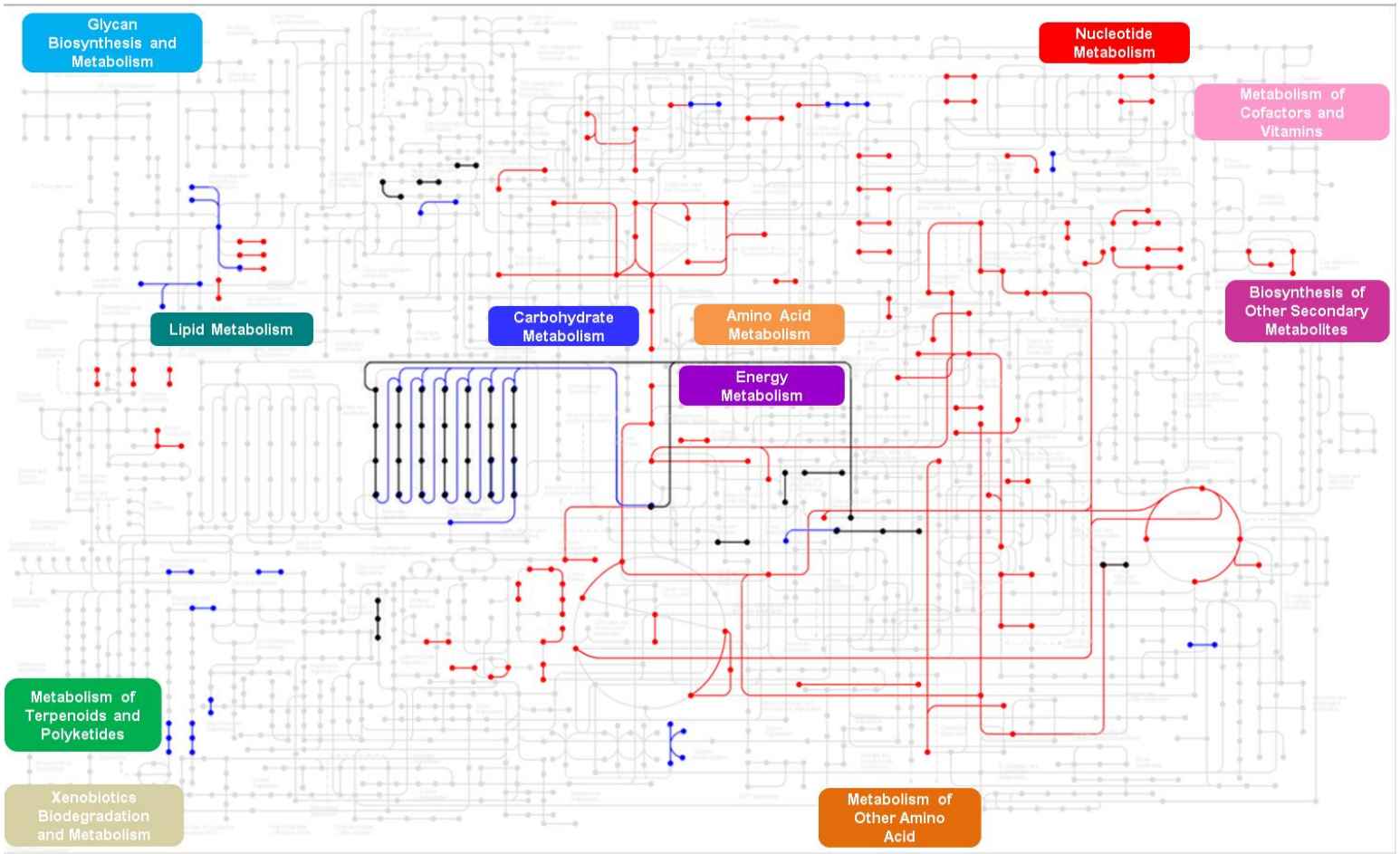

Figure IV.10. Diet Influences Different Metabolic Pathways on CLD Proteome in D5KO Mice
KEGG analysis was used to determine proteins in the metabolic pathways that were depleted (red), enriched (blue), or unchanged (black) on CLD HF-re-fed D5KO compared to WT.

are that Plin2 deletion impairs lipid accumulation induced by acute re-feeding fasted mice a HF diet; that normal zone specificities of hepatic lipid accumulation associated with HF diet re-feeding are disrupted in Plin2-null mice; that Plin2 loss reduces the size and alters the protein composition of CLD; and that dietary fat content and Plin2 interact in regulating CLD protein composition. Collectively, these results provide direct evidence that Plin2 is a physiologically important determinant of hepatic lipid accumulation and CLD properties, and that it may contribute to how the liver integrates metabolic responses to increased lipid exposure.

The Role of Plin2 in Hepatic Metabolism and Lipid Accumulation

The ability of Plin2 deletion to prevent obesity and fatty liver in mice re-fed HF diet for prolonged periods is associated with reduced food intake, lower adiposity, and decreased positive energy imbalance [40]. In contrast, in the fasting and re-feeding model, I found that the effects of Plin2 loss on hepatic lipid properties of HF re-fed mice were not associated with alterations in body or liver weights, adiposity, or reduction in food intake. Indirect calorimetry experiments further demonstrated that Plin2 deletion did not affect the general metabolic properties of the mice prior to, or in response to, fasting. Although the magnitude of RER values of D5KO mice re-fed the LF diet was less than that found for WT mice, overall the RER responses of D5KO mice to re-feeding LF- or HF-diets were physiologically appropriate and consistent with those of WT mice. Thus, within the context of fasting and re-feeding with a HF diet, my results are consistent with the hypothesis that Plin2 plays a direct role in regulating hepatic lipid properties that is independent of effects on energy consumption, body weight or substantial alterations in metabolic responses to fasting and re-feeding.

Specific Functions of Plin2 in Hepatocyte Lipid Biology

[40]The degree to which members of the PLIN family are able to substitute for one another in regulating cellular lipid properties remains an open question. Plin3 shares significant sequence and structural similarity to Plin2 [132, 133], and based on cell culture evidence [125], it has been suggested that Plin3 is able to substitute for loss of Plin2 in regulating lipid storage. However, data from this study add to the growing body of evidence that Plin3 does not fully substitute for loss of Plin2 in regulating HF diet re-feeding effects on lipid accumulation, or CLD properties in the mouse liver [37, 38, 40]. My data also adds to evidence that Plin5 does not compensate for Plin2 loss in regulating hepatic CLD accumulation in response to prolonged HF diet feeding [40].

Conversely, results showing that Plin2 loss did not significantly affect hepatic lipid levels, their zonal distribution, or CLD size in fasted mice re-fed the LF diet suggest that its hepatic functions may be influenced by diet and/or the metabolic properties of the liver. Additional studies are required to understand how diet, metabolism, and Plin2 interact in regulating hepatic lipid accumulation. However, my proteomic data demonstrating that the effects of Plin2 loss on CLD protein compositions depend on the fat content of the diet, and indirect calorimetry data demonstrating that Plin2 loss selectively affected RER values of LF-re-fed mice, provide evidence that interactions may involve more than one mechanism. Interestingly, my observation that LF diet re-feeding of fasted D5KO mice led to an increase in CLD levels of Plin3 relative to that observed in HF-re-fed mice, suggests that the hepatic functions of Plin3 also may be influenced by diet and/or metabolism. Understanding how diet, hepatic metabolism, and the functions of Plin2, and possibly other PLIN family members, are integrated in regulating hepatic lipid accumulation will be addressed in future studies.

Plin2 Contributes to the Zone Dependence of Hepatic Lipid Accumulation

The metabolic functions of hepatocytes are understood to vary according to the specific hepatic zone in which they are located, and to reflect nutrient, metabolite, hormone and oxygen concentration gradients in the hepatic blood supply that decrease or increase from zone 1 to zone 3 [134, 135]. Previous studies in rodents have shown that fasting and re-feeding a high carbohydrate diet induces lipogenic gene expression that begins in zone 1 and progresses to zone 3 [136]. However, lipid accumulation responses were not reported in these studies, and zone specific responses to re-feeding fasted animals a HF diet have not been previously identified. My results show that significant zone-specific responses in lipid accumulation following fasting and re-feeding occur only in mice re-fed with the HF diet. Combined with data in WT mice showing that hepatic lipid content in LF-re-fed animals is reduced relative to that of HF-re-fed animals, differences in the zone specificity of lipid accumulation provide evidence that the mechanisms underlying LF- and HF-diets effects on lipid accumulation are spatially distinct within the liver parenchyma.

The mechanisms determining zone specificity of hepatic lipid accumulation are likely to be complex, and may include zone-specific differences in several of the processes regulating hepatic lipid metabolism. For instance, *de novo* lipid synthesis and lipid oxidation activities of the liver have been reported to be zone specific [137, 138]. My finding that the zone specificity of lipid accumulation in HF-re-fed mice is disrupted by loss of Plin2, suggest that the processes regulating lipid storage associated with elevated amounts of dietary lipids may also exhibit zone specificity. Additional studies are needed to understand how Plin2 contributes to the zone dependence of lipid

accumulation. However, Plin2 expression and lipid accumulation are increased by hypoxia [139, 140], which is more pronounced in zone 3 compared to other zones [59]. Thus, zone specificity of lipid accumulation in HF-re-fed WT mice may reflect, in part, hypoxia driven Plin2 expression in zone 3.

Plin2 Regulation of CLD Properties

CLD size reflects the quantity of stored lipid, and possibly other aspects of their function [123]. Hepatocyte CLD size is influenced by diseases, or exposure to drugs and toxic agents that disrupt hepatic metabolism, and can vary over a considerable range [59, 141]. My observations that the average CLD diameter in livers of fasted WT mice re-fed the HF diet are significantly larger than those of LF-re-fed mice, demonstrate that the dietary fat content is another physiological influence of hepatic CLD size in WT mice.

It is unclear what determines variations in hepatic CLD size. Observations in mice chronically fed HF diets with or without ethanol, suggest that larger CLD found in livers of ethanol-exposed animals may be related to differences in PLIN family member composition, and/or to post-translational modification of CLD associated proteins [59]. However, definitive evidence those members of the PLIN family are physiologically important regulators of hepatic CLD size has been lacking. My data, documenting that Plin2 loss results in a 50% reduction in hepatic CLD size compared to WT mice re-fed LF- or HF-diets, provide the first direct evidence that Plin2 is a physiologically important determinant of hepatic CLD size. Further, the finding that Plin3 and Plin5 coat the smaller hepatic CLD found in D5KO mice demonstrates functional differences exist in the abilities of PLIN family members to regulate CLD growth.

Plin2 Scaffolding Functions

How Plin2 regulates hepatic lipid accumulation and CLD size are not understood in detail. Multiple cell culture and *in vivo* experiments suggest that Plin2 functions as a barrier to lipolysis and that this function is the primary mechanism by which it regulates CLD lipid storage functions [142, 143]. However, the possibility that PLIN proteins have scaffolding functions that link CLD protein composition and properties to the cells metabolic status has also been raised [113]. Previous studies documenting effects of dietary fat content on CLD protein composition, including Plin2 levels, in livers of fasted and re-fed WT mice [116] are consistent with possible functional linkages between hepatic CLD protein composition and the liver's metabolic status. Evidence from the present study, demonstrating that Plin2 is a physiological determinant of the protein composition and size of hepatic CLD, support the concept that it possesses scaffolding functions that regulate CLD lipid storage functions in the liver. Additional work is needed to formally establish this concept. However, the observations that dietary fat content influences the effects of Plin2 deletion on hepatic CLD protein composition are consistent with it having scaffolding functions, and the possibility that these scaffolding functions contribute to the coordination of hepatic CLD protein composition with the liver's metabolic properties.

In summary, my study demonstrates that Plin2 is a physiologically important determinant of hepatic lipid accumulation associated with re-feeding fasted animals a HF diet. The function of Plin2 in the liver appears to be specifically related to regulating the ability of CLD to accommodate increased lipid storage, as Plin2 is not essential for CLD formation, or apparently for lipid storage induced in response to de novo lipogenesis. My observations also provide the first evidence that Plin2 possesses scaffolding functions

that contribute to its role in regulating CLD properties and possibly to integrating lipid storage and metabolic functions of the liver.

CHAPTER V

CONCLUSIONS AND DISCUSSION

Summary and Conclusion

Cytoplasmic lipid droplets are now being recognized to play important roles in cellular homeostasis. In the liver, CLD provide a temporary, yet dynamic depot for TG storage that hepatocytes can access based upon the energy demands of the cell. The dysregulation of TG storage is the hallmark of hepatic steatosis [11]. Access to mass spectrometry based proteomics has improved our ability to identify the proteins that coat the CLD phospholipid monolayer through the analysis of more than 15 proteomic profiles of CLD from different tissues and cell lines [42, 61, 74-82, 92, 93]. My thesis work is the first to provide information about the proteomic profile of isolated CLD from the liver, and the first to exam the effects of two independent variables, environment (diet), and genetics (loss of Plin2) on CLD proteome. From the data presented in this thesis, I propose that Plin2 is a necessary scaffolding protein that is required for the interactions of specific enzymes that help to facilitate metabolic reactions (Figure V.1). Furthermore, the perilipin proteins act as adaptor proteins that can interact with the surface of the CLD monolayer and various organelles to facilitate metabolic functions. The data provided in this thesis are evidence that the CLD proteomic profile reflects the metabolic status of the liver, through alterations in CLD size and quantity, differences in the composition of proteins associated with specific metabolic enzymes, and through changes in pathways involved in metabolic processes (Figure V.2).

The vast amount of data generated from a single proteomics experiment can be significant. Isolated CLD contained 75-125 proteins after the use of a stringent criterion

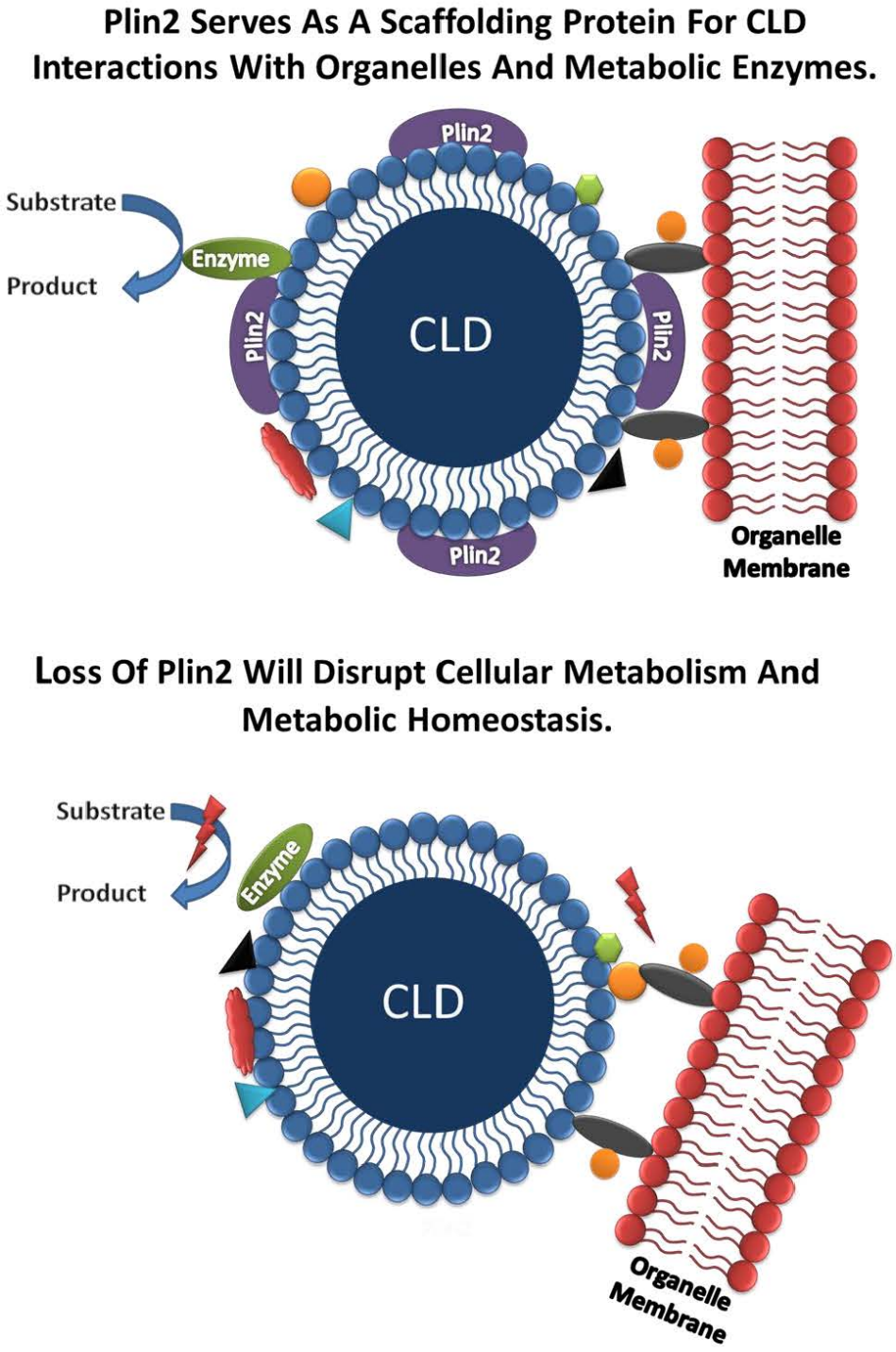

Figure V.1 Model of CLD Interactions with Organelle Membrane and Enzymes on the CLD in the Presences (A) or Absence (B) of Plin2

to determine which proteins to include in the profile. I was able to obtain evidence of complex protein interactions involving discrete metabolic pathways on isolated hepatic CLD utilizing web-based programs for analysis (STRING and KEGG). These findings suggest that CLD may act as metabolic platforms by sequestering and enhancing interactions among enzymes of specific metabolic pathways, including those involved in methionine-choline and glucogenic metabolism. Evidence also suggests the loss of Plin2 on CLD from HF re-fed animals may disrupt pathways that were once intact such as the loss of enzymes from FA metabolic pathways. The proposal that CLD function in the compartmentalization of metabolic pathway reactions is analogous to the known functions of other organelles, such as mitochondria, in compartmentalizing specific biological functions. Alternatively, the CLD may provide an additional level of regulation by excluding specific enzymes within a given pathway, which may be controlled through the expression of specific perilipin proteins.

Multiple studies have shown CLD are associated with various organelles. The most dramatic evidence for this support comes from the interaction between Plin5 and the mitochondria. Fractionation experiments have demonstrated how Plin5 can be localized to both the mitochondria and the CLD, and how disrupting the interactions of Plin5 can inhibit both TG storage and oxidation via mitochondria β-oxidation pathway [46]. This concept was further supported by proteomics data from isolated skeletal muscle CLD, which showed significant numbers of mitochondrial proteins within the enriched CLD fraction [82]. My work has shown that WT and D5KO mice had significant differences in the number of organelle specific proteins that were enriched with the isolated CLD. Isolated CLD from D5KO animals had fewer ER and peroxisomal associated proteins,

but had a significantly greater numbers of cytoplasmic proteins than CLD isolated from WT mice. There is still much work that is needed to make significant conclusions about these data. However, one could surmise the loss of interactions between CLD and organelles in the D5KO mice could lead to disruption of lipid metabolism through uncoupling of CLD to ER or peroxisomes.

In addition to proteomic profiles, I was also able to demonstrate that CLD size changed according to diet. In general, CLD generated from WT animals consuming LFD were much smaller than those on HFD. My observations that Plin2 loss reduces CLD size in mice re-fed the HFD, bun not the LFD, suggests that Plin2 plays a diet specific role in regulating the ability of CLD to store TG. The nature of these interactions between Plin2 and diet involved in regulating TG storage in CLD has not been identified. However, chylomicrons are the source of FA substrates for hepatic TG synthesis in HF re-fed mice, whereas FA mobilized from adipose, or synthesized de novo within the liver, are the source of FA used for hepatic TG synthesis in LF re-fed mice. Thus Plin2 may be functionally linked to lipoprotein lipase depended uptake and transport of dietary fatty acids into the liver.

Significance to Human Health

The purpose of biomedical research is to increase our understanding of biological systems in the effort to further our ability to improve human health. Obesity, type II diabetes, and non-alcoholic fatty liver disease have become a major health epidemic throughout the world. Understanding the complex mechanisms that lead to these diseases are an important foundation for finding new interventions in combating these health problems. The work presented here examines how the dynamic natures of the protein

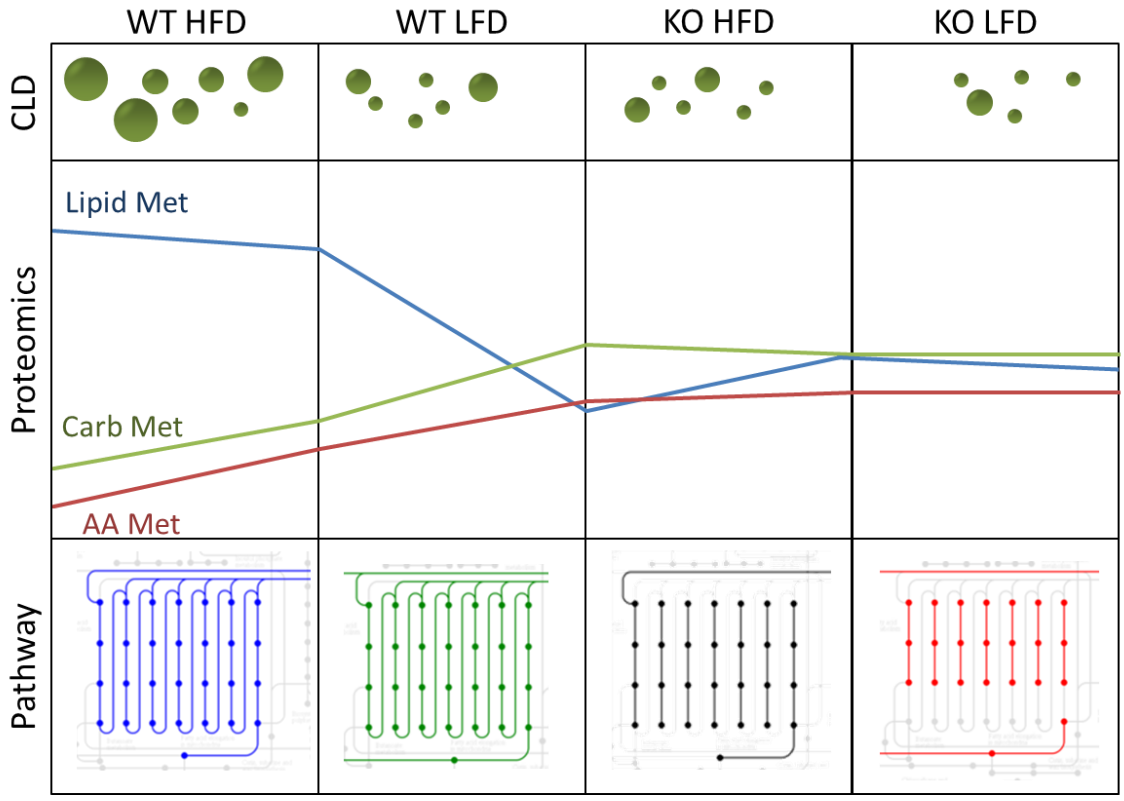

Figure V.2 Summary of Data from WT and D5KO Studies in Chapters III and IV

composition of CLD are influenced by diet and genetics. There are still many questions that must be answered before moving forward with translational studies in humans. However, it is clear that Plin2 plays an important role in the metabolic regulation of CLD in the mouse hepatocytes. Moreover, these data support numerous studies linking high fat diets to changes in overall metabolism. These data also suggest that diets high in fat change the metabolic composition in the liver compared to low fat diets.

Drug Targets

Much of biomedical research has focused over the years on finding potential drug targets to combat various diseases, and this has become the generic answer to the

fundamental questions regarding the validity of research, specifically in publicly funded university settings. The proteomics data presented here provides many potential drug targets that may help to decrease the severity of hepatic steatosis, most notably Plin2. The primary question that remains to be answered about Plin2 is what role does it play in overall metabolic function in the liver, and what is the role of other perilipin proteins such as Plin3 and Plin5 in prevention of CLD accumulation in hepatocytes? Moreover, additional work is needed to understand how the loss of Plin2 influences the total metabolic activity of an organism. It is clear that in the absence of Plin2 CLD accumulation can occur during fasting, and over longer durations of feeding high fat diet Plin2 deficient animals appear to be resistant to obesity and hepatic steatosis. Targeting proteins like Plin2 may lead to decreasing hepatic steatosis and even obesity. However, this may also lead to disruptions in metabolic homeostasis that result in additional side effects. Given the significant numbers of individuals, and the extraordinary cost involved in treating diseases and complications from obesity, all viable treatment options should be explored.

Personalized Medicine

The advances in technology, which have exponentially increased our understanding of the basic molecular and biochemical changes that lead to disease, have also increased our ability to examine the molecular and biochemical differences between individuals. The notion of individual personalized medicine is more pertinent to the data presented in my thesis than a generic argument of defining a new drug target. Beyond drugs that could target Plin2, further studies in humans should be explored to determine if those individuals who appear to be more prone to obesity and hepatic steatosis possess

genetic factors, such as single nucleotide polymorphisms (SNP) or genetic dysregulation of proteins that have been identified on the CLD. Recently Magne et al. discovered a SNP in the human form of Plin2 that was found to decrease hepatic steatosis and serum TG [144]. This discovery is further evidence that personalized medicine will be an important tool towards combating human disease, but proteomics data, such as those from my study, provides a potential list of targets that could be more fully investigated. This information may provide insight for individual treatment through understanding the specific metabolic demands, sensitivity towards particular nutrients, and alteration of hormones that may be regulated through complex pathways in part through the protein profile of CLD specific to individual genetic composition.

Future Directions

CLD as a Platform for Enzyme Activity

The thesis work I present here opens the door to many more questions. Are CLD capable of providing a platform for enzymatic reactions to take place? The cytosol is described as being a matrix for cellular reactions. CLD could provide proteins the necessary scaffold to efficiently perform enzymatic reactions in an organized manner. CLD proteins like Plin2 and Plin5, which are suggested to associate with specific organelles like the ER and mitochondria, could direct CLD to specific compartments of the cytosol depending on the metabolic demands of the cell. Although I have been able to provide support for this idea, there has yet to be a significant biochemical study to prove this hypothesis. In order to address this question several experiments should be performed. I would first determine if isolated hepatic CLD maintained any ability to undergo enzymatic reactions. The ideal technology for performing this experiment would

be the use of non-targeted mass spectrometry based metabolomics. Large quantities of isolated CLD would be necessary. I would begin looking at reactions involving C-13 labeled glucose and tracking the progression of glucose over time to determine if glucose oxidation were taking place on the isolated CLD. Based on these results, I would continue with other substrates, from identified pathways such as the methionine-choline pathway, which has been identified as a target of NAFLD.

Proteomics

To gain a true insight into the hepatic CLD of D5KO mice, I would embark on a series of proteomic experiments to determine how the loss of Plin2 changes the total liver proteome. The data presented in my thesis assumes the loss of Plin2 only affects the CLD proteome. I would examine the isolated CLD proteome from fasted mice at different time points to determine if there is a significant difference in the CLD coat during fasting. This would also be advantageous to examine in a D5KO liver specific KO model, and a rescue experiment with Plin2 Adenovirus to determine if the proteomic profile returns to the WT CLD proteome.

REFERENCES

1. Barness, L.A., J.M. Opitz, and E. Gilbert-Barness, *Obesity: genetic, molecular, and environmental aspects.* Am J Med Genet A, 2007. **143A**(24): p. 3016-34.

2. Unger, R.H., et al., *Lipid homeostasis, lipotoxicity and the metabolic syndrome.* Biochim Biophys Acta, 2010. **1801**(3): p. 209-14.

3. Hill, M.J., D. Metcalfe, and P.G. McTernan, *Obesity and diabetes: lipids, 'nowhere to run to'.* Clin Sci (Lond), 2009. **116**(2): p. 113-23.

4. Greenberg, A.S., et al., *The role of lipid droplets in metabolic disease in rodents and humans.* J Clin Invest, 2011. **121**(6): p. 2102-10.

5. Contos, M.J. and A.J. Sanyal, *The clinicopathologic spectrum and management of nonalcoholic fatty liver disease.* Adv Anat Pathol, 2002. **9**(1): p. 37-51.

6. Tolman, K.G., et al., *Spectrum of liver disease in type 2 diabetes and management of patients with diabetes and liver disease.* Diabetes Care, 2007. **30**(3): p. 734-43.

7. Bellentani, S., et al., *Prevalence of and risk factors for hepatic steatosis in Northern Italy.* Ann Intern Med, 2000. **132**(2): p. 112-7.

8. Tominaga, K., et al., *Prevalence of fatty liver in Japanese children and relationship to obesity. An epidemiological ultrasonographic survey.* Dig Dis Sci, 1995. **40**(9): p. 2002-9.

9. Nadeau, K.J., G. Klingensmith, and P. Zeitler, *Type 2 diabetes in children is frequently associated with elevated alanine aminotransferase.* J Pediatr Gastroenterol Nutr, 2005. **41**(1): p. 94-8.

10. Schwimmer, J.B., et al., *Prevalence of fatty liver in children and adolescents.* Pediatrics, 2006. **118**(4): p. 1388-93.

11. Raman, M. and J. Allard, *Non alcoholic fatty liver disease: a clinical approach and review.* Can J Gastroenterol, 2006. **20**(5): p. 345-9.

12. Reynolds, K. and J. He, *Epidemiology of the metabolic syndrome.* Am J Med Sci, 2005. **330**(6): p. 273-9.

13. Tang, A., et al., *Nonalcoholic fatty liver disease: MR imaging of liver proton density fat fraction to assess hepatic steatosis.* Radiology, 2010. **267**(2): p. 422-31.

14. Altman, R., *Die Elementarorganisem und ihre Beziehungen zu den Zellen.* (Leipzig: Veit, 1890.

15. Wilson, E., *The Cell in Development and Inheritance.* New York: Macmillan, 1896.

16. Greenberg, A.S., et al., *Perilipin, a major hormonally regulated adipocyte-specific phosphoprotein associated with the periphery of lipid storage droplets.* J Biol Chem, 1991. **266**(17): p. 11341-6.

17. Tauchi-Sato, K., et al., *The surface of lipid droplets is a phospholipid monolayer with a unique Fatty Acid composition.* J Biol Chem, 2002. **277**(46): p. 44507-12.

18. Yen, C.L., et al., *Thematic review series: glycerolipids. DGAT enzymes and triacylglycerol biosynthesis.* J Lipid Res, 2008. **49**(11): p. 2283-301.

19. Martin, S. and R.G. Parton, *Lipid droplets: a unified view of a dynamic organelle.* Nat Rev Mol Cell Biol, 2006. **7**(5): p. 373-8.

20. Ploegh, H.L., *A lipid-based model for the creation of an escape hatch from the endoplasmic reticulum.* Nature, 2007. **448**(7152): p. 435-8.

21. Robenek, H., et al., *Adipophilin-enriched domains in the ER membrane are sites of lipid droplet biogenesis.* J Cell Sci, 2006. **119**(Pt 20): p. 4215-24.

22. Brasaemle, D.L., *Thematic review series: adipocyte biology. The perilipin family of structural lipid droplet proteins: stabilization of lipid droplets and control of lipolysis.* J Lipid Res, 2007. **48**(12): p. 2547-59.

23. Chong, B.M., et al., *The adipophilin C terminus is a self-folding membrane-binding domain that is important for milk lipid secretion.* J Biol Chem, 2011. **286**(26): p. 23254-65.

24. Jiang, H.P. and G. Serrero, *Isolation and characterization of a full-length cDNA coding for an adipose differentiation-related protein.* Proc Natl Acad Sci U S A, 1992. **89**(17): p. 7856-60.

25. Buechler, C., et al., *Adipophilin is a sensitive marker for lipid loading in human blood monocytes.* Biochim Biophys Acta, 2001. **1532**(1-2): p. 97-104.

26. Corsini, E., et al., *Induction of adipose differentiation related protein and neutral lipid droplet accumulation in keratinocytes by skin irritants.* J Invest Dermatol, 2003. **121**(2): p. 337-44.

27. Faber, B.C., et al., *Identification of genes potentially involved in rupture of human atherosclerotic plaques.* Circ Res, 2001. **89**(6): p. 547-54.

28. Schmidt, S.M., et al., *Induction of adipophilin-specific cytotoxic T lymphocytes using a novel HLA-A2-binding peptide that mediates tumor cell lysis.* Cancer Res, 2004. **64**(3): p. 1164-70.

29. Steiner, S., et al., *Induction of the adipose differentiation-related protein in liver of etomoxir-treated rats.* Biochem Biophys Res Commun, 1996. **218**(3): p. 777-82.

30. Wang, X., et al., *Induced expression of adipophilin mRNA in human macrophages stimulated with oxidized low-density lipoprotein and in atherosclerotic lesions.* FEBS Lett, 1999. **462**(1-2): p. 145-50.

31. Heid, H.W., et al., *Adipophilin is a specific marker of lipid accumulation in diverse cell types and diseases.* Cell Tissue Res, 1998. **294**(2): p. 309-21.

32. Masuda, Y., et al., *ADRP/adipophilin is degraded through the proteasome-dependent pathway during regression of lipid-storing cells.* J Lipid Res, 2006. **47**(1): p. 87-98.

33. Brasaemle, D.L., et al., *Adipose differentiation-related protein is an ubiquitously expressed lipid storage droplet-associated protein.* J Lipid Res, 1997. **38**(11): p. 2249-63.

34. Londos, C., et al., *Perilipins, ADRP, and other proteins that associate with intracellular neutral lipid droplets in animal cells.* Semin Cell Dev Biol, 1999. **10**(1): p. 51-8.

35. Motomura, W., et al., *Up-regulation of ADRP in fatty liver in human and liver steatosis in mice fed with high fat diet.* Biochem Biophys Res Commun, 2006. **340**(4): p. 1111-8.

36. Magnusson, B., et al., *Adipocyte differentiation-related protein promotes fatty acid storage in cytosolic triglycerides and inhibits secretion of very low-density lipoproteins.* Arterioscler Thromb Vasc Biol, 2006. **26**(7): p. 1566-71.

37. Imai, Y., et al., *Reduction of hepatosteatosis and lipid levels by an adipose differentiation-related protein antisense oligonucleotide.* Gastroenterology, 2007. **132**(5): p. 1947-54.

38. Chang, B.H., et al., *Protection against fatty liver but normal adipogenesis in mice lacking adipose differentiation-related protein.* Mol Cell Biol, 2006. **26**(3): p. 1063-76.

39. Russell, T.D., et al., *Mammary glands of adipophilin-null mice produce an amino-terminally truncated form of adipophilin that mediates milk lipid droplet formation and secretion.* J Lipid Res, 2008. **49**(1): p. 206-16.

40. McManaman, J.L., et al., *Perilipin-2-null mice are protected against diet-induced obesity, adipose inflammation, and fatty liver disease.* J Lipid Res, 2013. **54**(5): p. 1346-59.

41. Wolins, N.E., D.L. Brasaemle, and P.E. Bickel, *A proposed model of fat packaging by exchangeable lipid droplet proteins.* FEBS Lett, 2006. **580**(23): p. 5484-91.

42. Sato, S., et al., *Proteomic profiling of lipid droplet proteins in hepatoma cell lines expressing hepatitis C virus core protein.* J Biochem, 2006. **139**(5): p. 921-30.

43. Sztalryd, C., et al., *Functional compensation for adipose differentiation-related protein (ADFP) by Tip47 in an ADFP null embryonic cell line.* J Biol Chem, 2006. **281**(45): p. 34341-8.

44. Carr, R.M., et al., *Reduction of TIP47 improves hepatic steatosis and glucose homeostasis in mice.* Am J Physiol Regul Integr Comp Physiol, 2012. **302**(8): p. R996-1003.

45. Dalen, K.T., et al., *LSDP5 is a PAT protein specifically expressed in fatty acid oxidizing tissues.* Biochim Biophys Acta, 2007. **1771**(2): p. 210-27.

46. Wang, H., et al., *Perilipin 5, a lipid droplet-associated protein, provides physical and metabolic linkage to mitochondria.* J Lipid Res, 2011. **52**(12): p. 2159-68.

47. Lass, A., et al., *Adipose triglyceride lipase-mediated lipolysis of cellular fat stores is activated by CGI-58 and defective in Chanarin-Dorfman Syndrome.* Cell Metab, 2006. **3**(5): p. 309-19.

48. Wang, H., et al., *Unique regulation of adipose triglyceride lipase (ATGL) by perilipin 5, a lipid droplet-associated protein.* J Biol Chem, 2011. **286**(18): p. 15707-15.

49. Wolins, N.E., et al., *OXPAT/PAT-1 is a PPAR-induced lipid droplet protein that promotes fatty acid utilization.* Diabetes, 2006. **55**(12): p. 3418-28.

50. Ducharme, N.A. and P.E. Bickel, *Lipid droplets in lipogenesis and lipolysis.* Endocrinology, 2008. **149**(3): p. 942-9.

51. Haemmerle, G., et al., *Hormone-sensitive lipase deficiency in mice changes the plasma lipid profile by affecting the tissue-specific expression pattern of lipoprotein lipase in adipose tissue and muscle.* J Biol Chem, 2002. **277**(15): p. 12946-52.

52. Zimmermann, R., et al., *Fat mobilization in adipose tissue is promoted by adipose triglyceride lipase.* Science, 2004. **306**(5700): p. 1383-6.

53. Haemmerle, G., et al., *Defective lipolysis and altered energy metabolism in mice lacking adipose triglyceride lipase.* Science, 2006. **312**(5774): p. 734-7.

54. Lu, X., X. Yang, and J. Liu, *Differential control of ATGL-mediated lipid droplet degradation by CGI-58 and G0S2.* Cell Cycle, 2010. **9**(14): p. 2719-25.

55. Gruber, A., et al., *The N-terminal region of comparative gene identification-58 (CGI-58) is important for lipid droplet binding and activation of adipose triglyceride lipase.* J Biol Chem, 2006. **285**(16): p. 12289-98.

56. Gruber, A., et al., *The N-terminal region of comparative gene identification-58 (CGI-58) is important for lipid droplet binding and activation of adipose triglyceride lipase.* J Biol Chem, 2010. **285**(16): p. 12289-98.

57. Chang, B.H., et al., *Absence of adipose differentiation related protein upregulates hepatic VLDL secretion, relieves hepatosteatosis, and improves whole body insulin resistance in leptin-deficient mice.* J Lipid Res, 2010. **51**(8): p. 2132-42.

58. Guo, Y., et al., *Lipid droplets at a glance.* J Cell Sci, 2009. **122**(Pt 6): p. 749-52.

59. Orlicky, D.J., et al., *Chronic ethanol consumption in mice alters hepatocyte lipid droplet properties.* Alcohol Clin Exp Res, 2011. **35**(6): p. 1020-33.

60. Wahlig, J.L., et al., *Impact of High-Fat Diet and Obesity on Energy Balance and Fuel Utilization During the Metabolic Challenge of Lactation.* Obesity (Silver Spring), 2011.

61. Wu, C.C., et al., *Proteomics reveal a link between the endoplasmic reticulum and lipid secretory mechanisms in mammary epithelial cells.* Electrophoresis, 2000. **21**(16): p. 3470-82.

62. Croze, E.M. and D.J. Morre, *Isolation of plasma membrane, golgi apparatus, and endoplasmic reticulum fractions from single homogenates of mouse liver.* J Cell Physiol, 1984. **119**(1): p. 46-57.

63. Russell, T.D., et al., *Cytoplasmic lipid droplet accumulation in developing mammary epithelial cells: roles of adipophilin and lipid metabolism.* J Lipid Res, 2007. **48**(7): p. 1463-75.

64. Lei, T.C., et al., *Label-free imaging of trabecular meshwork cells using Coherent Anti-Stokes Raman Scattering (CARS) microscopy.* Mol Vis, 2011. **17**: p. 2628-33.

65. Tokuyasu, K., *Application of cryoultramicrotomy to immunocytochemistry.* J Microscopy, 1986. **143**: p. 139-149.

66. Chong, B.M., et al., *The adipophilin C-terminus is a self-folding membrane binding domain that is important for milk lipid secretion.* J Biol Chem, 2011.

67. Bhala, N., et al., *The natural history of nonalcoholic fatty liver disease with advanced fibrosis or cirrhosis: an international collaborative study.* Hepatology, 2011. **54**(4): p. 1208-16.

68. Fabbrini, E., S. Sullivan, and S. Klein, *Obesity and nonalcoholic fatty liver disease: biochemical, metabolic, and clinical implications.* Hepatology, 2010. **51**(2): p. 679-89.

69. Straub, B.K., et al., *Differential pattern of lipid droplet-associated proteins and de novo perilipin expression in hepatocyte steatogenesis.* Hepatology, 2008. **47**(6): p. 1936-46.

70. Athenstaedt, K., et al., *Identification and characterization of major lipid particle proteins of the yeast Saccharomyces cerevisiae.* J Bacteriol, 1999. **181**(20): p. 6441-8.

71. Binns, D., et al., *An intimate collaboration between peroxisomes and lipid bodies.* J Cell Biol, 2006. **173**(5): p. 719-31.

72. Cermelli, S., et al., *The lipid-droplet proteome reveals that droplets are a protein-storage depot.* Curr Biol, 2006. **16**(18): p. 1783-95.

73. Beller, M., et al., *Characterization of the Drosophila lipid droplet subproteome.* Mol Cell Proteomics, 2006. **5**(6): p. 1082-94.

74. Liu, P., et al., *Chinese hamster ovary K2 cell lipid droplets appear to be metabolic organelles involved in membrane traffic.* J Biol Chem, 2004. **279**(5): p. 3787-92.

75. Bartz, R., et al., *Dynamic activity of lipid droplets: protein phosphorylation and GTP-mediated protein translocation.* J Proteome Res, 2007. **6**(8): p. 3256-65.

76. Brasaemle, D.L., et al., *Proteomic analysis of proteins associated with lipid droplets of basal and lipolytically stimulated 3T3-L1 adipocytes.* J Biol Chem, 2004. **279**(45): p. 46835-42.

77. Cho, S.Y., et al., *Identification of mouse Prp19p as a lipid droplet-associated protein and its possible involvement in the biogenesis of lipid droplets.* J Biol Chem, 2007. **282**(4): p. 2456-65.

78. Umlauf, E., et al., *Association of stomatin with lipid bodies.* J Biol Chem, 2004. **279**(22): p. 23699-709.

79. Fujimoto, Y., et al., *Identification of major proteins in the lipid droplet-enriched fraction isolated from the human hepatocyte cell line HuH7.* Biochim Biophys Acta, 2004. **1644**(1): p. 47-59.

80. Turro, S., et al., *Identification and characterization of associated with lipid droplet protein 1: A novel membrane-associated protein that resides on hepatic lipid droplets.* Traffic, 2006. **7**(9): p. 1254-69.

81. Wan, H.C., et al., *Roles and origins of leukocyte lipid bodies: proteomic and ultrastructural studies.* Faseb J, 2007. **21**(1): p. 167-78.

82. Zhang, H., et al., *Proteome of skeletal muscle lipid droplet reveals association with mitochondria and apolipoprotein a-I.* J Proteome Res, 2011. **10**(10): p. 4757-68.

83. Sokolovic, M., et al., *The transcriptomic signature of fasting murine liver.* BMC Genomics, 2008. **9**: p. 528.

84. Zhang, F., et al., *Gene expression profile change and associated physiological and pathological effects in mouse liver induced by fasting and refeeding.* PLoS One, 2011. **6**(11): p. e27553.

85. den Boer, M., et al., *Hepatic steatosis: a mediator of the metabolic syndrome. Lessons from animal models.* Arterioscler Thromb Vasc Biol, 2004. **24**(4): p. 644-9.

86. Bergen, W.G. and H.J. Mersmann, *Comparative aspects of lipid metabolism: impact on contemporary research and use of animal models.* J Nutr, 2005. **135**(11): p. 2499-502.

87. Lissner, L., et al., *Dietary fat and the regulation of energy intake in human subjects.* Am J Clin Nutr, 1987. **46**(6): p. 886-92.

88. Parks, E.J. and M.K. Hellerstein, *Thematic review series: patient-oriented research. Recent advances in liver triacylglycerol and fatty acid metabolism using stable isotope labeling techniques.* J Lipid Res, 2006. **47**(8): p. 1651-60.

89. Nan, X., E.O. Potma, and X.S. Xie, *Nonperturbative chemical imaging of organelle transport in living cells with coherent anti-stokes Raman scattering microscopy.* Biophys J, 2006. **91**(2): p. 728-35.

90. Hodges, B.D. and C.C. Wu, *Proteomic insights into an expanded cellular role for cytoplasmic lipid droplets.* J Lipid Res, 2010. **51**(2): p. 262-73.

91. Goodman, J.M., *The gregarious lipid droplet.* J Biol Chem, 2008. **283**(42): p. 28005-9.

92. Bouchoux, J., et al., *The proteome of cytosolic lipid droplets isolated from differentiated Caco-2/TC7 enterocytes reveals cell-specific characteristics.* Biol Cell, 2011. **103**(11): p. 499-517.

93. Ding, Y., et al., *Proteomic profiling of lipid droplet-associated proteins in primary adipocytes of normal and obese mouse.* Acta Biochim Biophys Sin (Shanghai), 2012. **44**(5): p. 394-406.

94. Dalen, K.T., et al., *PPARalpha activators and fasting induce the expression of adipose differentiation-related protein in liver.* J Lipid Res, 2006. **47**(5): p. 931-43.

95. Orlicky, D.J., et al., *Multiple functions encoded by the N-terminal PAT domain of adipophilin.* J Cell Sci, 2008. **121**(Pt 17): p. 2921-9.

96. Yoshiuchi, K., et al., *Pioglitazone reduces ER stress in the liver: direct monitoring of in vivo ER stress using ER stress-activated indicator transgenic mice.* Endocr J, 2009. **56**(9): p. 1103-11.

97. Lee, A.H., et al., *Regulation of hepatic lipogenesis by the transcription factor XBP1.* Science, 2008. **320**(5882): p. 1492-6.

98. Prattes, S., et al., *Intracellular distribution and mobilization of unesterified cholesterol in adipocytes: triglyceride droplets are surrounded by cholesterol-rich ER-like surface layer structures.* J Cell Sci, 2000. **113 (Pt 17)**: p. 2977-89.

99. Finkelstein, J.D., *Methionine metabolism in liver diseases.* Am J Clin Nutr, 2003. **77**(5): p. 1094-5.

100. Teng, Y.W., et al., *Deletion of betaine-homocysteine S-methyltransferase in mice perturbs choline and 1-carbon metabolism, resulting in fatty liver and hepatocellular carcinomas.* J Biol Chem, 2011. **286**(42): p. 36258-67.

101. Rubio-Aliaga, I., et al., *Alterations in hepatic one-carbon metabolism and related pathways following a high-fat dietary intervention.* Physiol Genomics, 2011. **43**(8): p. 408-16.

102. Browning, J.D. and J.D. Horton, *Molecular mediators of hepatic steatosis and liver injury.* J Clin Invest, 2004. **114**(2): p. 147-52.

103. Yamaguchi, K., et al., *Inhibiting triglyceride synthesis improves hepatic steatosis but exacerbates liver damage and fibrosis in obese mice with nonalcoholic steatohepatitis.* Hepatology, 2007. **45**(6): p. 1366-74.

104. Begriche, K., et al., *Drug-induced toxicity on mitochondria and lipid metabolism: mechanistic diversity and deleterious consequences for the liver.* J Hepatol, 2011. **54**(4): p. 773-94.

105. Nagle, C.A., E.L. Klett, and R.A. Coleman, *Hepatic triacylglycerol accumulation and insulin resistance.* J Lipid Res, 2009. **50 Suppl**: p. S74-9.

106. Ohsaki, Y., et al., *Biogenesis of cytoplasmic lipid droplets: from the lipid ester globule in the membrane to the visible structure.* Biochim Biophys Acta, 2009. **1791**(6): p. 399-407.

107. Hodges, B.D. and C.C. Wu, *Proteomic insights into an expanded cellular role for cytoplasmic lipid droplets.* J Lipid Res. **51**(2): p. 262-73.

108. Sunden, S.L., et al., *Betaine-homocysteine methyltransferase expression in porcine and human tissues and chromosomal localization of the human gene.* Arch Biochem Biophys, 1997. **345**(1): p. 171-4.

109. Kirpich, I.A., et al., *Integrated hepatic transcriptome and proteome analysis of mice with high-fat diet-induced nonalcoholic fatty liver disease.* J Nutr Biochem, 2011. **22**(1): p. 38-45.

110. Oh, T.S., et al., *Time-dependent hepatic proteome analysis in lean and diet-induced obese mice.* J Microbiol Biotechnol, 2011. **21**(12): p. 1211-27.

111. Grimsrud, P.A., et al., *A quantitative map of the liver mitochondrial phosphoproteome reveals posttranslational control of ketogenesis.* Cell Metab, 2012. **16**(5): p. 672-83.

112. Fu, S., et al., *Polysome profiling in liver identifies dynamic regulation of endoplasmic reticulum translatome by obesity and fasting.* PLoS Genet, 2012. **8**(8): p. e1002902.

113. Brasaemle, D.L., *The perilipin family of structural lipid droplet proteins: Stabilization of lipid droplets and control of lipolysis.* J Lipid Res, 2007. **48**: p. 2547-2549.

114. Fabbrini, E., et al., *Intrahepatic fat, not visceral fat, is linked with metabolic complications of obesity.* Proc Natl Acad Sci U S A, 2009. **106**(36): p. 15430-5.

115. Stefan, N., K. Kantartzis, and H.U. Haring, *Causes and metabolic consequences of Fatty liver.* Endocr Rev, 2008. **29**(7): p. 939-60.

116. Crunk, A.E., et al., *Dynamic Regulaiton of Hepatic Lipid Droplet Properties by Diet.* PLoS One, 2013. **8**(7): p. e67631.

117. Wahlig, J.L., et al., *Impact of high-fat diet and obesity on energy balance and fuel utilization during the metabolic challenge of lactation.* Obesity (Silver Spring), 2012. **20**(1): p. 65-75.

118. Klapper, M., et al., *Fluorescence-based fixative and vital staining of lipid droplets in Caenorhabditis elegans reveal fat stores using microscopy and flow cytometry approaches.* J Lipid Res, 2011. **52**(6): p. 1281-93.

119. Jungermann, K., *Metabolic zonation of liver parenchyma: significance for the regulation of glycogen metabolism, gluconeogenesis, and glycolysis.* Diabetes Metab Rev, 1987. **3**(1): p. 269-93.

120. Evans, J.L., B. Quistorff, and L.A. Witters, *Zonation of hepatic lipogenic enzymes identified by dual-digitonin-pulse perfusion.* Biochem J, 1989. **259**(3): p. 821-9.

121. Brunt, E.M., *Pathology of fatty liver disease.* Mod Pathol, 2007. **20 Suppl 1**: p. S40-8.

122. James, O.F. and C.P. Day, *Non-alcoholic steatohepatitis (NASH): a disease of emerging identity and importance.* J Hepatol, 1998. **29**(3): p. 495-501.

123. Suzuki, M., et al., *Lipid droplets: size matters.* J Electron Microsc (Tokyo), 2011. **60 Suppl 1**: p. S101-16.

124. D'Agostino, R., *Tests for Normal Distribution* in *Goodness-Of-Fit Techniques*, M.D. RB D'Agostino and MA Stephens, Editor. 1986: New York.

125. Sztalryd, C., et al., *Functional compensation for adipose differentiation-related protein (ADFP) by TIP47 in an adfp nullembryonic cell line.* J Biol Chem, 2006. **281**: p. 34341-34348.

126. Ashburner, M., et al., *Gene ontology: tool for the unification of biology. The Gene Ontology Consortium.* Nat Genet, 2000. **25**(1): p. 25-9.

127. Kanehisa, M., et al., *From genomics to chemical genomics: new developments in KEGG.* Nucleic Acids Res, 2006. **34**(Database issue): p. D354-7.

128. Jiang, L., et al., *Leptin contributes to the adaptive responses of mice to high-fat diet intake through suppressing the lipogenic pathway.* PLoS One, 2009. **4**(9): p. e6884.

129. Hernandez Vallejo, S.J., et al., *Short-term adaptation of postprandial lipoprotein secretion and intestinal gene expression to a high-fat diet.* Am J Physiol Gastrointest Liver Physiol, 2009. **296**(4): p. G782-92.

130. Serino, M., et al., *Metabolic adaptation to a high-fat diet is associated with a change in the gut microbiota.* Gut, 2012. **61**(4): p. 543-53.

131. So, M., et al., *Analysis of time-dependent adaptations in whole-body energy balance in obesity induced by high-fat diet in rats.* Lipids Health Dis, 2011. **10**: p. 99.

132. Lu, X., et al., *The murine perilipin gene: the lipid droplet-associated perilipins derive from tissue-specific, mRNA splice variants and define a gene family of ancient origin.* Mamm Genome, 2001. **12**(9): p. 741-9.

133. Chong, B.M., et al., *Determinants of adipophilin function in milk lipid formation and secretion.* Trends Endocrinol Metab, 2011. **22**(6): p. 211-7.

134. Tsukada, K. and M. Suematsu, *Visualization and analysis of blood flow and oxygen consumption in hepatic microcirculation: application to an acute hepatitis model.* J Vis Exp, 2012(66): p. e3996.

135. Katz, N.R., *Metabolic heterogeneity of hepatocytes across the liver acinus.* J Nutr, 1992. **122**(3 Suppl): p. 843-9.

136. Kinlaw, W.B., P. Tron, and L.A. Witters, *Thyroid hormone and dietary carbohydrate induce different hepatic zonation of both "spot 14" and acetyl-coenzyme-A carboxylase: a novel mechanism of coregulation.* Endocrinology, 1993. **133**(2): p. 645-50.

137. Pashkov, V., et al., *Regulator of G protein signaling (RGS16) inhibits hepatic fatty acid oxidation in a carbohydrate response element-binding protein (ChREBP)-dependent manner.* J Biol Chem, 2011. **286**(17): p. 15116-25.

138. Evans, J.L., B. Quistorff, and L.A. Witters, *Hepatic zonation of acetyl-CoA carboxylase activity.* Biochem J, 1990. **270**(3): p. 665-72.

139. Saarikoski, S.T., S.P. Rivera, and O. Hankinson, *Mitogen-inducible gene 6 (MIG-6), adipophilin and tuftelin are inducible by hypoxia.* FEBS Letters, 2002. **530**(1-3): p. 186-190.

140. Gimm, T., et al., *Hypoxia-inducible protein 2 is a novel lipid droplet protein and a specific target gene of hypoxia-inducible factor-1.* FASEB J, 2010. **24**(11): p. 4443-58.

141. Day, C.P. and S.J. Yeaman, *The biochemistry of alcohol-induced fatty liver.* Biochim Biophys Acta, 1994. **1215**(1-2): p. 33-48.

142. Listenberger, L.L., et al., *Adipocyte differentiation-related protein reduces lipid droplet association of adipose triglyceride lipase and slows triacylglycerol turnover.* J Lipid Res, 2007. **48**: p. 2751-2761.

143. Sapiro, J.M., et al., *Hepatic triacylglycerol hydrolysis regulates peroxisome proliferator-activated receptor alpha activity.* J Lipid Res, 2009. **50**(8): p. 1621-9.

144. Magne, J., et al., *The minor allele of the missense polymorphism Ser251Pro in perilipin 2 (PLIN2) disrupts an alpha-helix, affects lipolysis, and is associated with reduced plasma triglyceride concentration in humans.* Faseb J, 2013. **27**(8): p. 3090-9.